This is to certify that the

dissertation entitled

A Theoretical and Experimental Investigation of the Chemical Kinetics of an Oxygen Microwave Discharge

presented by

Mary Lynn Brake

has been accepted towards fulfillment of the requirements for

Ph.D degree in Mechanical Engineering

Ronald L. Keeler
Major professor

Date 1/25/83

A THEORETICAL AND EXPERIMENTAL INVESTIGATION OF THE CHEMICAL KINETICS OF AN OXYGEN MICROWAVE DISCHARGE

By

Mary Lynn Brake

A DISSERTATION

Submitted to
Michigan State Unviersity
in partial fulfillment of the requirements
for the degree of

DOCTOR OF PHILOSOPHY

Department of Mechanical Engineering

1983

ABSTRACT

A THEORETICAL AND EXPERIMENTAL INVESTIGATION OF THE CHEMICAL KINETICS OF AN OXYGEN MICROWAVE DISCHARGE

By

Mary Lynn Brake

In this dissertation, the degree of dissociation and recombination of oxygen atoms produced in a microwave discharge in oxygen is examined by comparing theoretical models of the kinetic mechanisms to chemical titration data. A literature search is used to gain understanding of the chemical and relaxation kinetic mechanisms necessary for the formulation of the theoretical models.

A comparison of the theoretical models to experimental results shows that a one dimensional, temperature dependent model of the neutral species of the system can predict the oxygen atom concentration profile as measured by nitrogen dioxide titration. The model also indicates that the temperature of the gas is approximately 1000K and that an overall gas temperature and velocity increase is due to heating by the microwave discharge and not due to the enthalpy change of the species in the system.

ACKNOWLEDGMENTS

I would like to express my gratitude to Professor Ronald Kerber, my thesis advisor, for his encouragement and interest over the past three years. I would like to thank Professor Jes Asmussen and the students in the Laser and Plasma Labs for their suggestions and advice. I am also grateful to Professors T. Harvey Edwards, John McGrath and Jerry Nolen who served on my guidance committee.

I would especially like to thank the following friends: Mr. Jeffrey Hinkle for not only designing the oxygen microwave experiment, but making work, Dr. Thomas Pierce III for graciously providing me with copies of EPISODE and LSODI as well as advice in their usage, Dr. Robert Ball for many hours of badly needed computer consultation and Dr. Mary Beth Kazanski for her constant support and encouragement.

Last, be certainly not least, I would like to thank my parents, Richard and Jane Brake for their support these many years and I would like to thank my husband Bob, for enduring many long hours on the road, so that I might be able to finish this project.

TABLE OF CONTENTS

LIST OF TABLES

LIST OF FIGURES

LIST OF SYMBOLS

A = cross sectional area of the plasma containment tube (2.54 cm^2)

A_{ij} = Einstein coefficient, probability of spontaneous emission from state i to j

B' = rotational constant for upper rotational state (cm^{-1})

c = speed of light (3.0×10^{10} cm/sec)

C_p = specific heat (cal/mole-K)

$\vec{E}$ = electric field strength

E_i = energy of state i

f = mass flowrate (moles/sec)

F = External force

g = statistical weight

H = enthalpy (cal/gm) = $1/\rho \sum_i n_i H_i$

H_i = enthalpy of species i (cal/moles)

H_β = the second line in the Balmer series of hydrogen (4861Å)

h = Planck's constant (6.626×10^{-34} Joule-sec)

J' = upper rotational quantum number

J'' = lower rotational quantum number

k = Boltzmann's constant (1.38×10^{-23} Joules/K)

L = path length of emitted light

M = molecular weight (gm/mole)

n_i = species concentration (moles/cc)

n_e = electron density (cm^{-3})

N_{ij} = integrated radiance of an atomic line

P = pressure = $\Sigma_i n_i R'T = \rho RT$ (torr)

$\dot{P}_{NO_2}$ = pressure increase (torr/sec) of NO_2 into a known volume V_{NO_2}

R = R'/M (cm^2/sec^2-K)

R' = universal gas constant (8.3×10^7 ergs/mole-K)

S_i = entropy of a species (cal/mole-K)

T = temperature (Kelvin)

T_e = electron temperature

v = linear velocity of gas (cm/sec)

Z = partition function

τ = shear force

ρ = density (gm/cc)

λ = wavelength of light

$\Delta\lambda_S$ = full width at half height of a Stark broadened line

CHAPTER I

INTRODUCTION

1.1 Plasma Chemistry

All matter exists in one of four states; solids, liquids, gases, or plasmas. The first three states are the most familiar but plasmas are believed to be the most abundant, with as much as 99% of the universe existing in the plasma state.[1,2] A plasma is defined as any gaseous system containing a sufficient number of electrons and ions such that long range electromagnetic (Coulomb) forces dominate the behavior of the gas. Note that a normal gas acts as an insulator whereas a plasma acts as a conductor.[1]

A transfer from one state to another can be accomplished through a transfer of energy. Energy added to a solid causes it to melt and become a liquid. Heat added to a liquid results in vaporization and the formation of gases. As even more energy is pumped into a gas, molecules dissociate and neutral species ionize, creating ions and electrons. These free electrons continue to transfer energy to the rest of the gas through elastic and inelastic collisions.

In recent years, the uses of plasmas in chemistry have gained much attention.[3-6] There are many advantages

associated with using plasmas for producing chemical species. One of the biggest advantages is that the high temperatures of plasmas are associated with producing high yields of pure and ultra-pure substances[3] which may be impossible to produce at low temperatures. This ability to produce non-equilibrium species concentrations at low overall gas temperatures reduces the requirements for heat loss control and durable reactor materials.[4] Through optimization, plasma chemistry can not only improve product quality but can reduce labor and handling and reduce utilization of hazardous or costly chemicals.[5] Perhaps one of the most important contributions of plasmas in chemistry is the ability to "generate the precursors to the desired products, rather than to produce these products directly".[4]

There are many applications of plasma chemistry in industry, science and medicine. In particular, due to the reactive nature of oxygen, oxygen plasmas have a wealth of applications. Oxygen plasmas are used to improve the bond strength of industrial materials. Oxygen plasmas can isolate trace constituents in complex organic structures, so that chemical analysis can be used to identify the trace substances. Oxygen plasmas prepare specimens for microscopy in the process of surface etching, thin film deposition and "ashing". Oxygen plasmas are also used in

the fabrication of semiconductor devices by removing photoresist, depositing organic and inorganic dieletric films, and by etching surfaces. (See Reference 5 for details.)

Oxygen plasmas can be initiated in many ways; glow discharges, plasma jets, shock tubes, and radio frequency discharges to name a few. Microwave discharges are particularly suitable for plasma chemistry applications because they do not use electrodes which can become contaminated and because microwave power supplies have become both plentiful and inexpensive.[7]

Microwave discharges are characterized as gases which are partially ionized by absorption of radiation in the microwave region of the electro-magnetic spectrum. Generally, as a gas flows through a "resonant cavity" which contains the microwave radiation, it absorbs electrical energy. The electrons in the gas gain kinetic energy from interactions with the electric field and then transfer some of this energy through elastic and inelastic collisions to the neutral and ionic species of the gas. This energy transfer manifests itself in dissociation and ionization and in populating electronic, vibrational and rotational states as well as causing a thermal energy increase of the gas as a whole. When the gas leaves the reactor cavity, the electrons recombine with the ions and the gas relaxes

to an equilibrium state different from the pre-discharge state. This new state may be characterized by a different temperature, a different velocity or by a different mixture of atoms and molecules. (See Figure 1.1 for a schematic of plasma processes in a microwave discharge.)

A potentially useful application of microwave discharges is "free radical propulsion".[8] The free radical propulsion concept uses the fact that the gas exiting a microwave discharge is at a different state than the initial gas. Originally it was thought that spacecraft propulsion could be obtained from the thermal energy released when dissociated diatomics recombine exothermically.[8] It is the purpose of this dissertation to examine the effects of microwave fields on oxygen and to investigate the chemical kinetic mechanisms involved in the transfer of electrical to thermal energy. Such understanding will permit assessment of the use of oxygen plasmas or plasmas of similar gases for various applications including spacecraft propulsion. It will be shown that the thermal energy increase anticipated for spacecraft propulsion is due solely to neutral gas heating and <u>not</u> due to the chemical energy released in recombination.

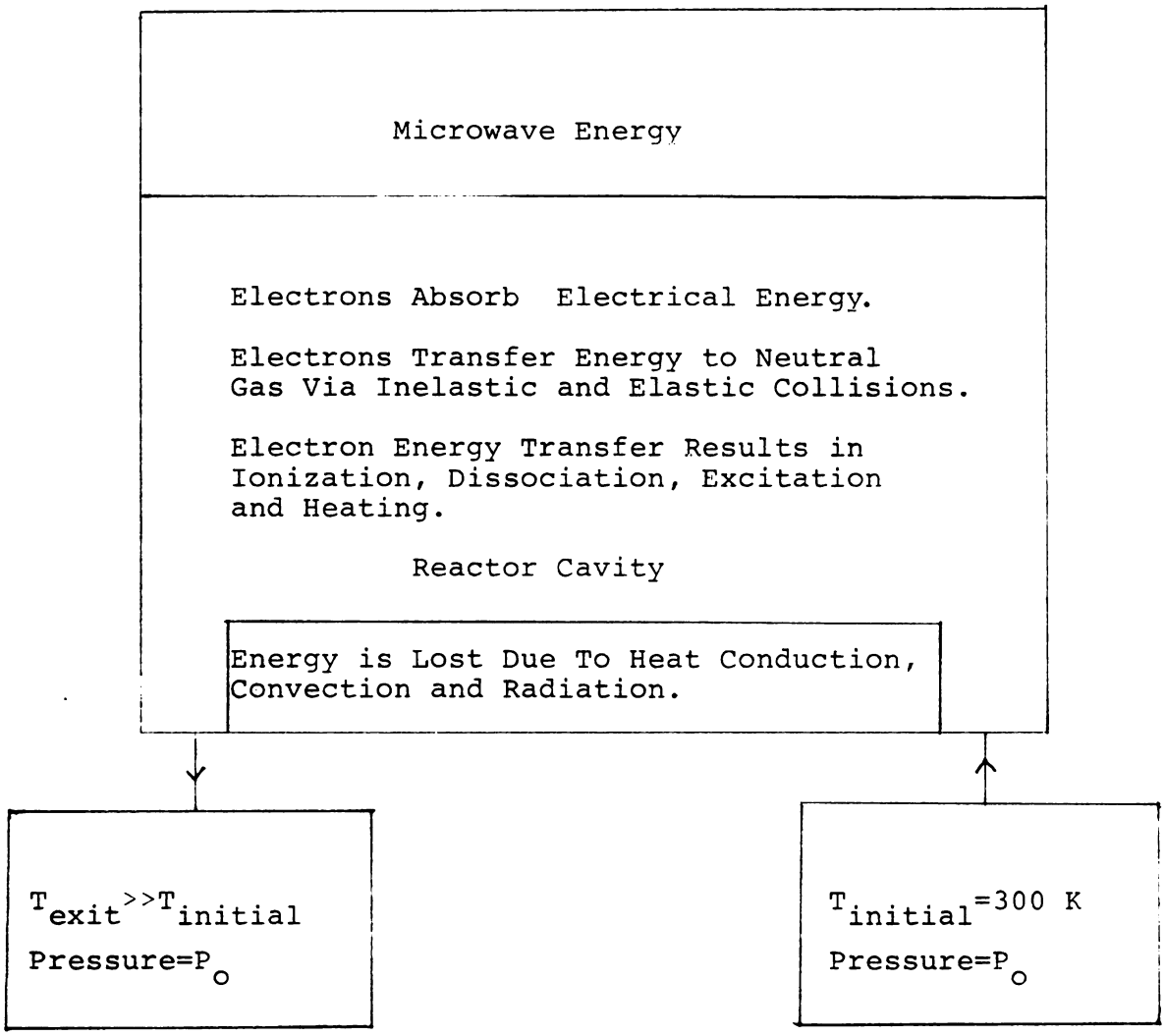

Figure 1.1. A schematic showing the energy processes in a microwave discharge.

1.2 Previous Models and Experiments

Oxygen plasmas have been examined in a variety of experiments and models. Bell and Kwong[9] examined two and three body recombination in a radio frequency discharge (13.56 MHz). Mearns and Morris[10] and Francis[11] have also examined three body recombination of oxygen atoms with oxygen molecules in a microwave discharge (2.54 GHz). These three studies did not however examine the role of electronically excited states of oxygen atoms and molecules. Bonnet[12] examined oxygen kinetic mechanisms for an electron beam controlled discharge in oxygen that did include excited species of oxygen molecules. Kocian[13] studied some of the same mechanisms as Bonnet but for a positive column discharge. Wayne[14] compiled an extensive literature review of oxygen kinetic mechanisms in discharges, however he has not examined these mechanisms in a model nor has he compared predictions of a model to experimental results.

Both Bell[5,9] and Bonnet[12] have used their model in computer simulations to make theoretical predictions about species concentrations as a function of time, atomic conversion (into molecules), power, pressure and electric field strength. Both include the effect of the electric field, where the electrical energy is absorbed wholly by

the electrons. Neither group however makes the distinction between the plasma inside the reactor cavity and the gas system outside the reactor cavity. Bell compares his model with the results of Mearns and Morris[10], but the data taken by Mearns and Morris was measured outside the reactor cavity (where presumably the electric field is not the same as in the reactor cavity and is possibly nearly zero). The amount of molecular conversion was linearly extrapolated back to the exit of the discharge but not into the discharge. To correctly make comparisons with experimental data taken outside the discharge and to make conclusions about the kinetic mechanisms, only that part of the discharge should be modeled.

1.3 Objectives of Present Research

The objective of this dissertation is to examine the change in oxygen as it travels through a reactor cavity containing a microwave field. This can only be accomplished by understanding the chemical kinetics of oxygen and how they affect the temperature and velocity of the gas. The specific objectives listed below are presented in the chronological order in which they were performed.

1. Identify the important chemical kinetic mechanisms of an oxygen discharge from the long list of possible reactions.
2. Determine the importance of electronically excited states to the chemical kinetics.
3. Determine the effect of temperature on the kinetic mechanisms.
4. Compare model predictions of the oxygen atom concentration of the gas after it has interacted with the microwave field with titration data. Examine the effects of temperature and velocity on the model.
5. Examine the overall changes in the oxygen gas due to interactions with the the microwave field.

The first objective is accomplished in Chapter II. A simple computer model is formulated that examines the importance of the many chemical reactions by determining which reactions dominate the chemical species derivatives as a function of time. The importance of electronically excited states is assessed at this time.

In Chapter III, a literature search of the temperature dependence of the rate coefficients of the important reactions found in Chapter II is discussed. Also, the forward rate coefficient for each important reaction is suggested. A summary of the important reactions and their

recommended rate coefficients is given in Appendix A.

The formulation of a model which includes the conservation of energy and momentum as well as the continuity equation for each species is formulated in Chapter IV. In Chapter VI the model is compared to experimental results of Chapter V, as well as other models. Velocity, temperature and $O_2(^1\Delta)$ formation predictions are made based upon the results of the model. Conclusions based upon the observations of this work are given in Chapter VII.

Electron and ion species collision processes are also very important in electrical discharges. (See Appendix E for a listing of some of the important charged species reactions in oxygen.) However, many experimental parameters such as the electron density, the electron temperature and the electron distribution function are needed to properly model these kinetic processes. These parameters are very difficult to measure in microwave discharges. Appendix C discusses emission spectroscopy techniques for determining electron density, electron temperature and gas temperature in argon and oxygen microwave discharges. In other works such as that of Dettmer[15] and Bonnet[12], electron and ion collision induced processes are discussed for oxygen in DC positive column and e-beam discharges.

CHAPTER II

SIMPLE MODELING

2.1 Simple Model Formulation

The first step in modeling the chemical kinetics of any system is to compile a list of the relevent mechanisms, (see Table 2.1). Generally, the neutral kinetic mechanisms important to this dissertation have been studied in ultra-violet flash photolysis of ozone and molecular oxygen, shock tube studies and electrical discharges. The vast majority of kinetic reactions were studied at one temperature only. The simple model discussed in this chapter examines the relative importance of the probable kinetic mechanisms of an oxygen gas system in chemical nonequilibrium, at the thermal equilibrium temperature of 300 K. Chapter III gives a comprehensive literature review of the temperature dependence of the most important mechanisms found in this chapter.

This model is based upon the mechanisms given by Wayne[14] and upon a similar model for an oxygen laser.[16] Atmospheric studies[17-23] have also provided possible kinetic mechanisms of systems comprised of oxygen. Most of the reactions are well documented and the different rate

Table 2.1 Rate Coefficients for Neutral Collision Partners in O_2 Dissociation.

Reaction	H(298K)	K_{equil}	Rate Coefficient	Method	Ref.
1. $O + O_3 \rightarrow 2O_2$	-93.7	5.8×10^{68}	4.0×10^{9}	photoionization	24
			$(6.6 \pm 0.6) \times 10^{9}$*	laser flash photolysis	25
			2.3×10^{9}	thermal decomposition	26
			$(1.5 \pm 0.3) \times 10^{10}$	mass spectroscopy	27
			$(5.3 \pm 1.1) \times 10^{9}$	photolysis	28
2. $O + O_3 \rightarrow O_2 + O_2(^1\Delta)$	-71.1	1.3×10^{52}	$2.7 \times 10^{9 \pm 2}$*	flowing afterglow	17
3. $O(^1D) + O_3 \rightarrow 2O_2$	-139.0	1.0×10^{100}	$(4.0 \pm 2.0) \times 10^{13}$	flash photolysis	29,30
			$(2.0 \pm 1.0) \times 10^{14}$*	flash photolysis	31
			$(1.6 \pm 0.1) \times 10^{14}$	photolysis	32
			$(2.1 \pm 0.2) \times 10^{14}$	photolysis/abs.spec.	32
			$(1.5 \pm 0.6) \times 10^{14}$	photolysis/em.spec.	33
4. $O(^1D) + O_2 \rightarrow O + O_2$	-45.4	4.0×10^{33}	$(3.0 \pm 3.0) \times 10^{13}$	flash phot./em.spec.	33
			$(2.4 \pm 0.6) \times 10^{13}$*	photolysis/em.spec.	34
			$(3.6 \pm 1.8) \times 10^{13}$	photolysis/em.spec.	35
			$(4.2 \pm 0.3) \times 10^{13}$	photolysis	32
			$(2.2 \pm 0.4) \times 10^{13}$	photolysis	36
5. $O(^1D) + O_2 \rightarrow O_2(^1\Delta) + O$	-22.8	8.8×10^{16}	6.0×10^{7}*	microwave discharge	37
6. $O(^1D) + O_2 \rightarrow O_2(^1\Sigma) + O$	-7.7	4.7×10^{5}	$(1.5 \pm 0.8) \times 10^{14}$*	flash photolysis	29,30
7. $O_2(^1\Sigma) + O_3 \rightarrow 2O_2 + O$	-12.3	4.3×10^{11}	$(4.0 \pm 0.5) \times 10^{12}$*	flash photolysis	29,30
			$(4.3 \pm 0.5) \times 10^{12}$	discharge/flash phot.	37,38
			$(1.4 \pm 0.3) \times 10^{13}$	flash photolysis	39

Table 2.1 continued

Reaction	H(298K)	K_{equil}	Rate Coefficient	Method	Ref.
8. $O_2(^1\Sigma) + O_2 \rightarrow 2O_2$	-37.7	8.4×10^{27}	1.8×10^{12}*		13
9. $O_2(^1\Sigma + O_2 \rightarrow 2O_2$	-37.7	8.4×10^{27}	6.6×10^{7}		40
			2.7×10^{8}	flash photolysis	38
			9.0×10^{7}	uv photolysis	35
			9.0×10^{7}*	discharge/flow	41
			6.0×10^{7}	microwave discharge	37
10. $O_2(^1\Sigma) + O_3 \rightarrow 2O_2 + O$	-37.7	8.4×10^{27}	$(1.5\pm0.6)\times10^{13}$	flash phot./em.spec.	33
			4.2×10^{12}*	microwave discharge	41
11. $O_2(^1\Delta) + O_3 \rightarrow 2O_2 + O$	+2.87	2.28	$(2.1\pm0.3)\times10^{9}$	photo-ionization	24
			$(1.7\pm0.5)\times10^{9}$	microwave discharge	42
			$(2.7\pm1.3)\times10^{9}$	microwave discharge	43
			$(1.5\pm0.3)\times10^{9}$	photo-ion/discharge	44
			$(2.2\pm1.0)\times10^{9}$*	photolysis	45
12. $2O_2(^1\Delta) \rightarrow O_2(^1\Sigma) + O_2$	-7.5	2.4×10^{5}	1.4×10^{6}	microwave discharge	37
			1.2×10^{6}	microwave discharge	46
			$(1.2\pm0.3)\times10^{7}$*	microwave discharge	47
13. $O_2(^1\Delta) + O_2 \rightarrow 2O_2$	-22.6	4.5×10^{16}	$(1.3\pm0.5)\times10^{6}$*	photolysis	48
			$(1.3\pm0.7)\times10^{6}$	photolysis	49
			$(1.4\pm0.1)\times10^{6}$	rf discharge	50
			$(1.0\pm0.6)\times10^{6}$	microwave discharge	41
			$(1.2\pm0.1)\times10^{6}$	discharge flow	51
14. $O_2(^1\Delta) + O \rightarrow O_2 + O$	-22.6	4.5×10^{16}	7.8×10^{7}*	rf discharge	50,52
15. $O + O + O \rightarrow O_2 + O$	-119.1	1.1×10^{85}	$(1.4\pm0.7)\times10^{15}$*	shock tube abs.	53
			$(1.6\pm0.3)\times10^{15}$	shock tube/dens.	54

Table 2.1 continued

Reaction	H(298K)	K_{equil}	Rate Coefficient	Method	Ref.
16. $O + O + O_2 \rightarrow O_2 + O_2$	-119.1	1.1×10^{85}	$(5.3\pm1.1)\times10^{14}$*	shock tube/dens.	54
			$(1.6\pm0.8)\times10^{14}$	shock tube/abs.	
			$(8.3\pm1.6)\times10^{14}$	shock tube/abs.	55
			2.3×10^{14}	shock tube/abs.	56
			5.1×10^{15}	shock tube/interferometer	57
17. $O + O_2 + O_2 \rightarrow O_3 + O_2$	-25.5	2.0×10^{16}	$(1.8\pm0.2)\times10^{14}$	flash photolysis	39
			1.3×10^{14}	thermal decomposition	26
			2.7×10^{14}	microwave discharge	58,59
			$(2.4\pm0.3)\times10^{14}$	microwave discharge	60
			$(2.0\pm0.1)\times10^{14}$*	flash photolysis	61
18. $O + O_2 + O_3 \rightarrow O_3 + O_3$	-25.5	2.0×10^{16}	2.9×10^{14}*	thermal decomposition	62,26
			3.2×10^{14}	thermal/pressure	63
19. $O \xrightarrow{wall} \frac{1}{2}O_2$	-56.6		$(6.0\pm2.0)\times10^{-5}$	microwave discharge	64
			1.6×10^{-4}	microwave discharge	65
			$(1.2\pm0.6)\times10^{-4}$*	ac discharge	66
20. $O(^1D) \xrightarrow{wall} \frac{1}{2}O$	-104.9		same as 19.		
21. $O_2(^1\Sigma) \xrightarrow{wall} O_2(^1\Delta)$	-15.1		1.0×10^{-2}*	microwave discharge	37,67
			$(0.9\pm0.2)\times10^{-2}$	microwave discharge	47
22. $O_2(^1\Delta) \xrightarrow{wall} O_2$	-22.6		2.0×10^{-5}*		67
23. $O_2(^1\Sigma) \xrightarrow{wall} O_2$	-37.7		2.2×10^{-3}*		17

Table 2.1 continued

Reaction	H(298K)	K_{equil}	Rate Coefficient	Method	Ref.
24. $O(^1D) \rightarrow h\nu$			6.7×10^{-3}*		17
25. $O_2(^1\Delta) \rightarrow h\nu$			2.6×10^{-4}*		17
26. $O_2(^1\Sigma) \rightarrow h\nu$			8.3×10^{-2}		17

* Values used in computer simulation

NOTE: All rate coefficients have the units of moles, cm^3 and seconds at 298K and H is in Kcal.

coefficients experimentally measured for each reaction agree well with one another (see Table 2.1). All of the reactions listed in Table 2.1 were included in the computer model and the asterisks denote the forward rate constant chosen for this model.

The first few electronically excited states of oxygen atoms and molecules are indicated in Table 2.2. As suggested by Wayne, the products of an electrical discharge of oxygen may contain an appreciable number of electronically excited states of oxygen. This model includes reactions that involve the first excited state of atomic oxygen $O(^1D)$ which is 1.96 eV above the ground state, and the first two excited states of molecular oxygen $O_2(^1\Delta)$ and $O_2(^1\Sigma)$ which are 0.98 eV and 1.64 eV above the ground state, respectively. States higher than 2.0 eV are very short lived and are assumed to have very small concentrations compared with the first excited states.

In modeling any system, a few initial assumptions must be made. In this model, the velocity of the flowing system remained constant and the pressure was allowed to vary. Also it is assumed that the electric field outside of the discharge was zero and that the electron and ion densities outside of the discharge were negligible. Also the temperature of the gas was set equal to 300 K, and the initial gas was assumed to be a homogeneous mixture of O,

Table 2.2. Excited states of O_2 and O

	STATE	ENERGY(eV)	Mean Radiative Lifetime (sec)
O_2 :	$^3\Sigma_g^-$	0.0	
	$^1\Delta_g$	0.98	3
	$^1\Sigma_g^+$	1.64	12.0
	$^3\Sigma_u^+$	4.3	0.03
	$^3\Sigma_u^-$	6.1	4.2×10^{-8}
O :	^3P	0.0	
	^1D	1.96	148.0
	$^1S_0$	2.22	0.80
	$^5S_2$	9.13	6.0×10^{-4}
	$^3S_1$	9.51	1.8×10^{-9}

O_2 , O_3 , $O(^1D)$, $O_2(^1\Delta)$ and $O_2(^1\Sigma)$. Also, for reactions that involve a third body M, it was assumed that this third body could be in the ground or excited states.

The rate of change of the concentrations with time is equal to the sum of all the populating effects minus the sum of all of the depopulating effects. The populating and depopulating effects included were chemical kinetics (two and three body), wall effects and spontaneous emission.

The reaction paths of the model are given in Table 2.1 along with the forward rate found in the literature. The chemical reactions may be written

$$\sum_i \alpha_{ri} N_i \underset{k_{br}}{\overset{k_{fr}}{\rightleftharpoons}} \sum_i \beta_{ri} N_i \qquad (2.1)$$

where N_i is the molar concentration of species i, α_{ri} and β_{ri} are stoichiometric coefficients and k_{fr} and k_{br} are the forward and backward rate coefficients respectively. To preserve detailed balancing, the backward rate coefficients are computed from the forward rate coefficients and the equilibrium constants by using the expression

$$K_{eq} = k_{fr} / k_{br} \qquad (2.2)$$

The equilibrium constants were calculated from values found in the JANAF (Joint Army Navy Air Force)[68] thermodynamic tables. If the perfect gas law is assumed, then the equilibrium constant is a function of temperature alone.

$$\ln K_{eq} = 1/RT \sum_i \nu_{ri} H_i + 1/R \sum_i \nu_{ri} S_i \qquad (2.3)$$

where H_i and S_i are the heats of formation and entropies of species i as found in the JANAF tables and $\nu_{ri} = \beta_{ri} - \alpha_{ri}$. Thus once the equilibrium constant is determined for a range of temperatures, the backward rate coefficient may be found. (See Appendix B)

The rate constants for wall recombination effects were calculated from the reported probability coefficients denoted by γ, where γ is the ratio of the frequency of collisions of atoms with the surface leading to recombination to the total frequency of collisions (see Table 2.1). The rate of wall recombination in a cylinder of radius r is equal to

$$k_{wall} = \sqrt{8kT/\pi m}\ \gamma/2r \qquad (2.4)$$

the particle flux at the surface, multiplied by the surface to volume ratio multiplied by the recombination probability γ. The mass of the particle hitting the wall is m, k is Boltzmann's constant and T is the translational temperature, which is 300 K for this model. A radius of 8.9 mm was used for these calculations.

The chemical rate equations form a nonlinear set of coupled differential equations of the form

$$\frac{d[n]}{dt} = \sum_i A_i - \sum_i B_i \qquad (2.5)$$

where A_i is the populating reaction rate for species n and B_i is the depopulating reaction rate for species n. These differential equations have been numerically solved using an integrating routine called EPISODE written by A. C. Hindemarsh and G. D. Byrne (obtained from the Argonne National Code Center).[80] The relative concentrations of different species and the pressure were varied and time histories of the concentrations and their derivatives have been studied.

Each reaction has a varying degree of importance depending upon the intial relative concentrations, the pressure and the amount of time evolved since reaction initiation. As will be shown, all of these factors can

affect species lifetime.

2.2 Simple Model Results

The ultimate purpose of this study is to determine the degree of recombination and dissociation of oxygen in a flowtube. The oxygen atom halflife is an important factor in determining where recombination occurs. Therefore, the input conditions were varied to determine the importance of individual species and reactions on oxygen atom halflife. (The "halflife" is the amount of time taken to decrease the oxygen atom population by one half its original value.) In addition to the concentrations as a function of time, the total reaction rate (the forward rate coefficient multiplied by the reactants minus the backward rate coefficient times the products) for each reaction was studied as a function of time also. These total reaction rates provided insight into the specific mechanisms which affected the time evolution.

Generally the most important reactions were found to be reactions 1, 2, 11, 14, 15, 16, 17, 19, and 22 for the input cases of mostly dissociated oxygen atoms with trace amounts of ozone and excited states. (These conditions best approximate experimental conditions.) The reactions that play the major role will be different for different

input conditions. Figure 2.1 shows a typical time history for 100% dissociation at 10 torr.

2.2.1 Effect of Molecular Oxygen

The effect of oxygen molecules on the oxygen atom halflife was studied by varying the O/O_2 ratio and keeping the initial pressure constant (10 torr) and all other concentrations equal to zero (Figure 2.2). The larger O/O_2 ratio shortens the halflife of oxygen atoms. This is due in part to the fact that at lower ratios (keeping the pressure constant) there are fewer oxygen atoms, so the probability of two atoms coming together and recombining is small. This can be observed in the fact that the total reaction rate of reaction 15 ($O + O + O = O_2 + O$) is much larger for large O/O_2 ratios than for for smaller ratios. Total reaction rates for reactions 16 and 17 (also three body reactions) are roughly the same for all ratios of O/O_2. The same is true for the wall recombination reaction rate. Also, near the beginning of the run (time less than 10^{-4}) reaction 7 ($O_2(^1\Sigma) + O_3 = 2O_2 + O$) and especially reaction 11 ($O_2(^1\Delta) + O_3 = 2O_2 + O$) run backward populating $O_2(^1\Delta)$, $O_2(^1\Sigma)$ and O_3. In particular, $O_2(^1\Delta)$ is produced to about the same degree regardless of input ratio, so it is at a much higher

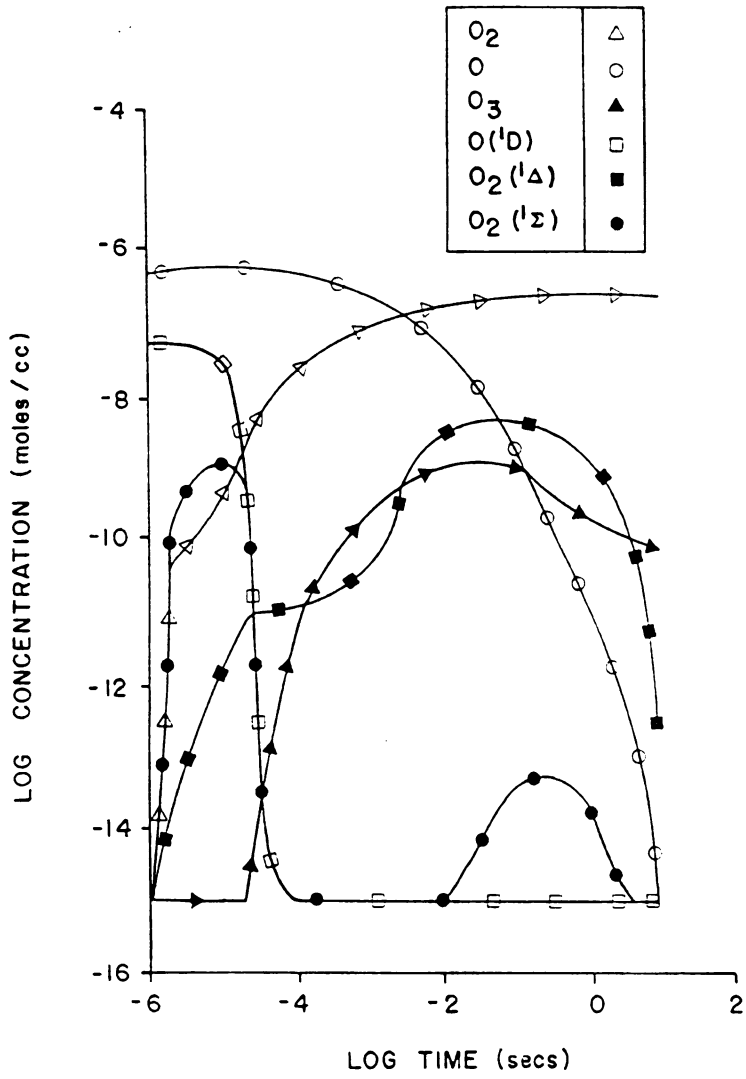

Figure 2.1 Time history of species concentrations. Initial conditions were 100% dissociation at an initial pressure of 10 torr where 10% of the initial O atom concentration was in the $O(^1D)$ state.

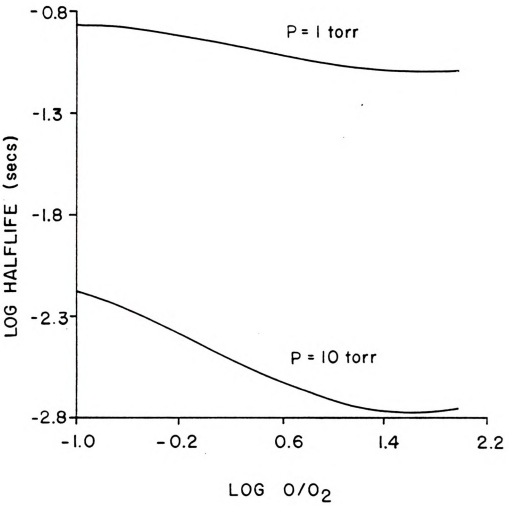

Figure 2.2 The effect of O/O_2 ratio on the halflife of atomic oxygen.

concentration compared with oxygen atoms, at lower O/O_2 ratios than at higher ratios, (as high as 10% of initial O atom concentration for O/O_2 = 0.1). The presence of $O_2(^1\Delta)$ was found to slightly increase the halflife of atoms. As time progresses (time greater than 0.01 seconds) reaction 11 runs in the forward direction to a significant degree and helps to populate the O atoms state. Thus at low O/O_2 ratios the larger relative fraction of $O_2(^1\Delta)$ would have a greater effect on O atom lifetime.

2.2.2 Effect of Excited Atomic Oxygen

The effect of $O(^1D)$ on the production and retention of O atoms was found to be negligible after the first few microseconds. The collisional halflife of $O(^1D)$ is found to be microseconds where typically, depending upon the pressure, the $O(^3P)$ ground state halflife is in the millisecond range. Two pressure cases (1 and 10 torr) were examined where the initial condition was 100% dissociation (i.e. all other species started out at zero concentration, so as not to mask the effect of $O(^1D)$). The initial amount of $O(^1D)$ (varied from 10%-50% of the initial oxygen atom concentration) was found to perturb the time history in the first few microseconds only. After these few microseconds, the time history was insensitive to initial $O(^1D)$

concentration. The $O(^1D)$ depletion mechanism is dominated by reactions 4 and 6 (two body collisional deactivation) and reactions 15 and 16 (three body recombination). These reactions all have large forward rate coefficients. These collisional reactions are all much faster than radiative decay. For the remaining studies the $O(^1D)$ concentration was initialized to zero.

2.2.3 Effect of Excited Molecular Oxygen

The effect of excited states of molecular oxygen was examined by varying their concentrations separately. A study at a pressure of 10 torr was examined where 60% of the gas has been dissociated into atoms. The $O_2(^1\Sigma)$ concentration was varied from 0-20% (of the remaining 40% molecular gas), leaving the initial $O_2(^1\Delta)$, O_3 and $O(^1D)$ set equal to zero. (The remainder of the gas was O_2 ground state.) It was discovered that the halflife of the oxygen atoms did not vary at all with increased $O_2(^1\Sigma)$ input. Like $O(^1D)$, $O_2(^1\Sigma)$ is quenched in microseconds.

The ratio of $O_2(^1\Delta)$ to total O_2 was varied from 0-100% at 1, 5 and 10 torr and 60% dissociation, (see Figure 2.3). The $O_2(^1\Delta)$ was found to have a weak effect on oxygen atom lifetime. Generally $O_2(^1\Delta)$ is longer lived than oxygen atoms. The $O_2(^1\Delta)$ helps to create oxygen

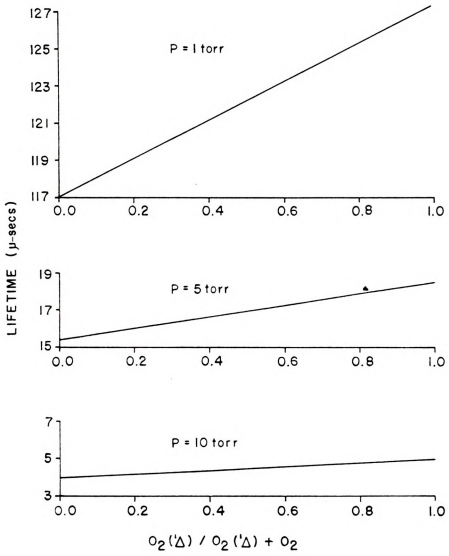

Figure 2.3 The oxygen atom halflife as a function of the input ratio of $O_2(^1\Delta)$ to total molecular oxygen.

atoms by reaction 11 ($O_2(^1\Delta) + O_3 = 2O_2 + O$). Ozone is produced as long as there is three body recombination by O + O_2 + M (reaction 17). However $O_2(^1\Delta)$ is gradually quenched by collisions with oxygen atoms and molecules (reaction 12-14) and with the wall, so it does not have a large effect on O atom lifetime.

The overall effect of excited states was studied by comparing this model to one that contained only reactions 1, 15, 16, 17, 18 and 19 (i.e. all reactions involving excited states in either products or reactants were removed.) When 100% dissociation is assumed (and zero initial excited state population) as much as a few percent of the initial oxygen atom concentration is turned into $O_2(^1\Delta)$. (Negligible amounts of $O(^1D)$ and $O_2(^1\Sigma)$ are also formed.) Generally, reactions 2 and 14 (recycling of O and $O_2(^1\Delta)$) are not important compared with three body recombination at the beginning of the run. In conclusion, the excited states (specifically $O_2(^1\Delta)$) do not affect the halflife of the oxygen atoms (when they are present in such small amounts) but they do affect the O atom concentration time history for times greater than the halflife, (see Figure 2.4). This is when reactions 2 and 14 become as important as three body and wall recombination. Since O atoms are abundant at the beginning of the run, small amounts of $O_2(^1\Delta)$ are produced by reaction 2. Also,

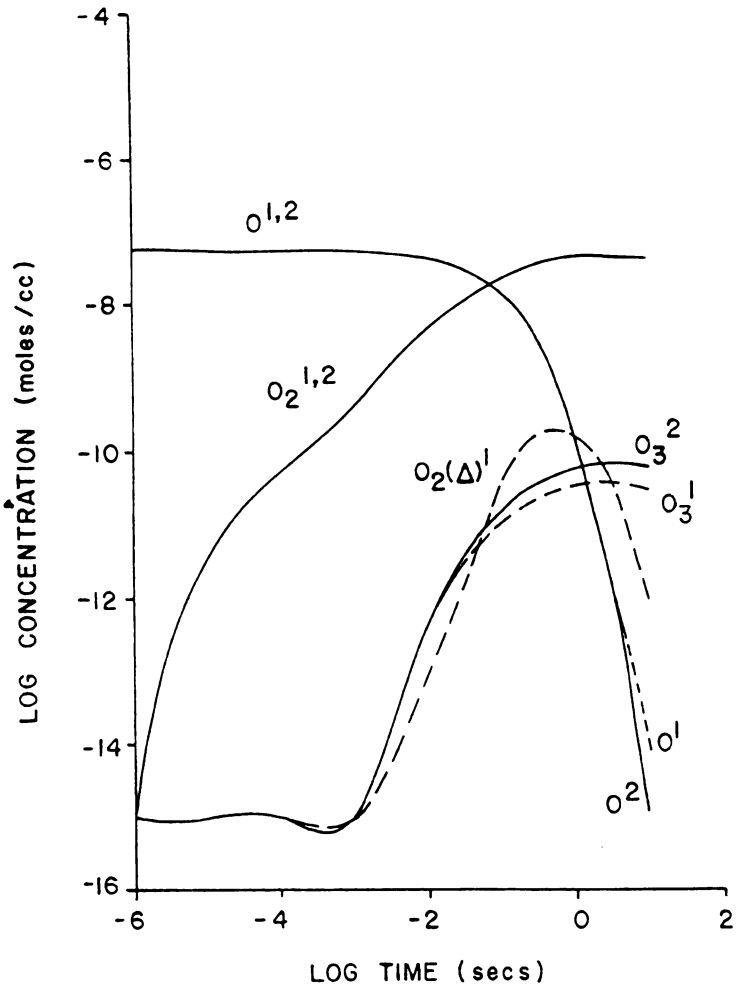

Figure 2.4 A comparison of two time histories at a pressure of 1 torr and 100% dissociation. 1) This model included both excited and ground state kinetics. 2) This model includes only ground state kinetics.

$O_2(^1\Delta)$ is more slowly quenched than O atoms recombine, therefore, reaction 11 will repopulate the O atom concentration near the end of the computer run (a few seconds) when the O atoms are otherwise consumed.

2.2.4 Effect of Ozone

The effect of ozone on oxygen atom lifetime was studied by adding ozone to a system consisting of only O atoms and varying the ratio of O_3/O (from 0-1) while keeping the pressure constant at 10 torr. As can be seen by Figure 2.5, the atomic lifetime is reduced by addition of ozone. This effect is dominated mainly by reactions 1 and 2 ($O + O_3$ = products). It is interesting to note that reaction 2 produces $O_2(^1\Delta)$ (as much as 10% of the original gas). Even though $O_2(^1\Delta)$ can enhance oxygen atom lifetime this effect cannot overcome reactions 1 and 2. Reaction 2 has such a large equilibrium constant and hence such a small backrate that it never runs in reverse.

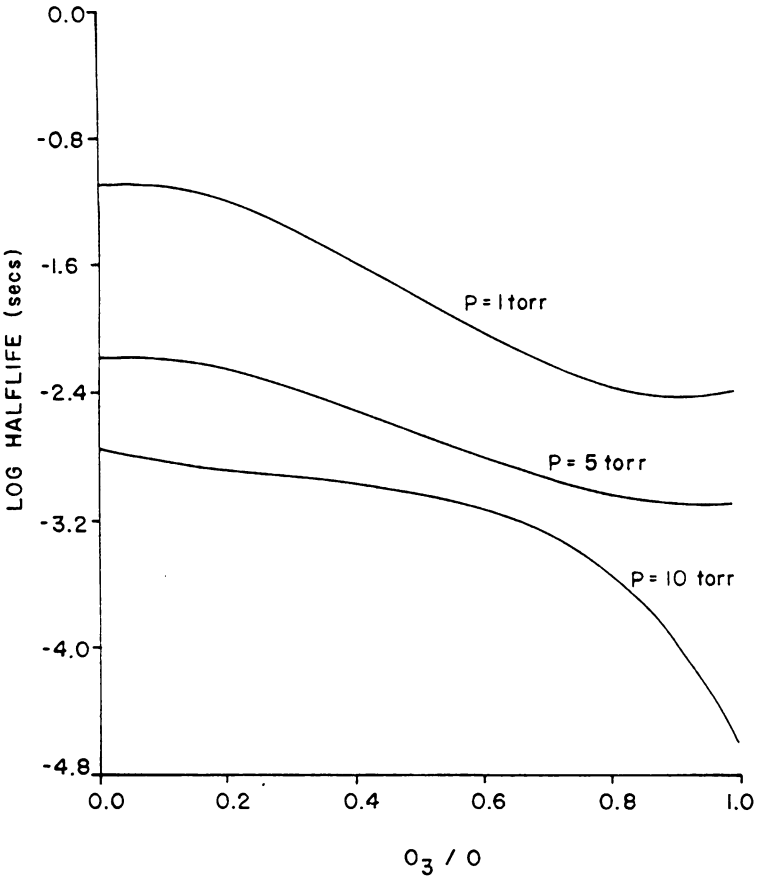

Figure 2.5 The effect of O_3/O on oxygen atom halflife. (All other initial concentrations were zero.)

2.2.5 Effect of Pressure

As expected, higher pressures cause oxygen atoms to recombine into molecules more rapidly. However the effect tends to level off near pressures of 1 torr and below (see Figure 2.6). The pressure study was used to examine the effects of radiative de-excitation and wall effects relative to collisional recombination and de-excitation. Since $O(^1D)$ is quenched fairly rapidly and since $O_2(^1\Sigma)$ is not produced to any great degree, there was very little radiative de-excitation in spite of their short radiative halflives. It was found that the radiative de-excitation of $O_2(^1\Delta)$ (to ground) was at least three orders of magnitude smaller than 2 body quenching (reaction 14) or wall quenching (reaction 22) for all pressures.

Wall recombination was found to be very important for low pressures (below 1.0 torr), about equal to three body recombination for intermediate pressures (10 torr), and not very important for high pressures (above 100 torr). Quenching of $O_2(^1\Delta)$ was about as important as 2 body quenching for low pressures and decreased in importance at higher pressures.

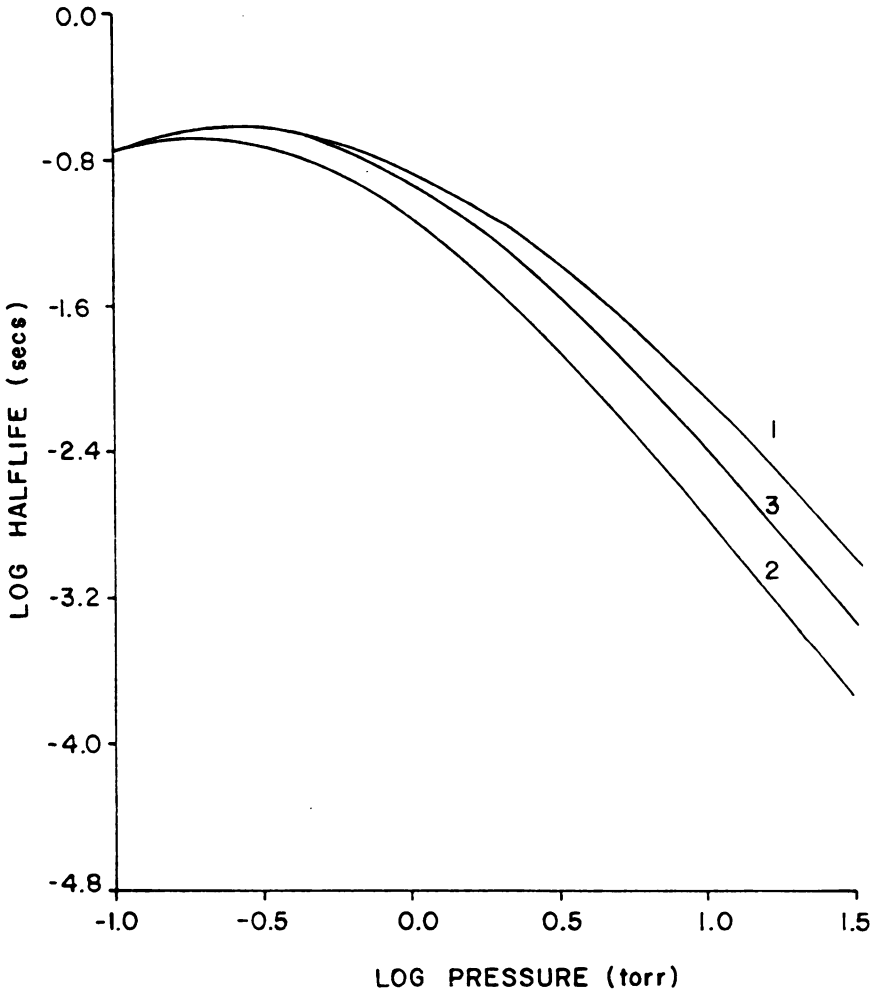

Figure 2.6 Effect of pressure on oxygen atom halflife. 1) The input ratio of $O:O_2$ was 1:10 with all other input concentrations equal to zero. 2) The input ratio of $O:O_2:O_2(^1\Delta)$ was 30:24:16. 3) 100% dissociation.

2.3 Summary and Conclusions

A kinetic model of an oxygen gas downstream of an electrical discharge and relevant rate-coefficient information found in the literature were presented. Rate coefficients recommended for this model are listed in Table 2.1. A computer simulation was used to examine the relative importance of various kinetic mechanisms involved in oxygen atom recombination. Calculations indicate that three body and wall recombination are important to O atom lifetime, but recombination is sensitive to other parameters as well. Low pressures, small O/O_2 ratios and $O_2(^1\Delta)$ were found to prolong the lifetime of O atoms. Ozone and high pressures were found to decrease O atom lifetime. Other higher excited states ($O_2(^1\Sigma)$ and $O(^1D)$) were found to have a negligible effect on O atom recombination.

CHAPTER III

OXYGEN KINETICS

3.1 Introduction to Literature Search

It was determined in Chapter II that two and three body reactions, as well as wall recombination, are important in determining the overall rate of oxygen atom recombination. Also it was determined that the only important electronic excited species is $O_2(^1\Delta)$. The first electronic state of atomic oxygen, $O(^1D)$, and $O_2(^1\Sigma)$, the second electronic state of molecular oxygen, were found to deactivate very quickly without significantly affecting the predictions of the kinetic simulation. Thus, the species included in the model of Chapter 5 are O, O_2, O_3 and $O_2(^1\Delta)$.

In simple models of electrical discharges of oxygen (e.g Bell and Kwong[9] and Mearns and Morris[10]) the kinetic rates are assumed to be constant and are evaluated at a temperature of 300 K. In general, these discharges are at much higher temperatures than 300 K and the temperature increases as the gas absorbs electromagnetic energy through inelastic and elastic collisions with electrons. Thus, it is important to know the temperature dependence of the

dominating mechanisms. The following review gives a summary of investigations that have determined kinetic rate constants either experimentally or theoretically for the important reactions involving oxygen under conditions of a typical experiment.

3.2 Two Body Reaction of Ozone and Oxygen

Many experimental studies have examined the temperature dependent rate constant of $O_3 + O_2 = 2O_2$ using flash photolysis or thermal decomposition of ozone. All experiments were performed near room temperature (200-400 K); however, in reviews by both Hampson[19] and Baulch[22], they recommend rate constants for use over a range of 200 K to 1000 K. As can be seen from Table 3.1, all of the rates are very close to being within experimental error of one another. The rate of Arnold and Comes[61] has been chosen as the recommended rate.

The product states of oxygen have not been well established. From an experimental study of thermal decomposition of ozone, Benson and Axworthy[62] note that reaction 1 (of Table 3.1) is exothermic by 93.2 kcal and the activation energy is 6.0 kcal. Therefore, there are 99.2 kcal of excess energy available to the products. If spin selection rules are obeyed in the collision of $O(^1P)$

Table 3.1 Temperature Dependent Rate Coefficients for Neutral Reactions of Oxygen

Reaction	Rate cc,mole,sec	Temperature Range	Reference
1. $O + O_3 \rightarrow O_2 + O_2$	$(2.96\pm0.21)\times10^{13}e^{(-3020/T)}$	340-384	62
	$(1.28\pm0.11)\times10^{13}e^{(-2337\pm26/T)}$	261-336	61
	$(2.4\pm0.5)\times10^{13}e^{(-2818\pm250/T)}$	780-910	69
	$1.2\times10^{13}e^{(-2410/T)}$	200-900	18
	$1.2\times10^{13}e^{(-2280/T)}$	200-900	22
	$1.14\times10^{13}e^{(-2300/T)}$	220-1000	19
	$(1.22\pm0.12)\times10^{13}e^{(-2276\pm105/T)}$	220-353	25
	$8.2\times10^{12}e^{(-2164\pm100/T)}$	300-523	28
reverse rate	$1.28\times10^{13}e^{(-50623/T)}$	200-900	18
2. $O + O_3 \rightarrow O_2 + O_2^*$	see text		
3. $O_2(^1\Delta) + O_3 \rightarrow 2O_2 + O$	$3.6\times10^{13}e^{(-2853/T)}$	296-360	43
	$2.7\times10^{13}e^{(-2828\pm180/T)}$	283-321	45
	$(4.0\pm1.5)\times10^{11}e^{(1560/T)}$	195-439	50
4.-5. $O_2(^1\Delta) + M \rightarrow O_2 + M$			
$M=O_2$	$1.3\times10^{6}(T/300)^{0.8}$	285-322	19
$M=O$	7.8×10^{7}	297	24
$M=N_2$	$(1.7\pm1.2)\times10^{9}$	297	24
$M=O_2$	$(1.3\pm0.05)\times10\ (T/300)^{0.78\pm0.32}$	285-322	45

Table 3.1 continued

Reaction		Rate cc, mole, sec	Temperature Range	Reference
6.-7. $O + O + M \rightarrow O_2 + M$				
$M=O_2$	k_f	$1.38\times10^{18} T^{-1} e^{(-171/T)}$	1000-8000	18
	k_r	$2.75\times10^{19} T^{-1} e^{(-59700/T)}$		
	$k_f(O_2)/k_f(Ar) = 10.8$			
M=Ar	k_r	$1.79\times10^{18} T^{-1} e^{(-59700/T)}$	3300-7500	53
M=O	k_r	$1.6\times10^{23} T^{-2} e^{(-59700/T)}$ $\pm$ 50%		
$M=O_2$	$k_r(O_2) = 2*k_r(Ar)$			
$M=O_2$	k_f	$1.6\times10^{18} T^{-1}$	3000-6000	54
M=O	k_f	$4.8\times10^{18} T^{-1}$		
M=Ar	k_f	$2.5\times10^{16} T^{-0.5}$	5000-180000	56
	$k_f(O) = 25*k_f(Ar)$			
	$k_f(O_2) = 9*k_f(Ar)$			
$M=O_2$	k_f	$(2.5\pm0.5)\times10^{17} T^{-1}$	2000-4000	55
$M=O_2$	k_r	$1.08\times10^{25} T^{-2.5} e^{(-59380/T)}$	3000-5000	73
	k_f	$1.03\times10^{22} T^{-2}$		

Table 3.1 continued

Reaction	Rate cc,mole,sec		Temperature Range	Reference
8.-9. $O + O_2 + M \rightarrow O_3 + M$				
$M=N_2$	k_f	$(9.4\pm1.0)\times10^{12}e^{(855\pm150/T)}$	680-860	69
	k_r	$(5.8\pm0.6)\times10^{14}e^{(-11650\pm150/T)}$		
$M=O_3$	k_f	$2.57\times10^{14}e^{(160/T)}$	70-130	63
	k_r	$1.6\times10^{16}e^{(-12150/T)}$		
$M=O_3$	k_f	$(6.0\pm0.33)\times10^{13}e^{(300/T)}$	333-380	62
	k_r	$(4.6\pm0.25)\times10^{15}e^{(-12077/T)}$		
	$k_r(O_3:O_2:N_2:He) = k_r(O_3)(1.0:0.44:0.41:0.34)$			
$M=O_2$	k_r	$2.96\times10^{13}e^{(447/T)}$		
$M=Ar$	k_f	$8.9\times10^{12}e^{(906\pm200/T)}$	180-373	26
	k_f	$3.3\times10^{12}e^{(1157/T)}$	180-1000	71
$M=Ar$	k_f	$(2.3\pm0.6)\times10^{13}e^{(525\pm70/T)}$	250-333	61
$M=O_2$	k_f	$(2.4\pm0.2)\times10^{13}e^{(635\pm18/T)}$		
$M=N_2$	k_f	$(6.6+0.8)\times10^{12}e^{(995\pm37/T)}$		
$M=Ar$	k_f	$1.3\times10^{14}(T/300)^{-1.93}$	200-1100	22
$M=N_2$	k_f	$2.0\times10^{14}(T/300)^{-2.23}$		
$M=O_3$	k_r	$9.9\times10^{14}e^{(-11400/T)}$		18
	k_f	$1.7\times10^{13}e^{(1060/T)}$		

Table 3.1 continued

Reaction	Probability for Reaction (γ)	Temperature Range	Reference
10. $O \xrightarrow{wall} \frac{1}{2}O_2$	1.2×10^{-4} $\pm 50\%$	297	66
	1.6×10^{-4}	297	65
	$(4.0-8.0) \times 10^{-5}$	297	64
	10^{-4}	297	75
11. $O_2(^1\Delta) \xrightarrow{wall} O_2$	2×10^{-5}	297	67

and a singlet ozone, then one of the product oxygen molecules must be in a triplet state. This implies that there is at most one electronically excited molecule (either $O_2(^1\Delta)$ at 22.5 kcal or $O_2(^1\Sigma)$ at 37.5 kcal). Consequently , Benson concluded that it is possible for one of the products to be in an electronically excited state with energy left over for vibrational and rotational excitation.

Jones and Davidson[69] have thermally decomposed ozone and observed vibrationally excited O_2 molecules from absorption spectra. They asssume the mechanism to be $O + O_3 = O_2(\text{excited}) + O_2$. (These were vibrationally excited ground state (electronic) molecules with vibration quantum number of v=10-16 with an average maximum intensity at v=13.) Jones and Davidson did not observe the vibrational spectra when all of the ozone was depleted (indicating that three body recombination is not responsible for producing the vibrationally excited states). Jones and Davidson did not discuss the possibility of electronically excited O_2 as a potential product.

Bader and Ogryzlo[70] looked at the production of $O_2(^1\Delta)$ and $O_2(^1\Sigma)$ by examining the emission spectrum of a 2.45 GHz discharge. The absence of particular vibrational bands indicates that they have very little vibrationally excited oxygen. They also concluded that emission due to

$O_2(^1\Sigma)$ is due to dimolecular complexes of $O_2(^1\Delta)$ rather than production by $O + O_3$, although they don't completely rule out electrically excited products of $O + O_3$. Their concentration of $O_2(^1\Delta)$ emission was low and they did not consider $O + O_3 = O_2(^1\Delta) + O_2(^3\Sigma)$

Clark, Jones and Wayne[24] measured the rate of reaction 1 under conditions where $O_2(^1\Delta)$ regeneration is unimportant and found that this matches other experiments that did have the possibility of $O_2(^1\Delta)$ regeneration. This, along with the results of quantum yield measurements, prompted Clark et al. to conclude that both oxygen molecules produced are in the electronic ground state.

3.3 Singlet Delta and Ozone

Findley and Snelling[45], in flash photolysis of O_3, and Becker[43], in a microwave discharge, obtained the same temperature dependent rate constant (within experimental error) for $O_2(^1\Delta) + O_3 = 2O_2 + O$ over a temperature range of 280-360 K. Clark, Jones and Wayne[24], have also measured this rate constant using a radio frequency discharge. They report a positive activation energy, even though they report that their rate increased with temperature. (Their reaction rate fits their data only if a negative activation energy is assumed.) If a sign error is assumed, their rate

constant still does not compare well with the other two reported rates. The rate of Findley or Becker is recommended.

3.4 Collisional Deactivation of Singlet Delta

Findley and Snelling[45] have examined the collisional deactivation of $O_2(^1\Delta)$ using uv photolysis of benzene-oxygen mixtures. They obtain a temperature dependent rate for collisional deactivation by O_2 (as well as other collisional partners). The effect of O or O_3 as collisional partners is not considered, since they assume that neither oxygen atoms nor ozone are produced in their system. Clark and Wayne[50], in a radio frequency discharge, determined an upper limit for the rate constant for collisional deactivation by O atoms at 297 K. They found that N atoms are more efficient than O atoms and that the N atom deactivation rate is not strongly temperature dependent. Since there is a lack of information on the temperature dependence of the O atom deactivation rate constant, the $T^{0.78}$ dependence found by Findley and Snelling for O_2 is recommended. Since reaction 3 has a much larger rate constant than reactions 4 or 5 it is assumed that deactivation of $O_2(^1\Delta)$ by O_3 is small in comparison with reaction 3.

Heidner and Gardner[67] included the possibility of deactivation of $O_2(^1\Delta)$ by collision with the wall in their studies of the kinetics of $O_2(^1\Delta)$ and iodine. Their value for a probability of deactivation is 2×10^{-5} as noted in Table 3.1.

3.5 Oxygen Atom Recombination

Recombination rates of oxygen atoms have generally been deduced from dissociation rates in shock tube studies at very high temperatures. The rate of recombination is found through relation (2.2) i.e. K_{eq} is equal to k_f divided by k_b, and the products and reactants are assumed to be in vibrational and rotational equilibrium. To check the validity of this assumption, Johnston[18] made a comparison of calculated recombination rates to measured recombination rates and concluded that $K_{eq}=k_f/k_b$ is satisfied.

In the recombination of oxygen atoms, there exists the possibility of producing electronically excited states of molecular oxygen. Clyne[71] concluded that neither O atoms nor H atoms recombine into electronically excited states with "allowed" transitions to the ground state of O_2 and H_2. In a review of singlet molecular oxygen, R. Wayne[72] commented that recombination does not significantly

contribute to $O_2(^1\Delta)$ (recall however that $O_2(^1\Delta)$ is difficult to detect).

In a shock tube study of Xe-O_2 mixtures by Rink and co-workers[54], rate determinations were made by comparing calculated density profiles with those obtained experimentally. Even though the rates were measured over a range of 3000 K-6000 K, they were unable to determine an exact temperature dependence of the recombination rate. They determined the limits on the exponent of the temperature dependence to be between -1/2 and -2, so they arbitrarily chose $T^{-1.0}$. (See Table 3.1)

Camac and Vaughan[53] used a uv light absorption technique to measure the O_2 dissociation rate in an O_2- Ar mixture by fitting data to the theoretical form of

$$C(D/RT)^{n-1/2} e^{(-D/RT)} \qquad (3.1)$$

where C, D and n are the parameters to be fit. For a temperature range of 3300 to 7500 K, with O_2 as the third body, they found that $C=6.0\times10^{-12}$ ($\pm$ 20%) cc/mole-sec^2 , D = 5.116 eV and n=1.5 $\pm$ 0.2. For O_2-O collisions, the best fit to the dissociation rate formula gives n=2.5 and $C=1.8\times10^{14}$ (with as much as 50% uncertainty). This was found by neglecting O_2- O_2 collisions. These values for C, D and n put an upper limit on the O_2-O collision rate of about $2k(Ar\text{-}O_2)$.) In addition, they found significant

coupling among the vibrational relaxation and dissociation processes above 8000 K where the relaxation rates for these reactions are comparable. This coupling could cause at least a factor of 2 decrease from the expected dissociation rate at the higher temperatures where vibrational equilibrium is not achieved.

Matthews[73] in another shock tube study (3000-5000 K), fits his data to the form

$$k_b = 5.2 \times 10^{10} T^{1/2} (59380/T)^3 e^{(-59380/T)} \qquad (3.2)$$

Matthews calculates the recombination rate to be $1.03 \times 10^{22} T^{-1/2}$.

Wray[56] has also determined the rate of dissociation in a shock tube study to be $k_b = 2.9 \times 10^{14} e^{(-59380/T)}$ with 20% uncertainty for M = Ar. He was able to determine the relative rates for Ar, O_2 and O as the third body: $k(Ar) = 1/9\ k(O_2) = 1/25\ k(O)$ for $T < 7700$ K. Wray also found that the time constant for dissociation was 60 times the time constant for vibrational relaxation at 5000 K but was only 1.4 times greater at 18000 K.

The recommended rate constants given in a review by Johnston[18] for the temperature range of 1000-8000 K are listed in Table 3.1. Below 1000 K, the experimental data lies below the extrapolated curve of data taken at higher

temperatures. (This may be due to the fact that data taken at room temperature is heavily corrected for the "ozone mechanism" of $O_3 + O = 2O_2$). Johnson does not recommend a rate for M=O, but he does recommend $k(O_2) = 10.8\ k(Ar)$.

Several recombination rates are plotted as a function of temperature in Figure 3.1. Although some of the rates were calculated and not measured directly and the temperature dependence is not well known, they are within an order of magnitude of one another for the temperature range of 1000-2000 K. The rates of Wray[56] and Matthews[73] are particularly close in this region. A discussion of the most probable rate is made in Chapter VI.

3.6 Ozone Formation

The formation of ozone from recombination of an oxygen atom and an oxygen molecule has been investigated by the thermal decomposition of ozone in a variety of experiments. Zaslowsky et al.[63] have measured the rate of decomposition of ozone over a temperature range of 115-130 K assuming M = O_3 for large concentrations of ozone. (See Table 3.1.) They determined an equilibrium constant and obtain a forward rate coefficient.

Benson and Axworthy[62] in a similar experiment measured the decomposition of ozone using M = O_3 and found

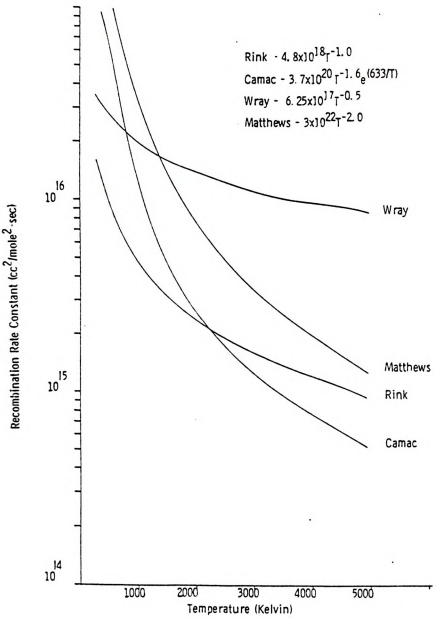

Figure 3.1 Recombination rate constant as a function of temperature as suggested by various studies.

relative efficiencies for M = O_3 to M = O_2 and M = N_2 of 1.0:0.44:0.41. They also determined an equilibrium constant and a forward rate constant that is in good agreement with Zaslowsky.[63] In a more recent paper[26], they corrected their value of $k_f(O_2)$ to be $2.96 \times 10^{13} e^{(447/T)}$ to allow for new thermodynamic values.

In a shock tube study, Jones and Davidson[69] measured the decomposition of ozone in Ar and N_2 at higher temperatures than the previous experiments (680-860 K). Based upon results of their experiment, they concur that Benson's relative efficiency O_2:N_2 of 1:0.41 is correct.

The formation of ozone was also studied by Clyne et al.[74] by decomposition of O_2 in Ar by means of a radio frequency discharge between 180 and 373 K. They have incorporated the data of Jones and Davidson and calculated a forward rate of $3.3 \times 10^{2} e^{(1157/T)}$ valid from 180 K to 1000 K.

In the flash photolysis of ozone, Arnold and Comes[61] obtained dissociation rates for collisions with Ar, O_2 and N_2. (See Table 3.1.)

In literature reviews of the dissociation rate, Baulch et al.[22] and Johnston[18] recommend rates for a range of 200-1000 K.

All reported rate coefficients have similar temperature behavior, and the rate becomes constant at

temperatures greater than 1000 K (Figure 3.2). Johnston indicates that there is as much as 50% uncertainty in the measured rate constants.

3.7 Wall Recombination

The recombination of oxygen atoms on the walls of a glass tube has been examined in several studies[64-66,75]. Linnett and Marsden[66] produced oxygen atoms in AC and DC discharges. They found that the recombination coefficient γ varied very slightly with wall temperature. From 293 K to 673 K γ varied from $1x10^{-4}$ to $4x10^{-4}$ with γ = $1.2x10^{-4}$ ($\pm$ 50%) at room temperature. They concluded that wall recombination is a first order process and that a small addition of water vapor did not affect the wall recombination coefficient.

In a later study, Greaves and Linnett[65] produced O atoms in a microwave discharge and found that γ varied strongly with temperature; γ ranged from $1.6x10^{-4}$ to $1.4x10^{-2}$ for a temperature range of 293 to 873 K with the largest increase occurring for temperatures greater than 500 K. They tried unsuccessfully to fit the temperature data to an Arrhenius form of $\gamma = \gamma_o e^{(-E/kT)}$. They conclude that wall recombination is a first order process and speculate that the silica wall either absorbs an atom or

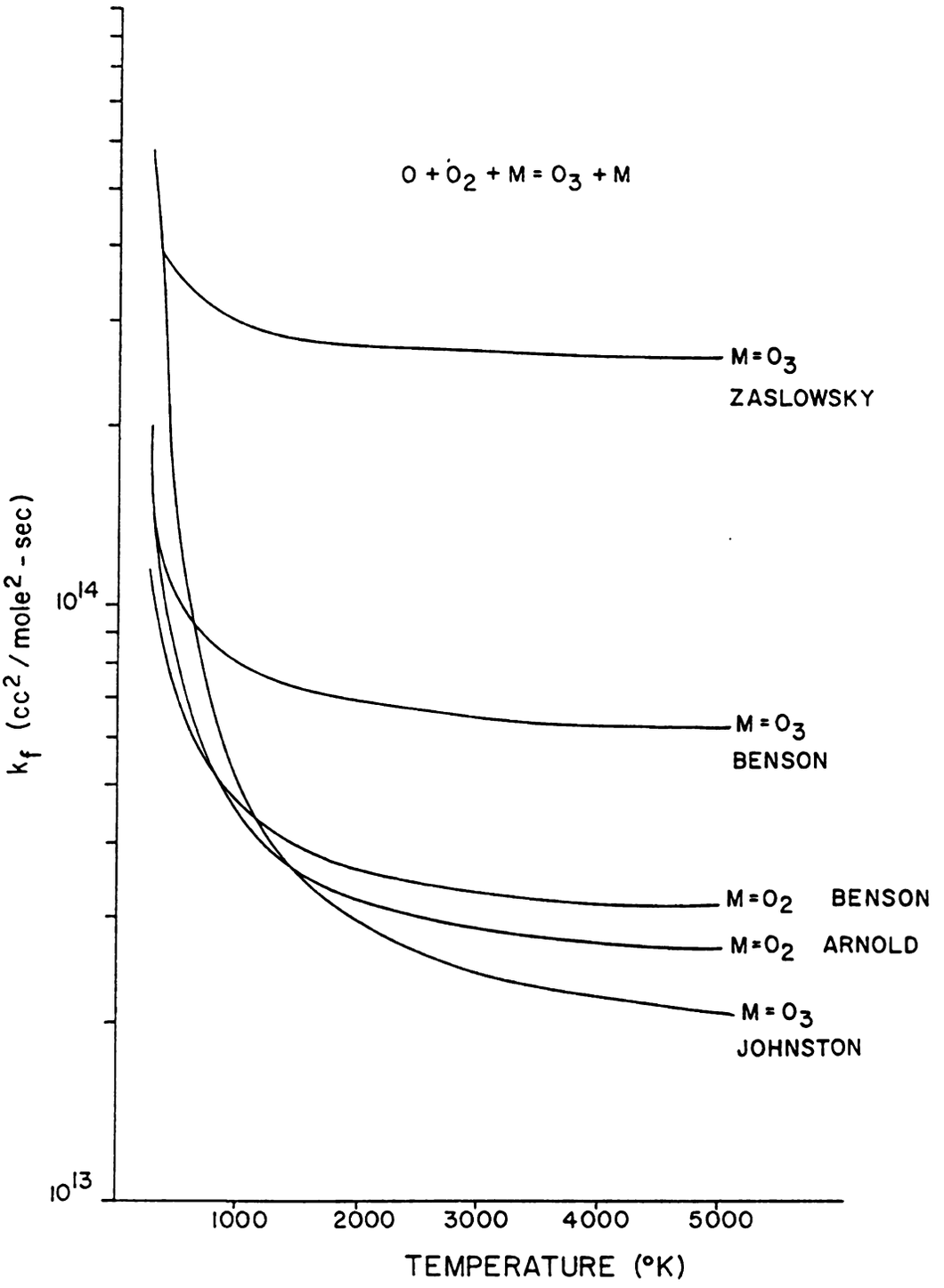

Figure 3.2 The formation rate of ozone as a function of temperature for $M = O_2$ and $M = O_3$ as suggested by the indicated investigators.

else releases an atom from a previously absorbed water molecule.

Williams and Mulcahy[64] measured γ by producing O atoms in a microwave discharge and determining the O atom concentration through titration with NO_2. They found γ = $4\text{-}8\text{x}10^{-5}$ for quartz at room temperature. This is 2-3 times smaller than previous measurements. They determined γ by measuring an overall rate of recombination and then subtracting the rate of three body recombination of O with O_2. (The other two studies[65,66] measured surface recombination at the wall only and not overall recombination. This difference in measurement technique could explain the difference in γ's.)

In a recent paper, Black and Slanger[75] concluded that between 18-36% of the atoms recombined produced O_2 in the first electronically excited state. They also find that the fraction of atoms recombined is consistent with a surface recombination coefficient γ of 10^{-4} for pyrex.

CHAPTER IV

MODEL FORMULATION

4.1 Model Assumptions

The goal of this chapter is to formulate a model that will predict the degree of dissociation and recombination of O_2 as a function of position in a flowtube after the gas has exited a discharge. This model is formulated to compare with results of a microwave discharge experiment,[76] therefore certain assumptions pertinent to that experiment are made. Experimental measurements were made downstream of the microwave cavity, so this model examines the gas after it has exited the discharge. In this region it is assumed that there are no electromagnetic forces and that neutral chemical kinetics dominate. Ion kinetics which could dominate in the reactor cavity are neglected. It is also assumed that the axial dependence of the properties measured are much more important than the radial dependence, so a one dimensional model is used. The gas is assumed to be contained in a constant area quartz tube under conditions where all wall effects such as friction and shear stress are negligible. Atom recombination on the wall however is significant and is included. The density, temperature, and velocity are

allowed to vary as a function of distance from the discharge. Conservation of mass, momentum, and energy and chemical kinetic mechanisms are used to establish differential equations necessary to solve for species concentrations, temperature, and velocity.

4.2 Conservation Equations

The conservation equations of a flowing, chemically reacting system are well known.[3, 77-79] If it is asssumed that all chemical species have the same average velocity v (because diffusion is small), and the same translational temperature T, the conservation of mass, momentum, and energy can be written as follows:

$$\frac{\partial \rho}{\partial t} + \frac{\partial (\rho v_i)}{\partial x_i} = 0 \qquad (4.1)$$

$$\frac{\partial (\rho v_i)}{\partial t} + \frac{\rho \partial (v_i v_j)}{\partial x_j} = - \frac{\partial P}{\partial x_i} + \frac{\partial \tau_{ij}}{\partial x_j} + F_i \qquad (4.2)$$

$$\frac{\partial(\rho e + 1/2\rho v^2)}{\partial t} + \frac{\partial(\rho v_j (H+1/2v^2))}{\partial x_j} = \frac{\partial(\tau_{ik} v_k)}{\partial x_j} + F_j v_j \quad (4.3)$$

where ρ is the density, x is the distance from the exit of the discharge, P is the pressure, τ is the shear stress, F is an external force, e is the internal energy, and H is the enthalpy. With the assumptions mentioned above and the steady state nature of the flow tube, the equations reduce to the following.

$$\frac{d(\rho v)}{dx} = 0 \qquad \text{Conservation of Mass} \quad (4.4)$$

$$\frac{d(\rho v^2)}{dx} = -\frac{dP}{dx} \qquad \text{Conservation of Momentum} \quad (4.5)$$

$$\frac{d(\rho v(H + 1/2v^2))}{dx} = 0 \qquad \text{Conservation of Energy} \quad (4.6)$$

Each equation can be manipulated into a form that can be used in the computer model.

4.2.1 Conservation of Mass

For conservation of mass, we have

$$\frac{d(\rho v)}{dx} = \sum_i \frac{d(M_i n_i v)}{dx} \qquad (4.7)$$

n_i is the concentration of each species in the gas, and M is the molecular weight of each species. The continuity equation for each species including the chemical generation term gives

$$v\frac{dn_i}{dx} = G_i - n_i\frac{dv}{dx} \qquad (4.8)$$

For example, for the reaction $O + O + M = O_2 + M$, $G_{O_2} = k_f[O^2][M] - k_b[O_2][M]$ where k_f is the forward rate constant and k_b is the backward rate constant, and $G_{O_2} = -2\,G_O$.

4.2.2 Conservation of Momentum

For conservation of momentum, we have

$$\frac{d(\rho v^2)}{dx} = (\rho v)\frac{dv}{dx} + v\frac{d(\rho v)}{dx} \qquad (4.9)$$

where $\frac{d(\rho v)}{dx} = 0$ from the continuity equation,

$$\rho v \frac{dv}{dx} = -\frac{dP}{dx} \qquad (4.10)$$

Now since $P = \sum_i n_i R'T$ where R' is the universal gas constant we have,

$$\rho v \frac{dv}{dx} = -\sum_i \frac{d(n_i R'T)}{dx} \qquad (4.11)$$

$$\rho v \frac{dv}{dx} = -R'T \sum_i \frac{dn_i}{dx} - \sum_i n_i R' \frac{dT}{dx} \qquad (4.12)$$

4.1.3 Conservation of Energy

For conservation of energy, we have

$$\frac{d(\rho v H + 1/2\, v^3)}{dx} = 0 \qquad (4.6)$$

but from the definition of H, $H = \sum_i n_i H_i$

$$\frac{d\left(\sum_i n_i H_i v + 1/2\rho v^3\right)}{dx} = 0 \qquad (4.13)$$

$$\frac{d\left(\sum_i n_i H_i v\right)}{dx} + 1/2\,\frac{d(\rho v)v^2}{dx} \qquad (4.14)$$

$$\text{but} \quad \frac{d\left(\sum_i n_i H_i v\right)}{dx} = \sum_i H_i \frac{d(n_i v)}{dx} + \sum_i n_i v \frac{dH_i}{dx} \qquad (4.15)$$

from the definition of $C_{pi} = \frac{dH_i}{dT}$, $\frac{dH_i}{dx}$ can be written as

$$\frac{dH_i}{dx} = \frac{dH_i}{dT}\frac{dT}{dx} = C_{pi}\frac{dT}{dx} \qquad (4.16)$$

and since $\frac{d(n_i v)}{dx} = G_i$ from the continuity equation,

$$\frac{d\left(\sum_i n_i H_i v\right)}{dx} = \sum_i H_i G_i + \sum_i n_i C_{pi} v \frac{dT}{dx} \qquad (4.17)$$

The second term in equation (4.6) can be written as

$$\frac{1}{2}\frac{d(\rho v)v^2}{dx} = \frac{v^2}{2}\frac{d(\rho v)}{dx} + \rho v\frac{dv}{dx} \qquad (4.18)$$

Since $\frac{d(\rho v)}{dx} = 0$ from the continuity equation

$$\frac{1}{2}\frac{d(\rho v)v^2}{dx} = \rho v^2\frac{dv}{dx} \qquad (4.19)$$

Now the energy equation becomes

$$\sum_i n_i C_{pi} v\frac{dT}{dx} + \sum_i \dot{H}_i G_i + \rho v^2\frac{dv}{dx} = 0 \qquad (4.20)$$

$$\sum_i n_i C_{pi}\frac{dT}{dx} + \sum_i H_i G_i\frac{1}{v} + \rho v\frac{dv}{dx} = 0 \qquad (4.21)$$

4.3 Differential Equations

For this particular model, four chemical species were included; O, O_2, and O_3 and $O_2(^1\Delta)$. The three conservation equations become six ordinary differential equations.

$$v\frac{d[O]}{dx} = G_O - [O]\frac{dv}{dx} \tag{4.22}$$

$$v\frac{d[O_2]}{dx} = G_{O_2} - [O_2]\frac{dv}{dx} \tag{4.23}$$

$$v\frac{d[O_3]}{dx} = G_{O_3} - [O_3]\frac{dv}{dx} \tag{4.24}$$

$$v\frac{d[O_2(^1\Delta)]}{dx} = G_{O_2(^1\Delta)} - [O_2(^1\Delta)]\frac{dv}{dx} \tag{4.25}$$

$$v\frac{dv}{dx} = -R'T\left(\frac{d[O]}{dx} + \frac{d[O_2]}{dx} + \frac{d[O_3]}{dx} + \frac{d[O_2(^1\Delta)]}{dx}\right) - \left([O] + [O_2] + [O_3] + [O_2(^1\Delta)]\right)R'\frac{dT}{dx} \tag{4.26}$$

$$0 = \frac{dT}{dx}\left([O]C_{pO} + [O_2]C_{pO_2} + [O_3]C_{pO_3} + [O_2(^1\Delta)]C_{pO_2(^1\Delta)}\right) + \frac{1}{v}\left(H_O G_O + H_{O_2} G_{O_2} + H_{O_3} G_{O_3} + H_{O_2(^1\Delta)} G_{O_2(^1\Delta)}\right) + v\frac{dv}{dx} \tag{4.27}$$

Note the coupling of the four species and the temperature and velocity derivatives. This system of differential equations is solved using Hindemarsh's routine LSODI[80] given initial conditions (i.e conditions at the

exit of the discharge). The initial conditions for comparison with the experiment were determined as follows; the initial velocity is determined from the measured flow velocity and the degree of dissociation. The initial temperature must be independently selected, since it was not measured. Note that the concentration derivatives were fifteen orders of magnitude or more smaller than the temperature and velocity derivatives. Therefore, under conditions typical of this experiment, it was necessary to use double precision on the Cyber 750. The initial species concentrations are determined from the titration measurements of oxygen atom concentration.

CHAPTER V

EXPERIMENTAL APPARATUS

5.1 Reactor Flow System

The microwave plasma flow system is shown in Figure 5.1 and discussed in detail in Reference 76. The plasma was contained in a 1.79 cm I.D. quartz tube coaxial with a cylindrical microwave cavity. The gas control system consisted of a high purity oxygen source (99.993%), a back pressure regulator, a back pressure monitor, a flowmeter, and a bellows metering valve. A constant back pressure of 1400 torr was maintained up to the metering valve. Downstream of the metering valve, oxygen entered the microwave cavity through a quartz containment tube which was coupled to a 58 CFM vacuum pump through a 5.1 cm I.D. pyrex suction line. Plasma pressure was monitored by a McLeod gauge located at the quartz to pyrex transition section. Discharges with molecular flowrates of 0.4 to 4.0 ml/sec and pressures of 8-16 torr were investigated. The flowmeter was calibrated for oxygen flow at atmospheric pressure, hence the densities given for these flowrates are the densities at atmospheric pressure.

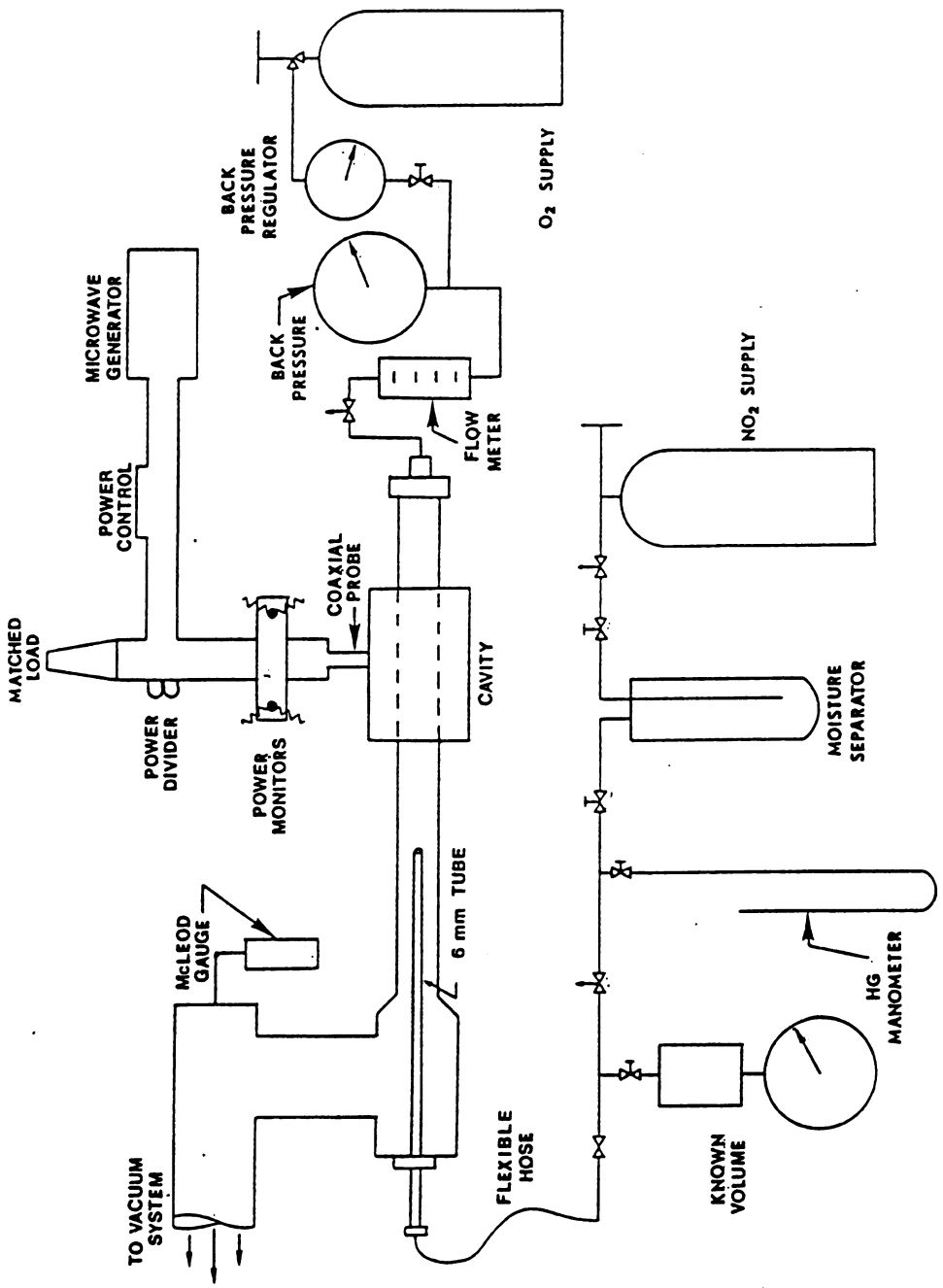

Figure 5.1 Experimental Apparatus

5.2 Plasma Cavity and Microwave System

A 2.44 GHz magnetron oscillator capable of delivering 1000 watts of continuous power was used as a microwave power source. The power was delivered through a water attenuator which allowed the power to be continuously varied from 200 to 800 watts. The magnetron was protected from reflected power by a circulator and a matched load.

The microwaves entered the reactor cavity through a directional coupler so that incident and reflected power could be monitored simultaneously. The power absorbed by the plasma was taken to be the incident power minus the reflected power. (Typically the reflected power was less than 5% of the incident power.) It was assumed that there was no drop in power between the power meters and the coaxial probe.

Power was coupled to the cylindrical water cooled cavity by an adjustable coaxial probe. The cavity had an I.D. of 17.8 cm and the length could be varied from 6-16 cm with a sliding short. A more detailed description has been given previously[7,81]. The cavity operates on a number of different modes depending upon cavity length, gas pressure and probe position. The cavity length and probe position were varied until maximum incident power and minimum reflected power were obtained. The optimal

conditions were found to be a cavity length of 9.3 cm and a probe depth of 7.6 cm from the cavity wall.

5.3 Nitrogen Dioxide Titration System

The nitrogen dioxide flow system consisted of a NO_2 supply cylinder, a liquid vapor separator maintained at constant temperature and pressure, a mercury manometer, a fine metering valve and a 6 mm outer diameter glass tube. This glass tube was positioned down the center of the discharge flow tube and had 43 centimeters travel towards or away from the plasma. The tip of the glass titration tube was rounded off, sealed, and eight pinholes were drilled 3 mm from the tube end (see Figure 5.2). These holes formed a ring in a single cross sectional plane so that the NO_2 met the oxygen in a cross flow pattern. This "maximized reagent mixing" and "provided titration analysis at any cross sectional plane downstream of the oxygen plasma discharge".[76] It was possible to determine the atom concentration at any point downstream of the discharge, including the exit plane of the reactor cavity. In other systems (e.g. Bell[9] or Mearns[10]) the number of oxygen atoms produced at the exit plane was determined by extrapolating data taken at one or two fixed spots downstream of the exit plane. Thus, this variable probe method of introducing NO_2 into the system was a big

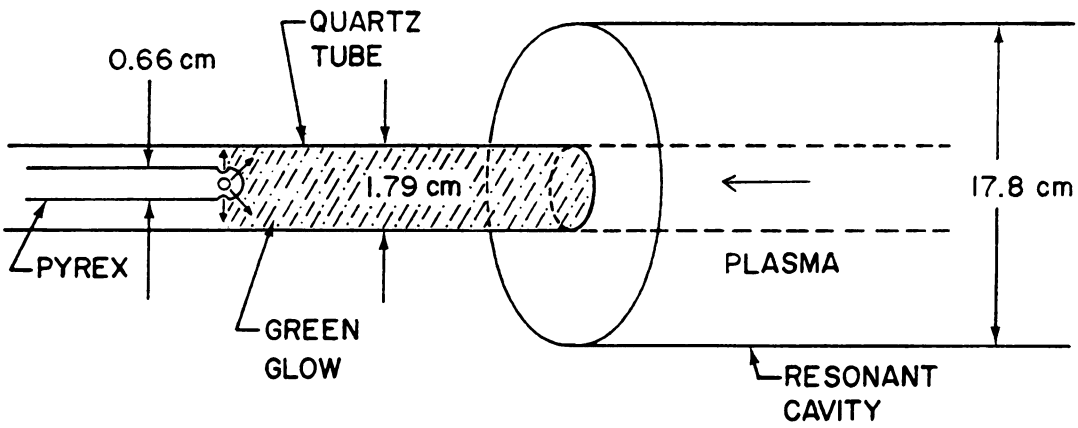

Figure 5.2 Nitrogen dioxide titration technique.

improvement over previous methods.

5.4 Titration Technique

The oxygen atom titration process is based upon the following reactions:

$$O + NO_2 = NO + O_2 \qquad (5.1)$$

with a forward rate coefficient[82] at 300 K of 3.3×10^{12} cc/mole-sec and

$$O + NO = NO_2 + h\nu \qquad (5.2)$$

with a forward rate coefficient[83] at 300 K of 1.5×10^{7} cc/mole-sec. In reaction 5.1, free oxygen atoms exiting the plasma are scavenged by NO_2 (see Figure 5.2) to produce nitric oxide and oxygen molecules. This reaction is very fast compared to reaction 5.2. If the initial free oxygen atom production exceeds the rate at which NO_2 is being introduced, then reaction 5.2 follows, producing green light which fills the whole flow system outside of the discharge. When the NO_2 is introduced at a rate equal to or exceeding the free oxygen atom production rate, the green glow downstream of the port is extinguished and the upstream green glow is highly localized. "When titrating in a darkened room, increasing the NO_2 flowrate

causes the glow to progress upstream, approaching the point of NO_2 introduction. This glow becomes sharper and more distinct until it appears to be a truncated cylinder" (see Figure 5.2).[76] At this point, the NO_2 flowrate exactly equals the oxygen atom flowrate and reaction 5.2 does not occur. Thus, by knowing the NO_2 flowrate, the oxygen atom flowrate can be inferred. The movable titration probe provides O atom determination at any cross section downstream of the discharge. (The accuracy of titration is discussed in Appendix C.)

The NO_2 was fed through a fine metering valve with the NO_2 source maintained in a constant temperature bath (300 K) in a liquid-vapor equilibrium. The back pressure of NO_2 was therefore 800 torr. Only vapor entered the titration line because the downstream pressure was never more than 16 torr which is well below the vapor-liquid point at 300 K and the liquid-vapor equilibrium vessel was 10 meters away from the titration experiment. No liquid was ever observed at the titration tip or at any point in the titration line. Due to the corrosive nature of NO_2, the titration endpoint flowrate was determined by directing the same gas flowrate into a known volume and monitoring the change in pressure as a function of time. This provided a molar flowrate which was one to one with the oxygen atom production rate.

The mass flowrate of NO_2, measured as a pressure increase ($\dot{P}_{NO_2}$) in a known volume (V_{NO_2}) can be related to the oxygen atom flowrate through the following relation:

$$\frac{\dot{P}_{NO_2} V_{NO_2}}{kT_{NO_2}} = \text{flowrate } NO_2 = \text{flowrate } O \qquad (5.3)$$

where T_{NO_2} is the temperature of NO_2 (300 K) and $\dot{P}_{NO_2}$ = dP/dt. The oxygen atom concentration can also be determined from $\dot{P}_{NO_2}$ by

$$[O] = \Omega \dot{P}_{NO_2} \qquad (5.4)$$

where $\Omega = V_{NO_2} / kT_{NO_2} vA$ if v (the linear velocity) is known. (A is the cross sectional area of the flowtube.) The percent of O_2 molecules converted to O atoms at any particular cross section can be calculated as one half the flowrate of O atoms divided by the initial O_2 flowrate. (This ratio is denoted as percent conversion throughout the text. Figures 5.3-5.5 show typical data.)

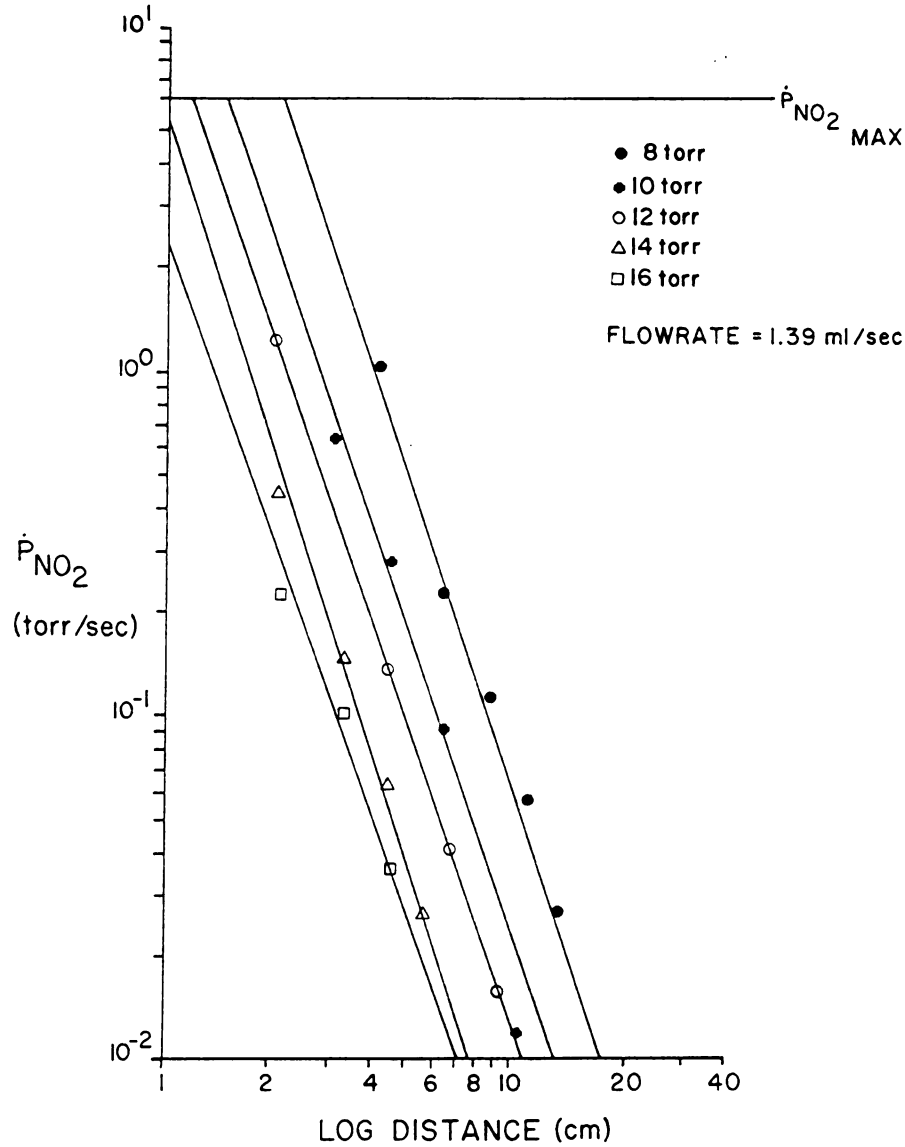

Figure 5.3 The effect of distance on oxygen atom concentration for several pressures.

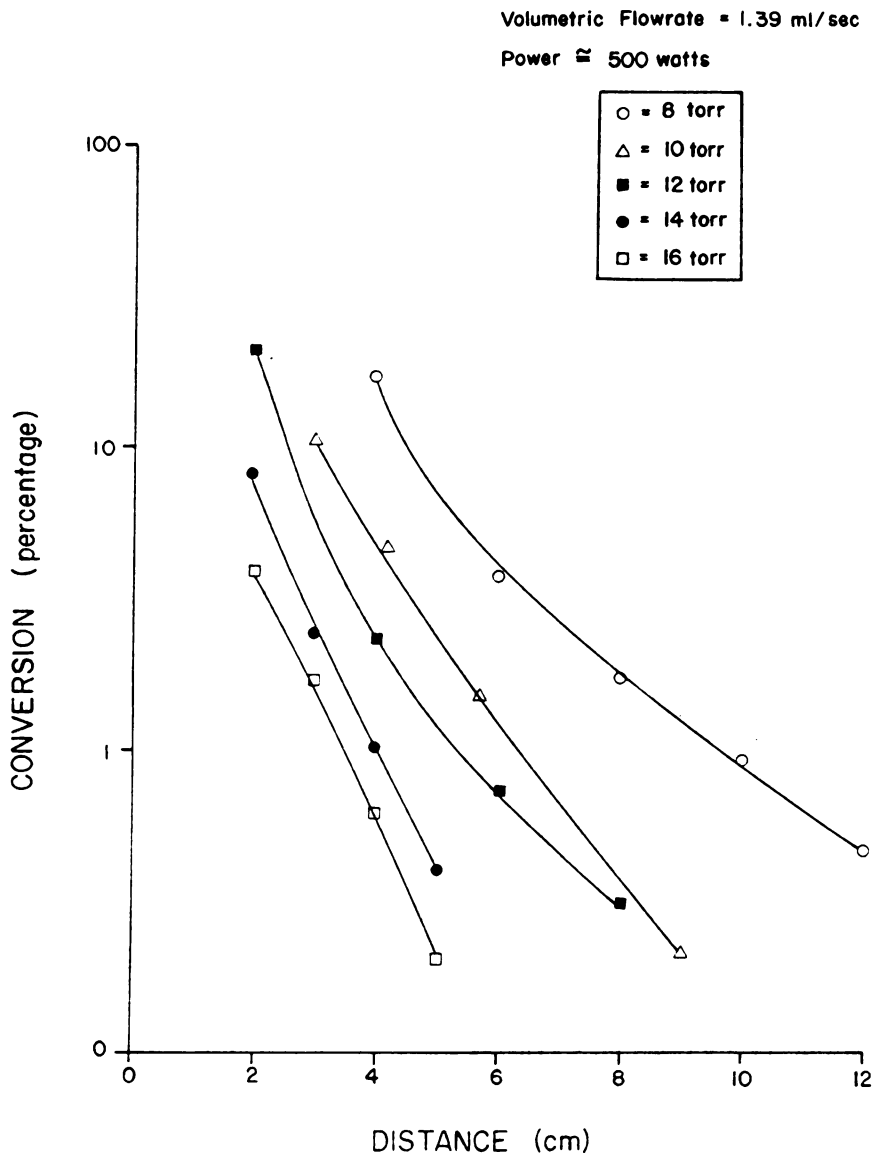

Figure 5.4 The amount of O_2 converted to atoms vs distance from the exit of the reactor cavity for several pressures.

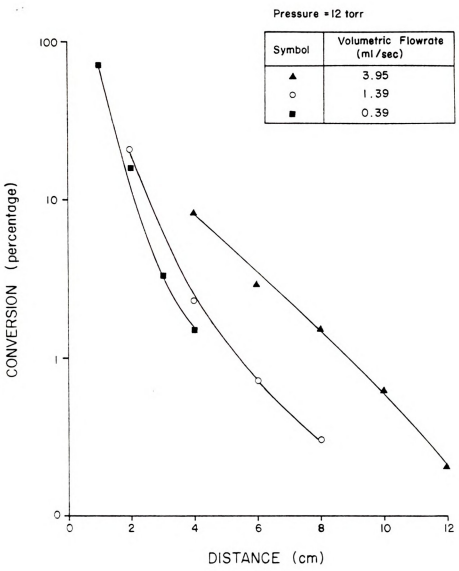

Figure 5.5 The amount of O_2 converted to atoms vs distance for several flowrates.

CHAPTER VI

RESULTS OF MODEL

6.1 Comparison of Model to Experimental Results

The effects of pressure, flowrate and power on oxygen atom production were investigated for the experimental parameters 8 to 16 torr, 0.4-4.0 ml/sec and 200-600 watts of absorbed power. Mearns and Morris[10] have suggested that it would be interesting to determine the oxygen atom concentration at the exit of the discharge. This was tried, but the addition of titrant at distances less than 2 cm caused a change in the plasma emission spectrum. As the atom concentration increases the NO_2 injection rate must also increase which implies that the closer to the cavity titration is performed, the larger the upstream penetration of NO_2. Therefore, the oxygen atom flowrate could not be determined in the exit plane without adversly affecting the plasma. It could however be determined a short distance away from the exit plane.

Titration data were measured from the exit of the discharge and not from the end of the plasma. The plasma tended to "blow out" of the cavity for pressures below 14 torr. (For example if the gas is composed of 100% O atoms,

$\dot{P}_{NO_2}$ has a maximum value of 6.0 torr/sec for a flowrate of 1.39 ml/sec. As can be seen by Figure 5.3, extrapolation of the data curves back to 1 cm indicates that $\dot{P}_{NO_2}$ is greater than this maximum for pressures less than 14 torr.) Consequently, the raw data required adjustment when compared to a theoretical model. The distance of titration from the plasma was determined by subtracting the distance the plasma extended from the resonant cavity. Thus, it appears that there was 100% dissociation for the pressures where extrapolation reaches this maximum value. The highest conversion actually measured was 70% at 12 torr and a flowrate of 0.4 ml/sec and 500 watts power absorbed.

Since the gas temperature of the experiment is not known, and the temperature as a function of distance in the model is known, the model results are converted into a $\dot{P}_{NO_2}$ (pressure increase of O atoms to a known fixed volume), so that a direct comparison of the model results can be made to the unaltered experimental data.

Figure 6.1 illustrates the fact that 3 body recombination of O atoms (reactions 6 and 7 of Table 3.1) and wall recombination of O atoms (reaction 10) are the important mechanisms. This case is typical of all of the experimental cases. As mentioned in the previous section, the reaction rate constant as a function of temperature is not always well known, especially for reactions 6, 7, and

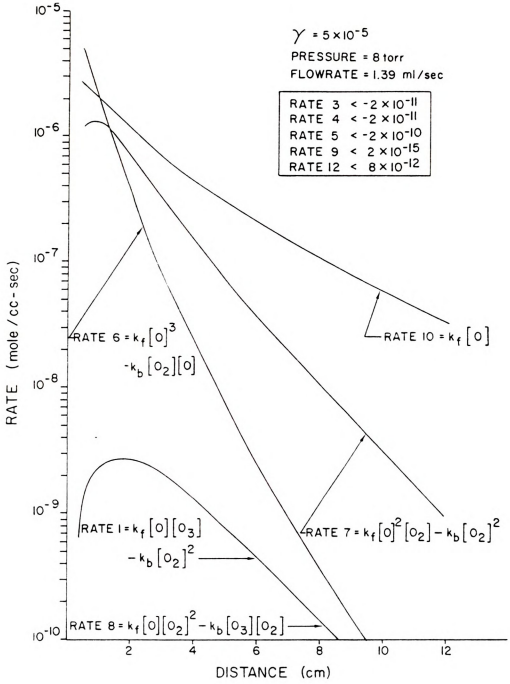

Figure 6.1 The model based net rates as a function of distance from the exit of the discharge.

10. Since reactions 6, 7 and 10 are so important, the effect of changing their rate constants to reflect uncertainties in their value was studied.

Typically within 3 cm downstream of the plasma, surface recombination rates dominate the kinetic mechanisms. Since wall recombination is a first order mechanism, the log-log plot of O atom concentration (in the form of $\dot{P}_{NO_2}$) as a function of distance greater than 2 or 3 cm, yields a straight line, the slope of which is dominated by the recombination probability coefficient γ . As can be seen by Figure 6.2, a recombination coefficient γ of $5x10^{-4}$ best fits the data at both 12 and 8 torr. This is slightly higher than that found by Linnett and Greaves[65], but the temperature of tube wall of the experiment may have been higher than 297 K. (See Appendix D).

A study was made of the effect of the three body recombination rate of reaction 6 and 7. The results (Figures 6.3-6.5) show the predicted mass flowrate of NO_2 using the rates of Wray[56], Matthews[73], Rink[54] and Camac[53]. (A wall recombination coefficient of $5.0x10^{-4}$ was used.)

At 8 torr (T=1200), Matthews and Wray's rates give the same predicted $\dot{P}$'s. This is due to the fact that the two rates are very close at 1200 K. For 12 torr where the temperature is assumed to be 1500 K, Wray's rate gives a better fit to the data. Figure 6.3 shows the results for

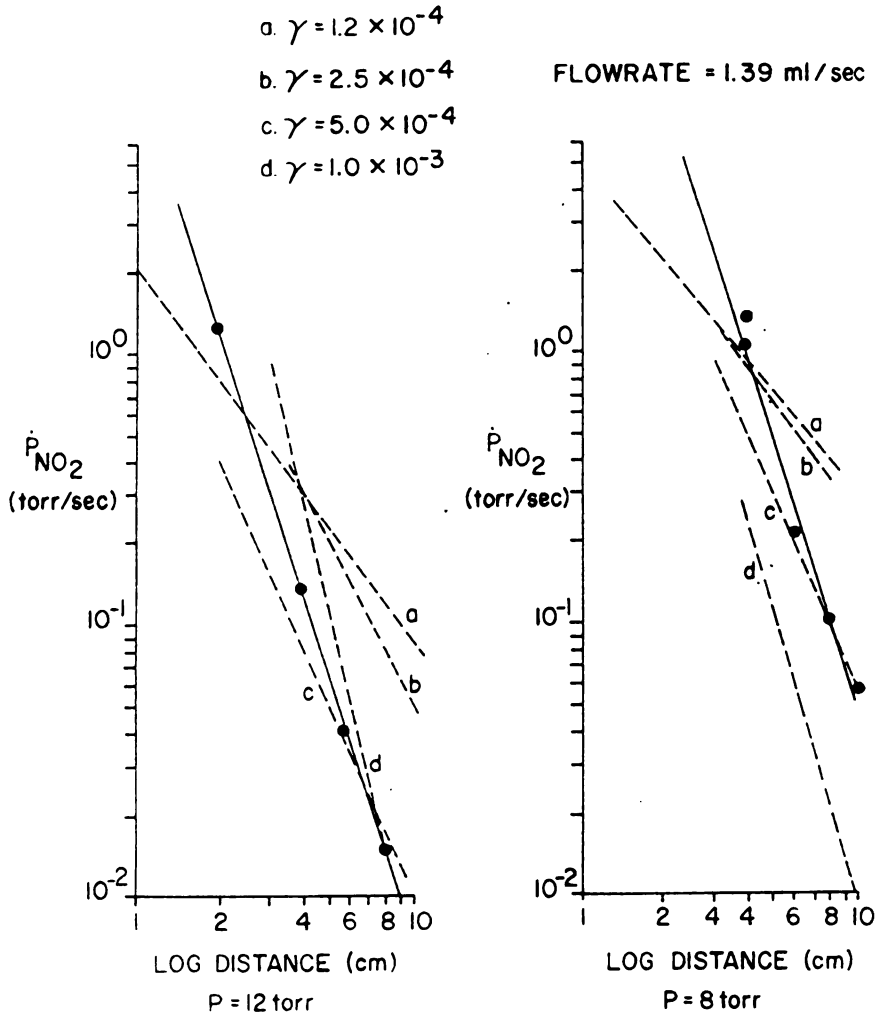

Figure 6.2 The solid line is the best fit to the titration data points. The dashed lines are the theoretical lines for different wall recombination coefficients. A recombination coefficient of 0.0005 was found to best approximate the data of the two cases of 8 and 12 torr.

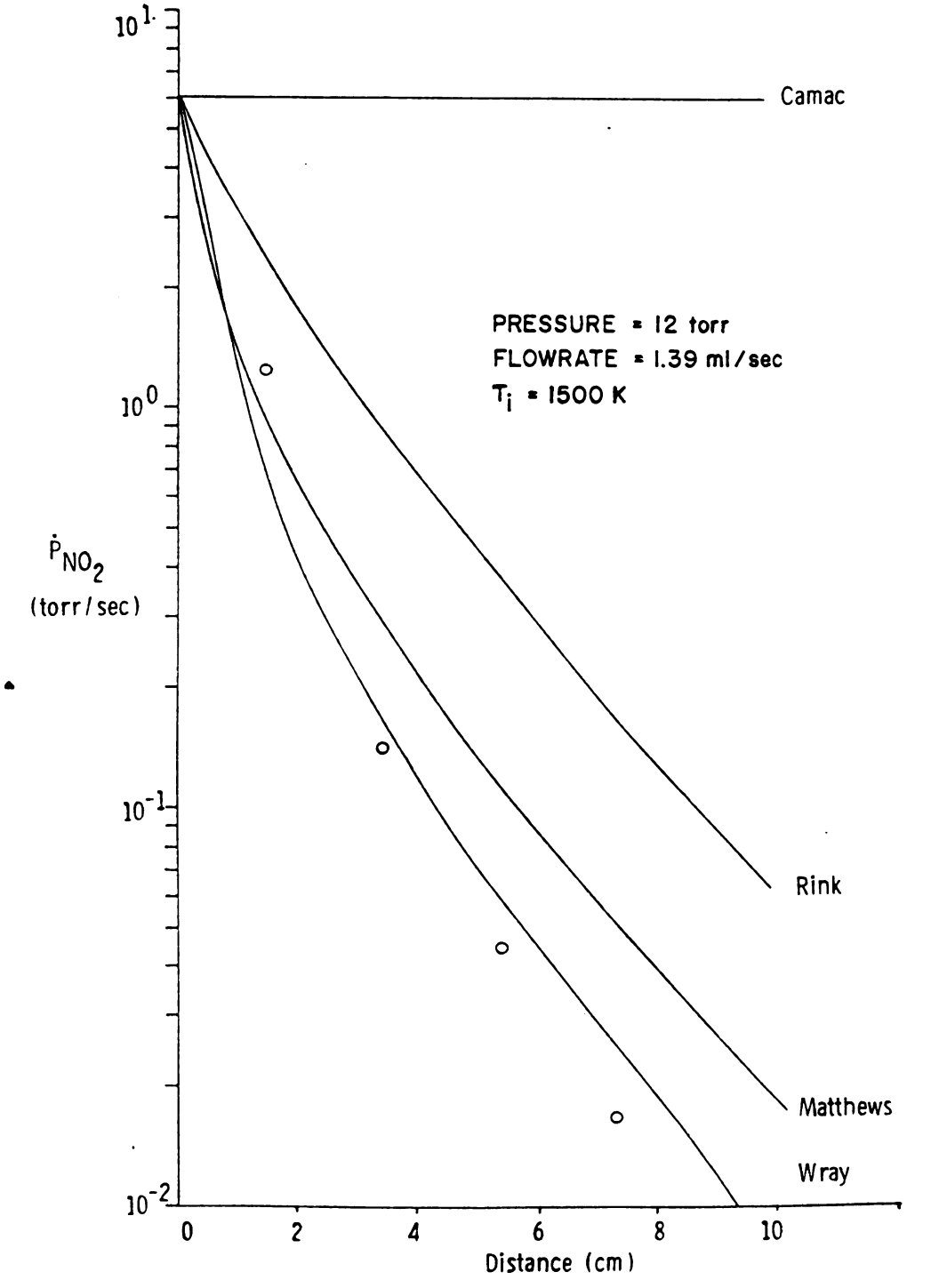

Figure 6.3 A comparison of predicted O atom mass flowrates with titration data using independently measured three body recombination rate coefficients.

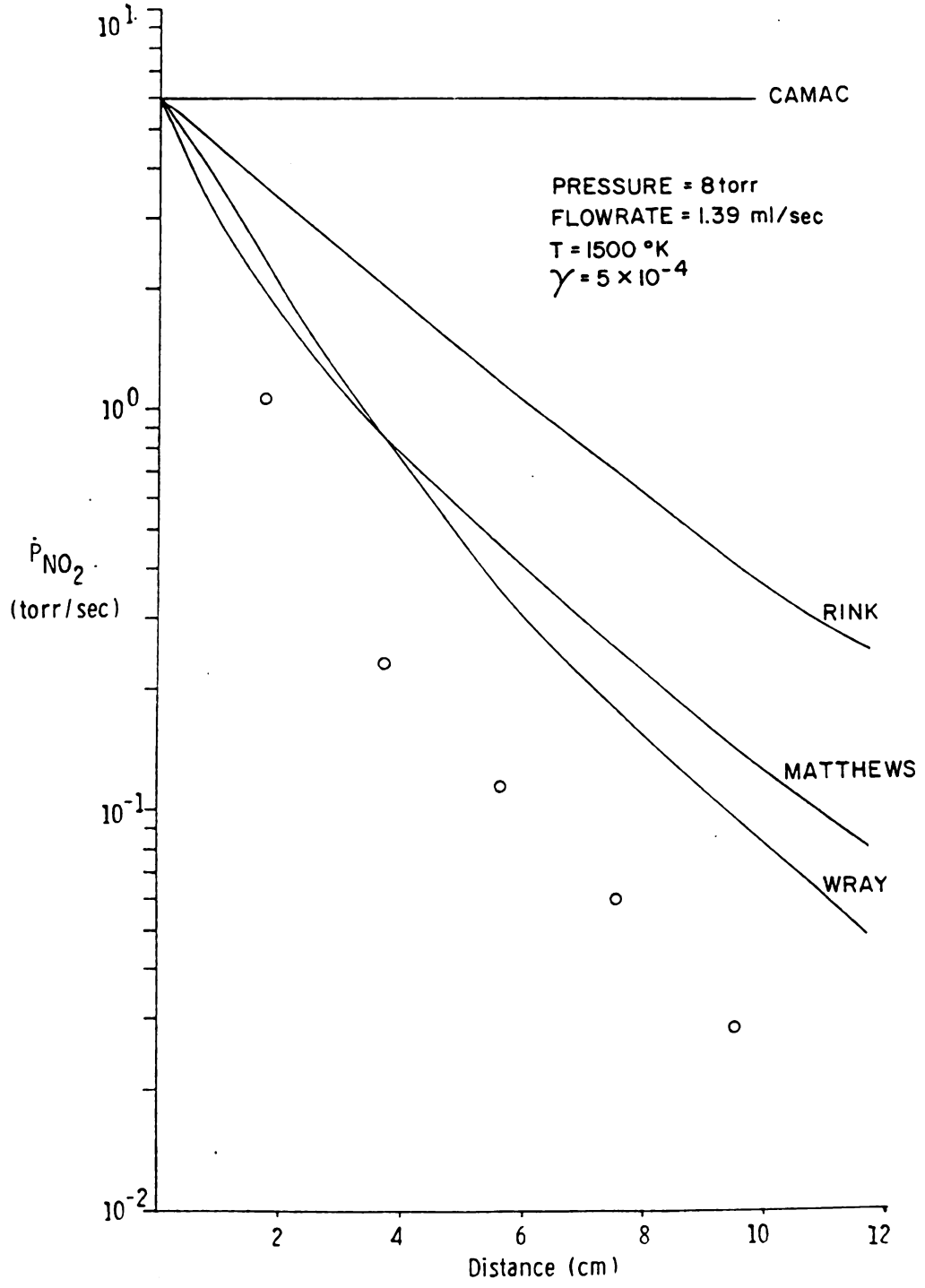

Figure 6.4 A comparison of predicted O atom mass flowrates with titration data using independently measureed three body recombination rate coefficients.

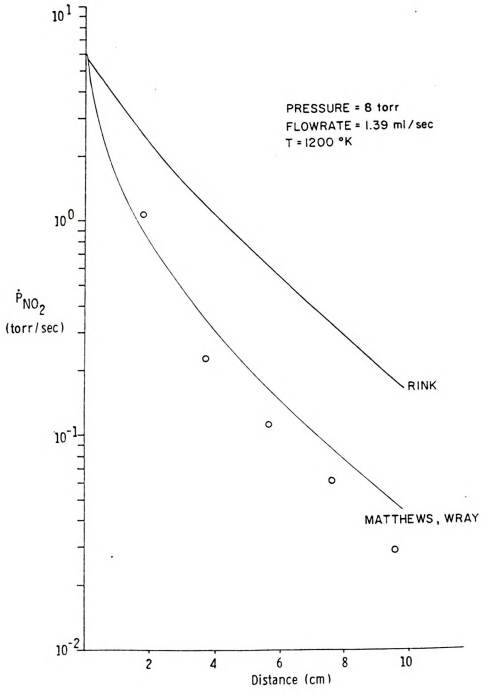

Figure 6.5 A comparison of predicted O atom mass flowrates with titration data using independently measured three body recombination rate coefficients.

the 8 torr and 1500 K case. It is obvious that this temperature is too high since the temperature affects where the curve falls, and not the shape of the curve. The rate coefficient predicted by Wray provides a curve which more closely matches that of the data.

The difference between the curve predicted using Matthews rate and the experimental data gets larger for increasing distance. Wray's rate is taken as the rate which best approximates this experiment.

Since there is some question in the literature as to the relative effectiveness of O and O_2 as third body partners in recombination, this effect was also studied by assessing the sensitivity of the model to variations in rate coefficients. The sensitivity of the model to the ratio of k_f (M=O_2) to k_f (M=O) of 1) 1:3 (as suggested by Wray) and 2) 3:1 as suggested in this paper is illustrated in Figures 6.6-6.7 for different temperatures. A ratio of 3:1 was found to fit the data better than a ratio of 1:3.

Once the reaction kinetics and the most probable rate constants were determined, the only input variable not known was the gas temperature at the discharge exit. Several cases, each at a different temperature, had to be examined for each set of initial conditions (see Figures 6.6-6.7). Thus, the temperature was fit to the data in this manner. Using a wall recombination probability of γ =

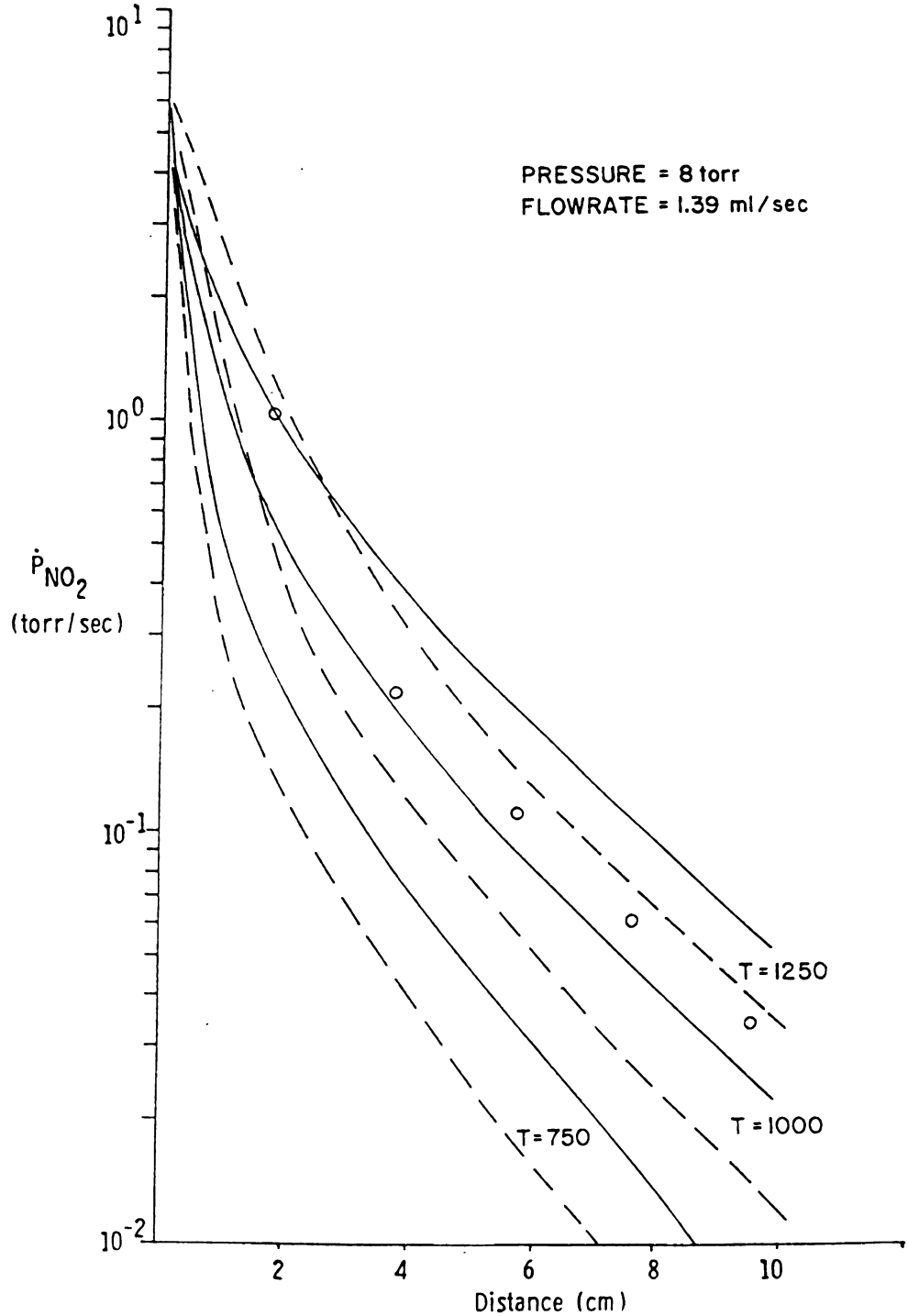

Figure 6.6 The dashed line indicates the model predictions using a 3:1 ratio of relative efficiencies of O_2:O for three body recombination. The solid lines show the model predictions using a 1:3 ratio as suggested by Wray[56].

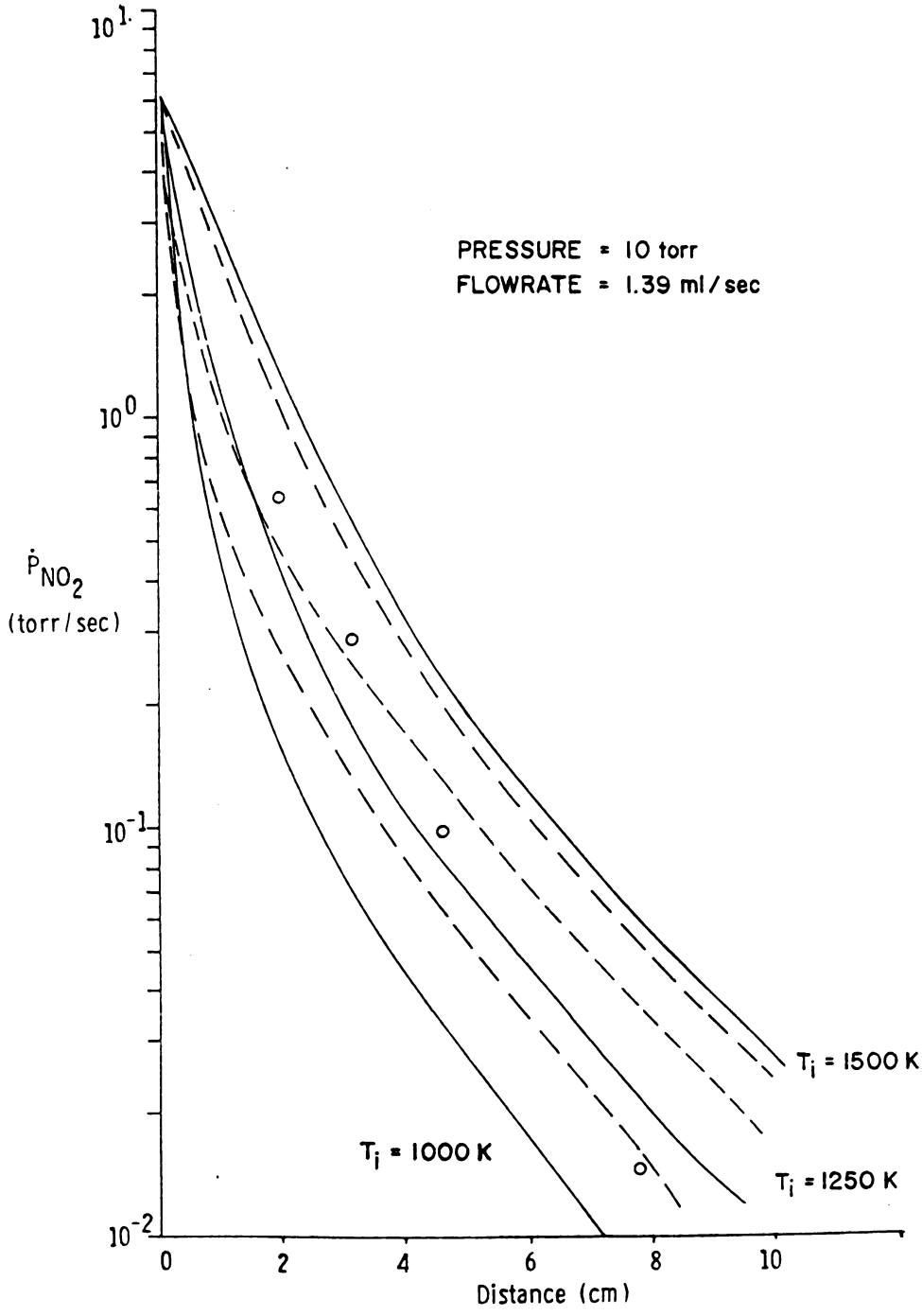

Figure 6.7 The solid line indicates the model predictions using a 3:1 ratio of relative efficiencies of O_2:O for three body recombination. The dashed lines show the model predictions using a 1:3 ratio as suggested by Wray[56]

$5x10^{-4}$ and Wray's rate for three body recombination with a factor of 1:3 for $k_f(M=O_2)/k_f(M=O)$ several cases were investigated. (See Figures 6.8-6.17.) For the cases where the flowrate was 1.39 ml/sec, the theoretical curve fits the titration data well. For lower and higher flowrates at pressures of 12 and 16 torr, the predicted results did not match as well.

The effect of temperature was investigated by varying the input temperature of the model (i.e. the temperature at the exit of the discharge) and examining $\dot{P}_O$ at a fixed position of 1.8 cm downstream of the plasma, assuming 100% dissociation of the molecular gas at the exit of the discharge. As illustrated by Figure 6.18 the number of O atoms remaining at that fixed distance increases with temperature. In other words, the lifetime of the O atoms increases with temperature. Also plotted in Figure 6.18, are titration measurements as a function of absorbed power. Figure 6.18 shows that there is a one-to-one correspondence between absorbed power within the resonant cavity and the exit temperature of the gas, i.e. doubling the absorbed power from 300 W to 600 W results in a doubling of exit temperature from 1000 K to 2000 K. Thus, the exit temperature of the gas is linearly proportional to the amount of power absorbed by the plasma.

The oxygen atom concentration at a fixed location of

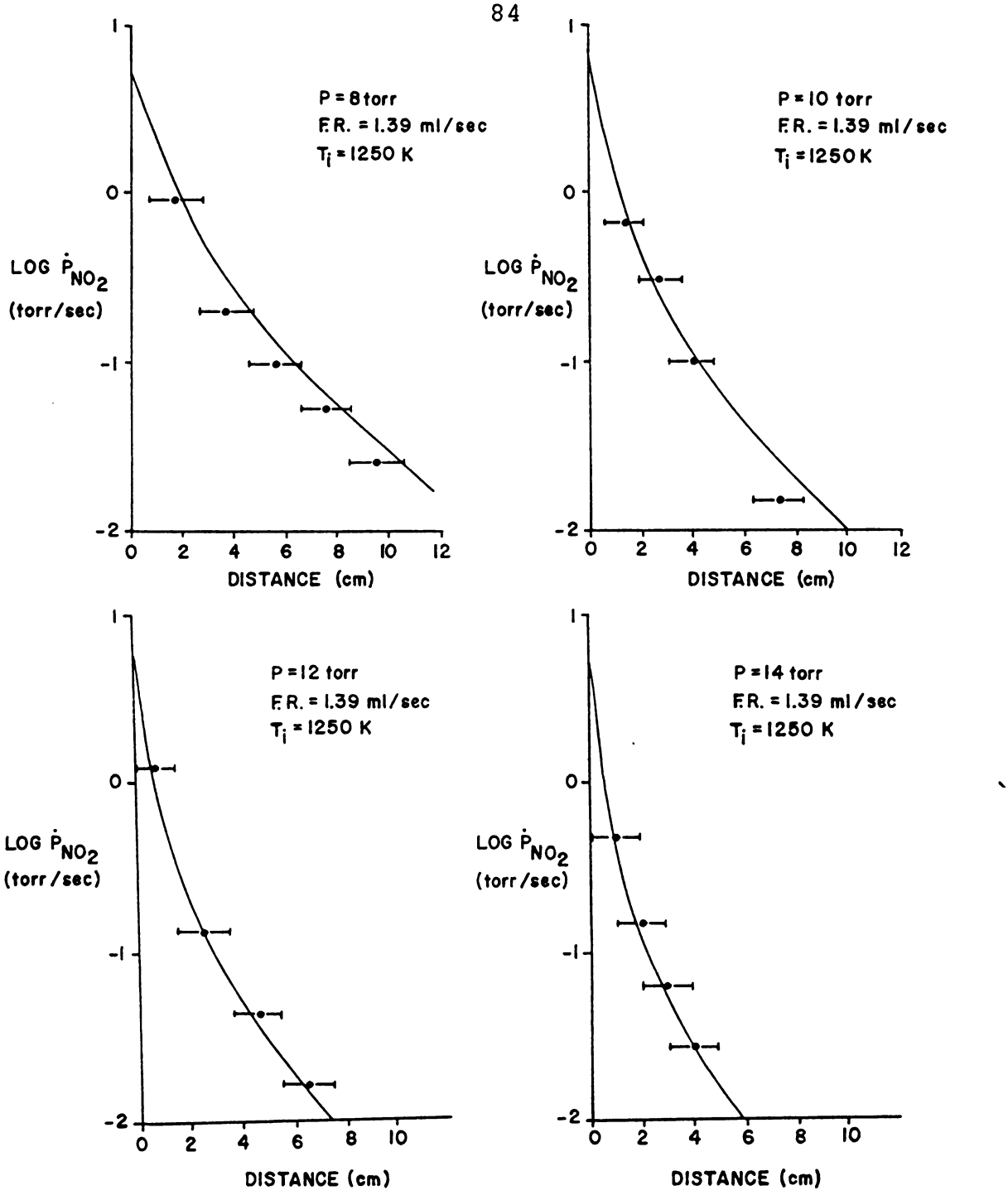

Figures 6.8-6.11 The solid line indicates the model predictions for O atom decay as a function of distance for several pressures and flowrates. The actual data points are indicated by the solid circles.

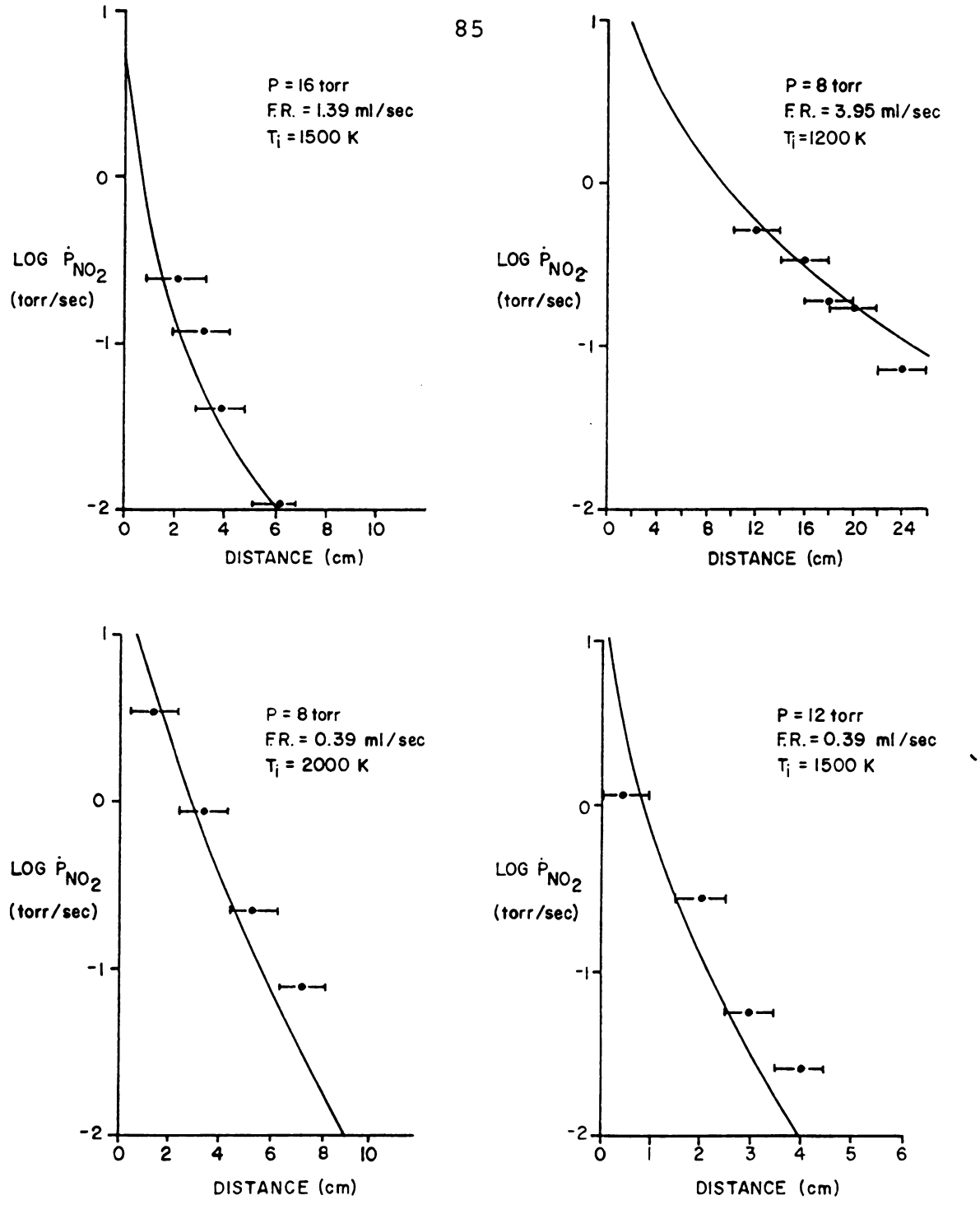

Figures 6.12-6.15 The solid line indicates the model predictions for O atom decay as a function of distance. The actual data points are indicated by the solid circles.

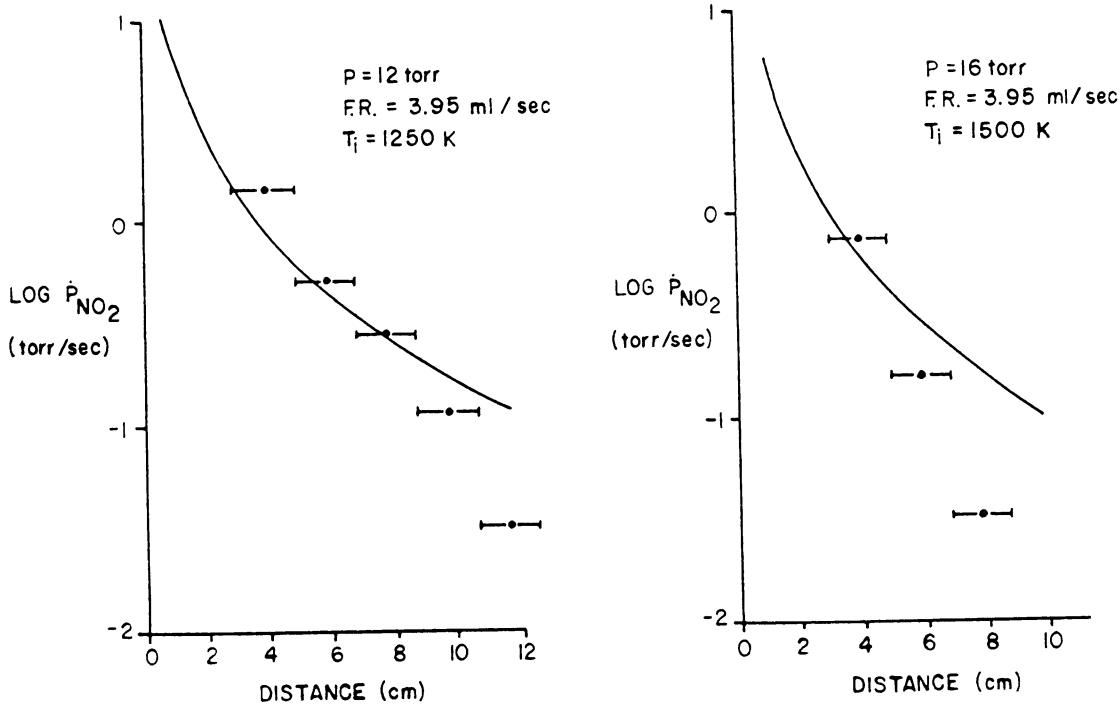

Figures 6.16-6.17 The solid line indicates the model predictions for O atoms decay as a function of distance. The actual data points are indicated by the solid circles.

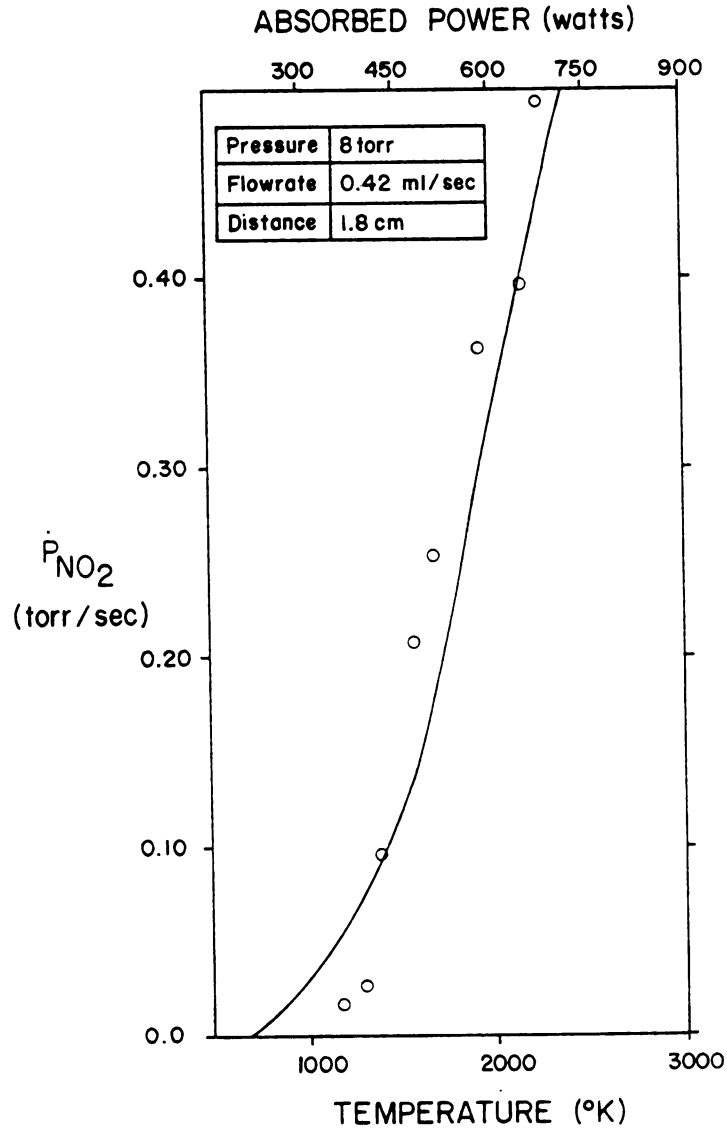

Figure 6.18 The data points represent the mass flowrate of NO_2 needed to titrate O atoms as a function of measured absorbed power. The theoretical curve is the mass flowrate of NO_2 as a function of discharge exit temperature.

1.8 cm from the end of the plasma was measured as a function of flowrate. As illustrated by Figure 6.19 a comparison of the model's predictions of O atom concentration as a function of flowrate for constant exit temperature do not match the experimental data. This implies that gases with different initial flowrates but with the same amount of absorbed power exit the reactor cavity with different temperatures. The "resident time" (amounts of time the incoming gas spends in the resonant cavity) is correspondingly larger for slower flowrates and shorter for faster flow rates. Naturally, it would be expected that a gas that is completely dissociated and moving with a slower flowrate would have a higher temperature than a similar gas moving with a faster flowrate for the condition where a constant amount of power is absorbed. It is possible to estimate the exit temperature of the experimental data at various flowrates for fixed pressure and fixed absorbed power by noting the points of intersection of the predicted curves with the experimental curve. These points are predicted by the model for a particular exit temperature and oxygen atom flowrate at a specific distance downstream of the discharge. Note that these points are uniquely determined by the temperature for a specific initial gas flowrate. When the exit temperatures are plotted as a function of the

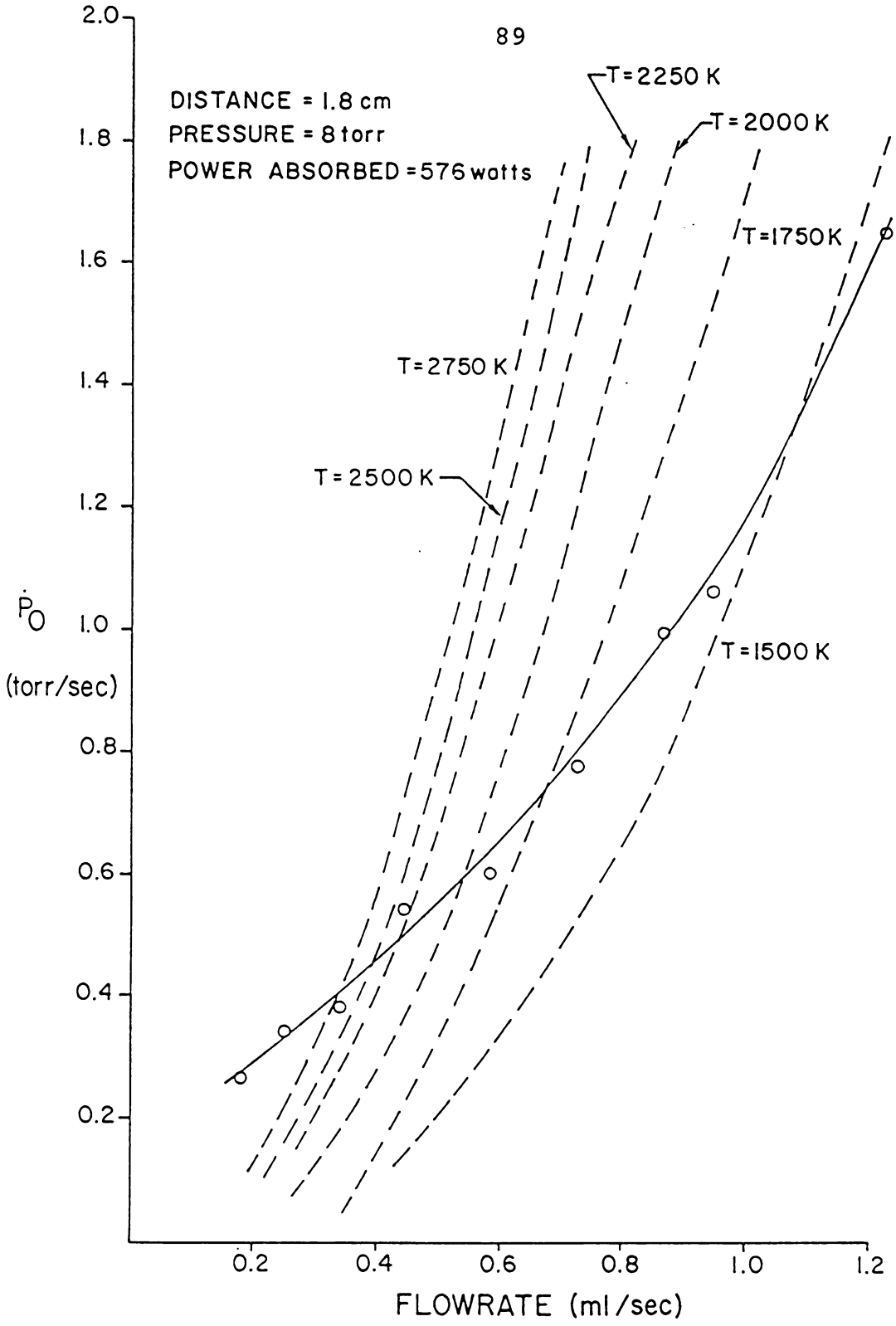

Figure 6.19 A comparison of the model predictions (dashed line) of the mass flowrate of NO_2 as a function of flowrate of initial O_2 for fixed temperatures at the exit of the discharge, and the actual mass flowrate measurements as a function of flowrate of initial O_2.

inverse of the flowrate , a straight line is obtained, (see Figure 6.20). Hence, the temperature times the flowrate gives the same constant value for a gas of constant pressure and constant absorbed power. Since the composition of the gas at the exit seems to be nearly 100% O atoms, this implies that the rate of energy absorbtion of the plasma is a constant.

It is possible to estimate the amount of absorbed energy of the plasma. Assume a typical case of 10 torr with a volumetric flowrate of 1.4 ml/sec where the gas heats up to an average temperature of 2000 K and then dissociates to near 100% oxygen atoms. The amount of energy necessary to heat the gas to 2000 K can be found from the relation $\dot{m}C_p\Delta T$, where $\dot{m}$ is the mass flowrate (grams/sec), C_p is the specific heat (approximately 9 cal/gram-K for O_2 at 1800 K) and ΔT is the change in temperature (2000 - 300) K. For this example, the heating of O_2 amounts to 3.6 Watts. If 500 Watts are absorbed by the plasma, the heating accounts for 0.7% of the incoming energy.

The amount of energy used in dissociation can be calculated by taking the mass flowrate in moles/sec and multiplying by the amount of energy needed to dissociate each mole. This is approximately 136 kcal/mole for oxygen, therefore it takes 32 Watts to totally dissociate oxygen at

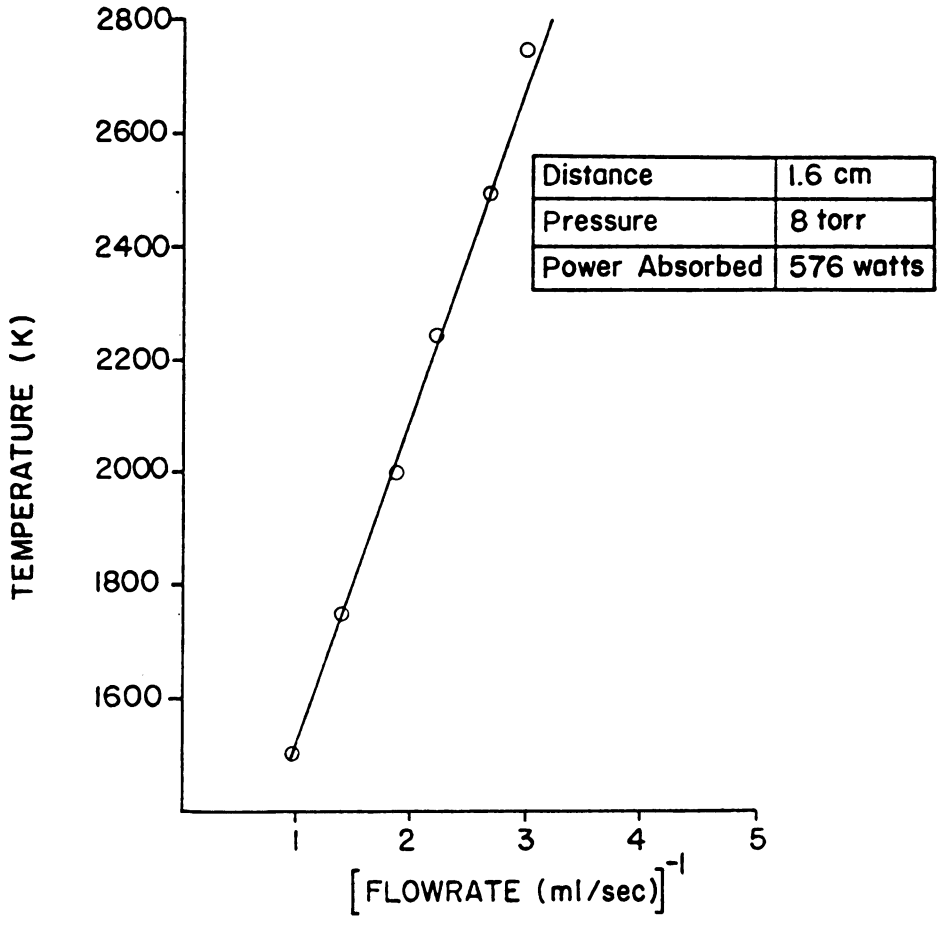

Figure 6.20 The semi-empirical temperatures as a function of inverse flowrate of initial O_2 as determined from Figure 6.19.

2000 K. This accounts for 6% of the incoming energy.

Another source of energy absorption is ionization. Using 12.2 eV for the ionization potential of O_2, it takes 66 Watts to 100% ionize the gas. In actuality the ratio of ions to neutrals is 10^{-4} for microwave plasmas (see Appendix D), so only 6.6×10^{-3} Watts are used in ionization.

Fournier et al.[85] lists many energy loss mechanisms in oxygen plasmas, due to inelastic processes such as dissociative attachment, electronic, vibrational and rotational excitation and three body attachment. These processes only take a very small fraction of the input energy.

Thus a plasma which absorbs 500 Watts uses 3.5 Watts to heat the gas, 32 Watts to dissociate the gas and a few Watts to ionize and excite the gas. Obviously, the majority of the energy is not used by the plasma. This energy is lost through conduction, convection and radiation heat transfer to the quartz containment tube and the surrounding air. The quartz tube had to be cooled with forced air, otherwise the tube started to melt. (The melting point of quartz is approximately 2000 K.)

In a recent study by Morin et al.[84], the energy loss due to heat transfer in a microwave discharge similar to this experiment, but using hydrogen rather than oxygen, has

been investigated. In this calorimetric experiment at Michigan State University, the amount of energy transfered to the cooling water and cooling air of the system was measured. They found that 25-35% of the input power could be accounted for in heat lost from the walls of the reactor and containment tube and heat lost from the cooling air regardless of the amount of incident power. They also found that an increase in gas flowrate results in a decrease in the amount of heat loss. However, in a second experiment[84] performed at National Aeronautrics and Space Administration-Lewis Lab, 66% of the input power was transfered to the air coolant. It is unclear where the remainder of the input energy of both experiments is lost. If it were coupled to the plasma as thermal energy, it would result in much higher temperatures than the 400-2000 K range measured by NASA-Lewis and the 1000-2000 K range predicted here.

As will be shown in Section 6.3, the kinetic energy of the post discharge gas is due solely to thermal heating of the gas by the microwaves and not due to the chemical energy released in recombination. If electrical to thermal energy conversion is the goal of a microwave plasma, something must be done to account for the input energy so that coupling a larger fraction of the input energy into the plasma can be achieved. In addition, smaller amounts

of input energy would be needed to heat the gas to present temperatures if the heat transfer losses could be reduced.

In summary, the computer model simulates experimental titration data quite well, particularly at the flowrate of 1.39 ml/sec. In addition, by judiciously selecting model parameters, matching the model predictions with the experimental results provides estimates of the plasma gas temperature, a parameter proven difficult to measure. It was found that the predicted gas temperature was linearly dependent on the power and that the temperature is inversely proportional to the flowrate. A wall recombination probability of 5×10^{-4}, and the three body recombination rate given by Wray were found to fit the data of this experiment best. It was also found that the majority of the input energy is lost, but what little energy is absorbed goes into heating and dissociating the gas.

6.2 Comparison with Other Experiments

The computer model presented here is the only model to date which can directly predict titration data as a function of distance. As mentioned in the Introduction, Bell[5,9] and Mearns[10] have developed computer simulations to model their experiments, but they do not make a

distinction between the gas outside of the reactor cavity where titration was performed and the gas inside the cavity where the electrical energy is absorbed. Their models do not predict their titration results, but only the trends of their results as a function of pressure, power and amount of conversion.

It is difficult to make a direct comparison between the model presented in this study and the experimental investigations of others because of the wide range of experimental conditions and apparatus (see Table 6.1). Typically, titration measurements were made at designed locations and not as a continuous function of distance. These titration measurements were reported as conversion ratios and were not given in their original form. However, several assumptions made in the model given in this study were found to be in agreement with other experiments.

Another major difference between this experiment and others is that the power density of this experiment was much larger than the power density of other experiments (see Table 6.1). The volume of the oxygen plasma of this experiment was approximately 23 cc assuming that the plasma uniformly filled the quartz tube. It would be expected that a higher power density would lead to higher neutral gas temperatures. Therefore, the neutral gas density of a plasma at 10 torr and 300 K, for example, would be the same

Table 6.1 Summary of Oxygen Discharge Experiments

1. P. Francis (11)
   - 2.54 GHz microwave discharge
   - 1 to 10 torr (pressure)
   - 6.0 - 125.0 ml/sec (flowrate)
   - 8 mm I.D. containment tube
   - 15 Watts (power input)
   - 2% maximum conversion (6 torr, 10 ml/sec)

2. J. Battey (87)
   - 13.56 MHz radio frequency discharge
   - 1 to 3 torr (pressure)
   - 1.67-15.0 ml/sec (flowrate)
   - 20.3 cm I.D. and 33 cm length (reactor geometry)
   - 0 to 200 Watts (power input)
   - 0.0093 W/cc (power density)
   - 7.5% maximum conversion (0.5 torr, 200 W)

3. A. Bell and K. Kwong (9)
   - 13.56 MHz radio frequency discharge
   - 2 to 4 torr (pressure)
   - 0.3-1.3 ml/sec (flowrate)
   - 8 cm by 2.5 cm pillbox (reactor geometry)
   - 0.59 W/cc (power density)
   - 49% maximum conversion (2 torr, 74 W)

4. A. Mearns and A. Morris (10)
   - 2.54 GHz microwave discharge
   - 0 to 10 torr (pressure)
   - two cylindrical cavities of volume 1) 2.1 cc and 2) 2.67 cc
   - 2.97 Watts/cc (power density)
   - 14 % maximum conversion (2 torr, 200 W)

5. This experiment
   - 2.4 GHz microwave discharge
   - 8 to 16 torr (pressure)
   - 0.2 to 4.0 ml/sec (flowrate)
   - 1.7 cm I.D. and 92 cm length (containment tube)
   - 200 to 700 Watts (power input)
   - 10 to 33 W/cc (power density)
   - 80% maximum conversion (12 torr, 500 W)

as a plasma at 1 torr and 300 K. Thus, it is difficult to make comparisons between experiments of similar pressures but different power densities and temperatures.

McCarthy[86] found that a 2.54 GHz discharge produces "free radicals" such as O atoms that are relatively long lived after leaving the discharge. He found that when the gas exited the discharge and entered a magnetic field or an electric field, it was not deflected, implying that the gas outside of the discharge was in fact neutral. So the assumption that the electrons have spontaneously recombined with the ionic species upon exiting the discharge, (leaving only neutral radicals and molecules) is supported by McCarthy.

Mearns and Morris[10] modeled the kinetics of an oxygen microwave discharge. They assumed that the important mechanisms in their discharge were $O + O_2 + O_2 = O_3 + O_2$ and $O + \text{wall} = 1/2\ O_2 + \text{wall}$. Since they measured low O atom concentrations, they assume that $O + O + M = O_2 + M$ is negligible. They used an exponential extrapolation (based upon the forward rates of the above two reactions) of the NO_2 titration data to predict the amount of conversion at the exit of the discharge. There was no attempt to match their data to predictions made from their model, but instead they made generalizations based upon their calculated "conversions". They also calculated

"discharge residence times" based upon the flowrate of O_2 and O in the discharge and a temperature of 300 K.

Mearns and Morris conclude that the amount of O_2 converted to O atoms will increase with 1) a longer residence time, 2) a decrease in pressure or 3) an increase in absorbed power. However, from our present work we conclude that the conditions of this experiment yield maximum conversion. Hence, for a longer residence time, a decrease in pressure and an increase in absorbed power will increase the lifetime of O atoms downstream of the discharge, but not necessarily the amount of conversion. However, in the limit of low fractional conversion, the conclusions of Mearns and Morris hold. Increased residence time for the present experiment gave higher discharge temperatures.

Bell and Kwong[9] examined the dissociation of oxygen in a 13.56 MHz radio frequency discharge. They use NO_2 titration to determine the concentration of O atoms. Like Mearns and Morris[10], they also convert their data into percent conversion, but they do so by assuming that the flowrate of the atomic oxygen measured at the titration end point was identical to that at the exit of the discharge. (Their titration port was 5 cm downstream of the discharge cavity.) Bell and Kwong[9] measured the gas temperature using catalytic probes and found that the gas temperatures

increased with an increase in power, but not linearly as found in this study. They also found that the gas temperature increased as the flowrate was increased which is in direct opposition to our conclusions in the previous section. To explain this phenomenon, they assume that for low flowrates, the amount of dissociation is increased and since the thermal conductivity of atomic oxygen is greater than that of molecular oxygen, the heat loss by conduction would be enhanced by the presence of a large fraction of atoms. Thus, a gas with a low flowrate would have more cooling per unit mass than a gas at a high flowrate.

Bell and Kwong measured the gas temperature with a glass probe and they assumed that very little recombination occurs on the glass surface, which may or may not be a valid assumption. If recombination does occur to a large extent on glass surfaces, then the temperature measured on the probe surface would not only be due to the bulk gas temperature, but also due to the energy released during recombination, recombination being highly exothermic (120 kcal/mole). In addition, as the gas cools, the rate of recombination increases since its rate is temperature dependent. The net result is an increase in molecular gas formation surrounding the glass probe, and an overall decrease in thermal conductivity, (competing with the heat removal process suggested by Bell and Kwong). Better

temperature measurements need to be made to resolve this difference.

Bell and Kwong model the amount of conversion by examining the probable kinetics of the discharge itself. They assume that the gas is dissociated due to collisions with electrons. This process then competes with three body recombination of O atoms with other O atoms and O_2 molecules. Knowing the absorbed power, diffusion length, and electric field strength, they calculate the electron density. The electron density is included in the continuity equation for O atoms along with the rates of several chemical reactions and the amount of conversion for an assumed temperature of 297 K. The continuity equation is then solved for the amount of conversion as a function of power, pressure and flowrate. They do not make allowances for changes in temperature. Their model does not quantitatively predict their results, but it does predict qualitative effects that match those same effects found in their experiment. Like Mearns and Morris[10], they found that an increase in power and a decrease in pressure or flowrate will increase the amount of molecular to atomic conversion.

Battey[87] produced atomic oxygen in a 13.56 MHz discharge, and deduced properties of the oxygen plasma by measuring the stripping rate of photoresist from silicon

wafers contained within the oxygen plasma. He measured the effect of temperature by placing a silicon wafer on a large aluminum block in the discharge cavity and then monitored the temperature of the block. He also placed thermometers on the wall of reactor. He found that the temperature of the block and walls did not change during plasma operations, nor did it change as a function of atomic flowrate. This agrees, in part, with the predictions of the model in this study. As seen in Figure 6.21, the temperature of the gas rises only slightly when the gas exits the discharge but remains constant as the gas flows down the tube.

Battey[87] also measured the flowrate of NO_2 necessary to titrate atomic oxygen as a function of the flowrate of initial molecular oxygen in a range of 1.67 ml/sec to 15 ml/sec. He found that the O atom concentration was independent of the O_2 flowrate. i.e. the flowrate of atomic oxygen changes by the same factor as the flowrate of the total oxygen. This is supported by the results of this study at low flowrates. In Figure 6.19 at a flowrate of 0.45 ml/sec, P_{NO_2} = 0.52 torr/sec and at a flowrate of 0.9 ml/sec, P_{NO_2} = 1.02 torr/sec. Battey indicates, that at first glance, it would be expected that at higher flowrates, the O atom concentration would drop off due to reduced discharge residence times. He notes however, that

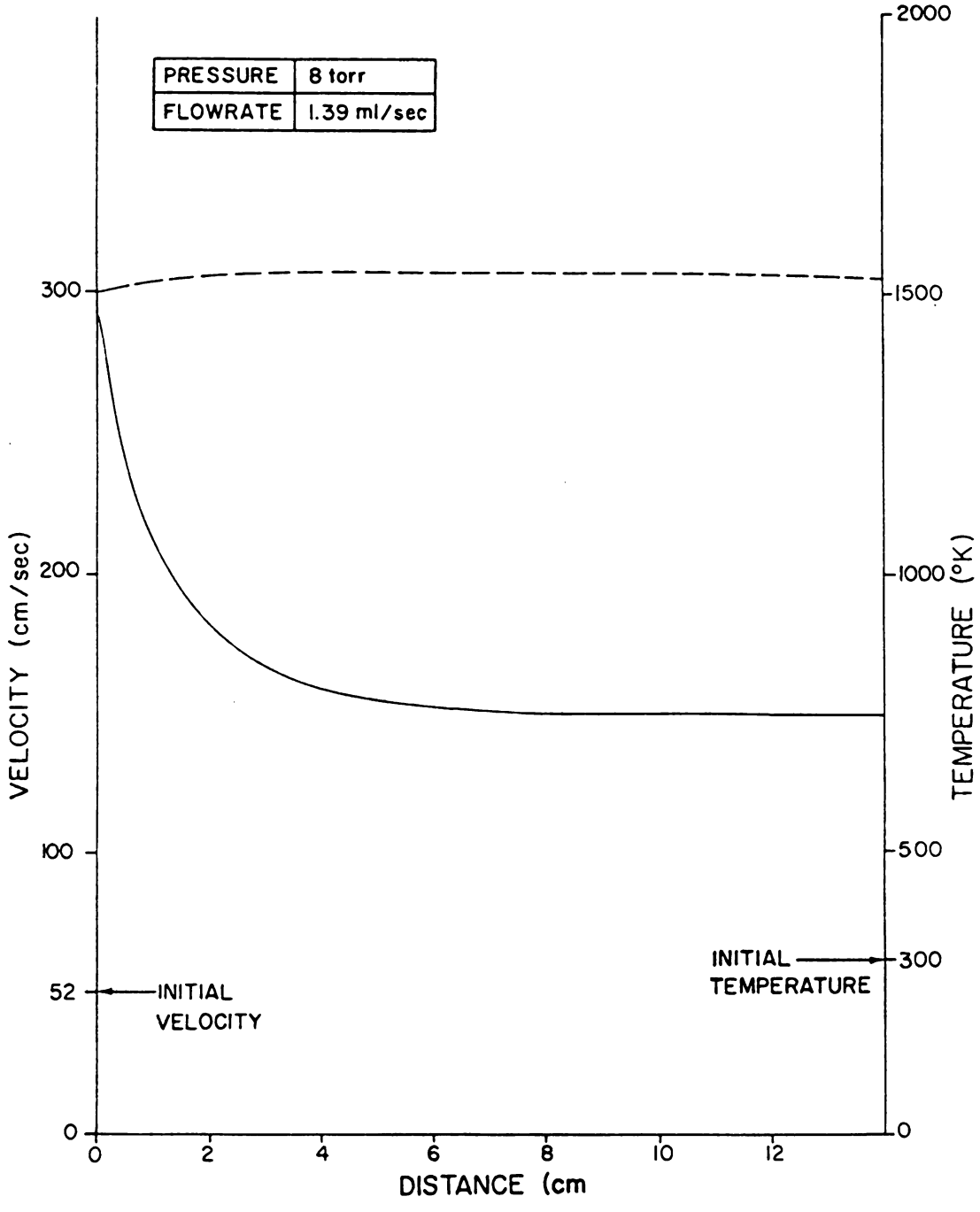

Figure 6.21 Velocity (solid line) and temperature (dashed line) predictions as a function of distance from the exit of the discharge.

lower flowrates (longer residence times) alllow for an increase in surface recombination between the exit of the discharge and the titration point. In this study 100% dissociation was implied by the titration data for all flowrates. Experimental data and modeling predictions indicate that there was a smaller fraction of O atoms remaining by the time the gas reached a specific titration point for the slower flowrates. This effect manifests itself due to the relative increase in surface recombination as well as three body recombination effects taking place during the extended travel time.

Francis[11] comes to the same conclusion as Battey.[87] He produced O atoms in a 2.54 GHz discharge and used e.p.r. techniques to observe the decay of the oxygen atoms. He states that when the inverse of the discharge residence time is much smaller than the rate of recombination, then the surface recombination rate constant determines the steady-state atom concentration and the atom concentration will be independent of flow velocity. In Figure 6.19 the surface recombination rate was much larger than the inverse of the residence time for low flowrates, and was somewhat larger than the inverse of the residence time for higher flows. This is why the curve is linear at lower flowrates. So in fact, it is the ratio of surface recombination to residence time that determines if the amount of O atoms

produced is dependent or independent of the flow velocity.

The assumption that radial and axial diffusion could be neglected was made in several experiments. Based upon a previous analysis, Bell and Kwong assume that the diffusion rate is slow enough in the direction of flow that it can be neglected. Mearns and Morris also neglect radial and axial diffusion, but they state that this is not necessarily a valid assumption, but that the available data on diffusion is not sufficiently accurate to include it. Francis states that the diffusion coefficient is inversely proportional to the density of the gas, so that the error in neglecting radial diffusion will increase with decreasing pressure and flow velocity. He calculates the diffusion coefficient for conditions similar to that in this experiment and finds that it is very small (to the point where it can be neglected) for pressures of 6 torr and above. Francis also calculates the viscous pressure drop by assuming Poiseuille flow. He finds that this can be neglected in the region of his experiment, which again was in the same region as that of this experiment.

In general, there is the concensus between the above experiments and the experiment modeled in this study, that increased flowrate, and increased absorbed power and a decrease in pressure will increase the observed O atom concentration at a fixed point downstream of the discharge.

There is some question as to the effect of the plasma parameters on temperature and more accurate measurements of temperature will have to be made before any conclusions can be drawn.

6.3 Temperature and Velocity Predictions

In the previous sections it was shown that a theoretical model could accurately predict oxygen atom concentrations as a function of distance from a microwave discharge, as well as match the pressure and flowrate trends of other experiments. The model was not quite as capable of predicting temperature trends of other experiments but it is very difficult to accurately measure temperature.

Neither this experiment, nor the experiments discussed in previous sections quantitatively measured other species known to be present in the discharge, nor did they measure velocity either at the exit of the discharge or after total recombination had occurred. This section discusses the model predictions for some of these parameters which have not been measured.

Velocity and temperature are important parameters in assessing the feasability of using a microwave discharge as a source for many potential applications such as momentum transfer which could be used for a rocket thruster. Figure

6.21 shows the typical temperature and velocity profiles. The difference between the final equilibrium temperature and the exit temperature is not large, but the overall temperature increase of the gas from 300 K before it enters the discharge to the final equilibrium (post discharge) temperature is large. This overall temperature increase appears to be due primarily to the absorption of energy in the microwave discharge and not due to the energy released in recombination downstream of the discharge.

The flow velocity on the other hand reaches a maximum at the exit of the discharge where the temperature is large and the average mass per particle is half that of the undissociated gas. As the dissociated gas recombines, the gas velocity decreases and reaches a value larger than that of the initial velocity but smaller than the velocity of the dissociated gas. It might have been anticipated that the velocity should continue to increase as the gas recombines because of the extra thermal energy released in the three body recombination, but this extra energy indicated by a slight temperature increase is not large enough to overcome the deceleration of the gas due to the decrease in the number of particles per unit volume and the increased mass per particle. (This assumes of course that the pressure remains constant throughout the flowtube. The model results show that the pressure actually increases

slightly (by 0.01 torr).)

The degree to which the temperature increases and the velocity decreases as a function of pressure outside of the discharge is illustrated in Figure 6.22. An increase in pressure causes an increase in the final temperature and a decrease in the final velocity. However, Figure 6.23 shows that at a constant pressure, an increase in exit temperature causes an increase in final velocity. So, for example, to maximize the final velocity requires a trade-off between minimizing the pressure and maximizing the exit temperature.

6.4 Singlet Delta Formation

The model predicts that O_2 and O are the only species of importance, by several orders of magnitude (see Figure 6.24). However, if $O_2(^1\Delta)$ is produced by recombination of O atoms with the wall, as suggested by Black and Slanger[75], $O_2(^1\Delta)$ concentration could also be significant. The solid lines of Figures 6.25 and 6.26 represent the concentration of O_2 and $O_2(^1\Delta)$ when all the O atoms that recombine at the wall do so into the electronic ground state of O_2 for a temperature of 2000 K. The dashed lines show the concentration of O_2 and $O_2(^1\Delta)$ when 30% of the O atoms recombined at the wall populate the $O_2(^1\Delta)$ state. For a temperature of 1000 K, a maximum of 4% (at 8 torr) and 2%

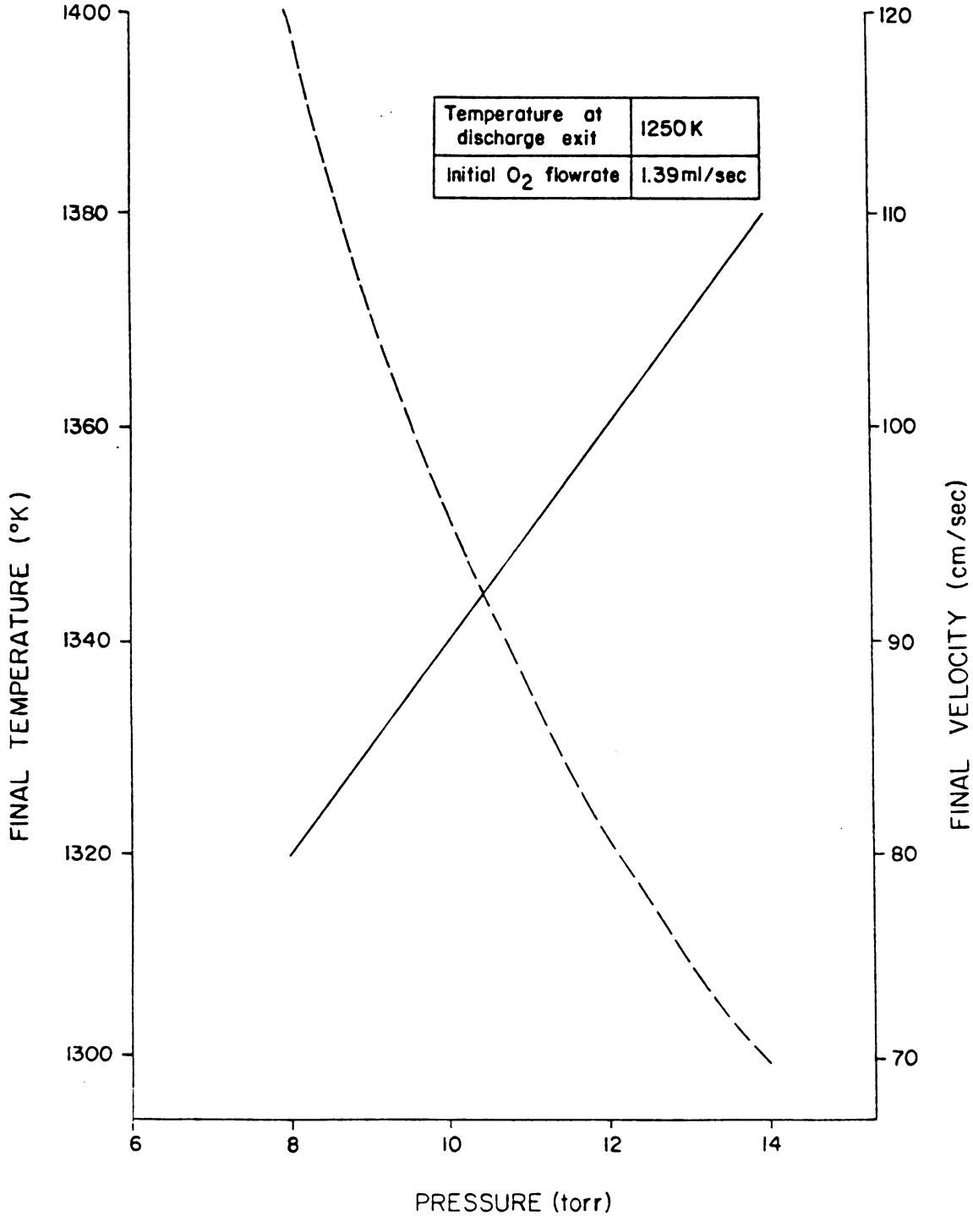

Figure 6.22 Model predictions of the final gas temperature (solid line) and velocity (dashed line) as a function of pressure.

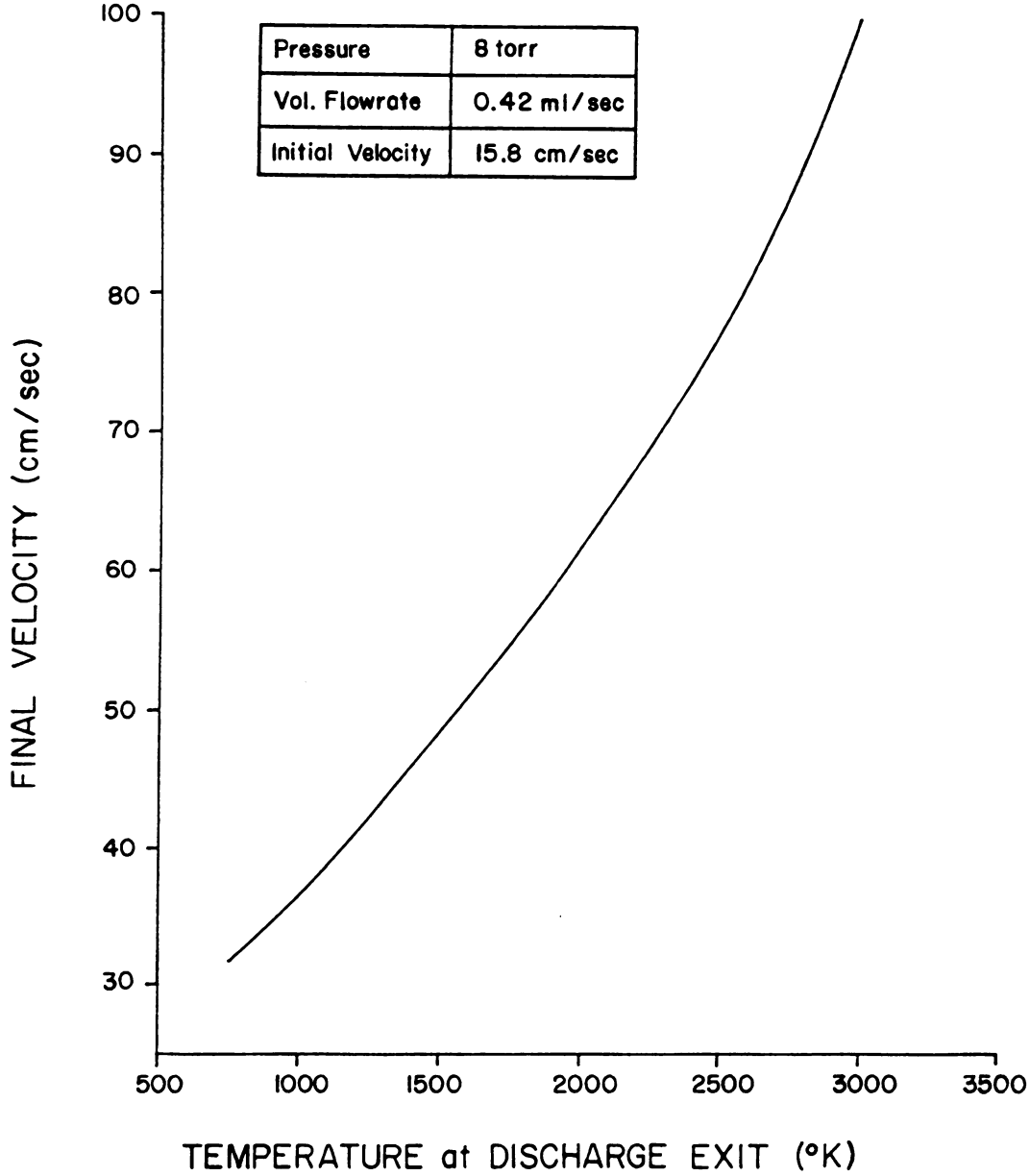

Figure 6.23 Model predictions of final velocity as a function of exit temperature.

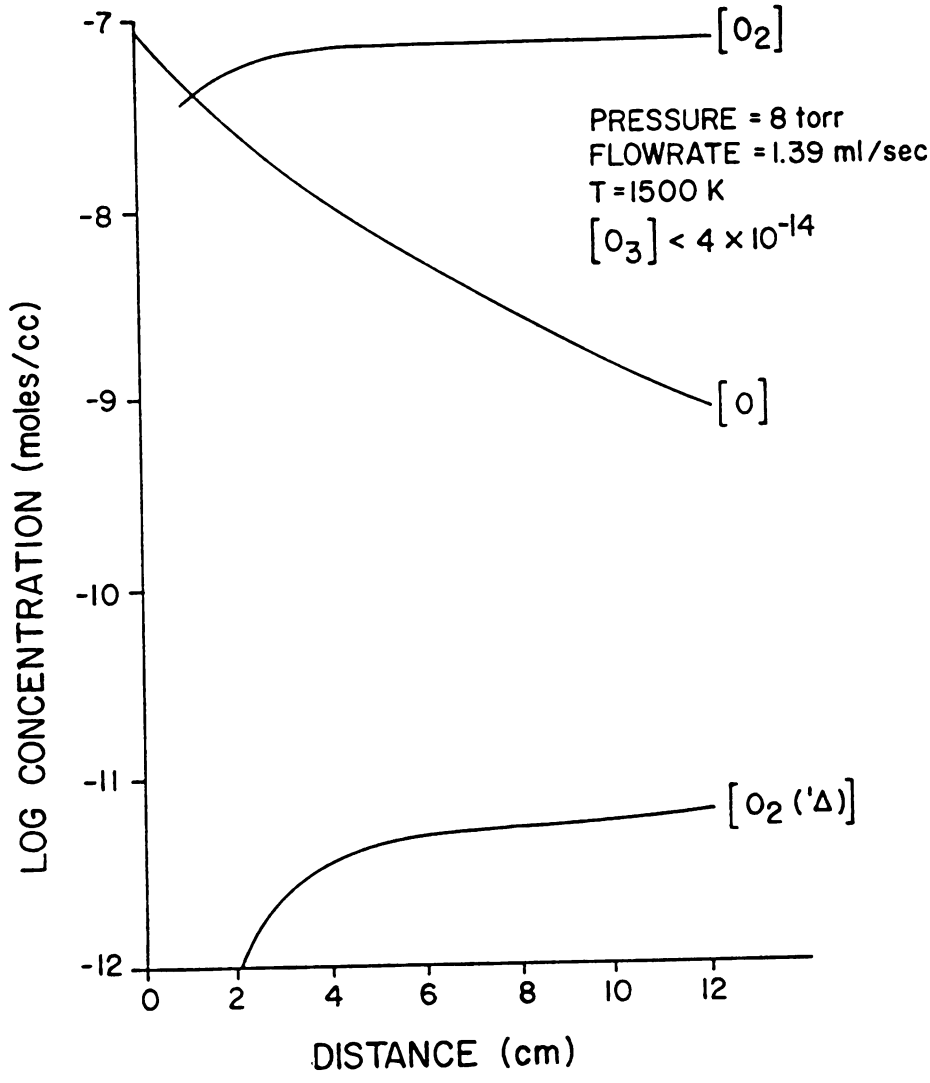

Figure 6.24 The concentrations of important species of an electrical discharge as a function of distance from the discharge.

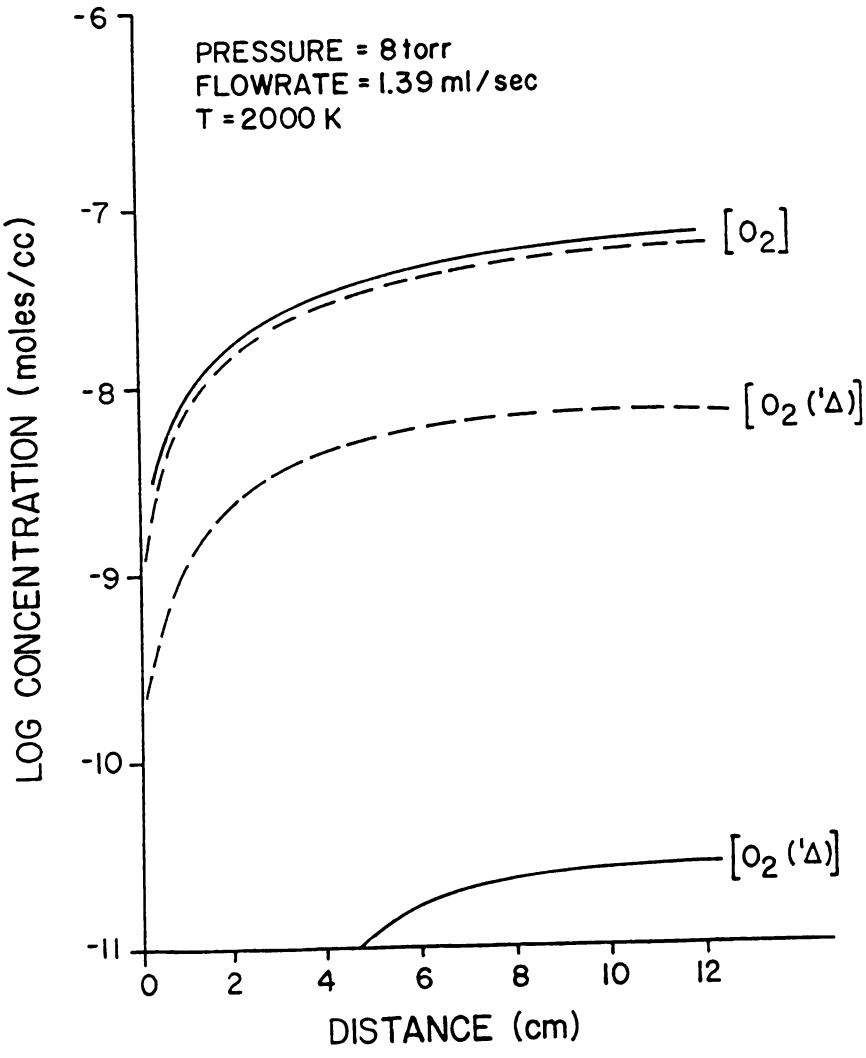

Figure 6.25 The solid lines indicate the O_2 and $O_2(^1\Delta)$ concentrations as a function of distance when all of the molecular oxygen formed by wall recombination is in the ground state. The dashed line indicates the concentrations when 30% of the wall recombination produces $O_2(^1\Delta)$.

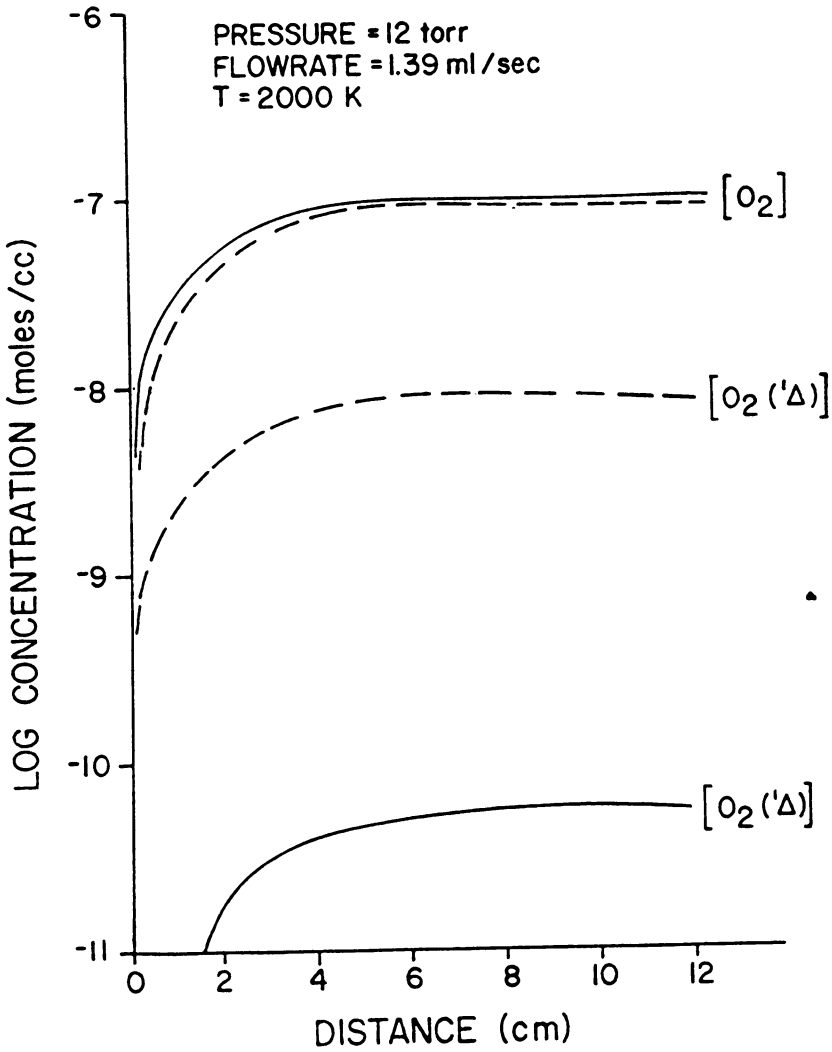

Figure 6.26 The solid lines indicate the O_2 and $O_2(^1\Delta)$ concentrations as a function of distance when all of the molecular oxygen formed by wall recombination is in the ground state. The dashed line indicates the concentrations when 30% of the wall recombination produces $O_2(^1\Delta)$.

(at 12 torr) of the total O_2 population was in the $O_2(^1\Delta)$ state. For a temperature of 2000 K, a maximum of 15% (at 8 torr) and 10% (at 12 torr) occurred very near the exit of the discharge (less than 2 cm). Thus, the concentration of $O_2(^1\Delta)$ could be large at low pressures and large temperatures, if O atoms recombine into electronically excited states at the wall.

CHAPTER VII

CONCLUSIONS

7.1 Conclusions

A one dimensional comprehensive model which predicts species concentrations, temperature and velocity profiles by solving the conservation of mass, momentum and energy equations can accurately predict the results of NO_2 titration of oxygen atoms produced in a microwave discharge as a function of distance. The assumptions used in the model based upon experimental evidence in this and other experiments includes negligible viscous pressure drop and negligible radial and axial diffusion, such that the gas remains in an homogeneous mixture throughout each cross sectional area.

The important neutral chemical kinetic mechanisms for oxygen which has interacted with a microwave discharge, as well as the probable rate coefficients of these reactions have been determined from computer modeling and comprehensive literature reviews. The most important mechanisms were found to be three body recombination and wall recombination. The oxygen atom lifetime was found to depend upon pressure and degree of dissociation as well as

the presence of $O_2(^1\Delta)$ and ozone. The presence of $O_2(^1\Delta)$ and $O(^1D)$ was found to have a negligible effect on the oxygen atom lifetime.

By matching the predictions of the computer model for oxygen atom concentrations as a function of distance to chemical titration results, it was found that the exit temperature was between 1000K and 2000K. It was also found that an increase in flowrate, temperature and power and a decrease in pressure would increase the amount of O atoms observed at a fixed point downstream of the discharge. The model also predicts that the final equilibrium state of the gas has a higher temperature and velocity than the initial equilibrium state. There is a very slight post discharge temperature increase due to the stored chemical energy released when the oxygen atoms recombine into molecules, but the majority of the temperature increase occurs in the discharage due to neutral gas heating. The velocity is largest at the exit plane of the discharge where the mass per particle is small and the temperature is large. The velocity decreases as the atoms recombine, resulting in a velocity smaller than at the exit plane but larger than the initial velocity.

A microwave plasma could be used for space-craft propulsion, but not for the reasons given in the intial "Free Radical Propulsion" concept. Neutral gas heating is

the main mechanism which increases the energy of the gas, not energy stored in the chemical bonds as originally proposed. "Electro-thermal Propulsion" has been suggested as a more appropriate label. Ongoing studies at National Aeronautics and Space Administration - Lewis Research Center in Cleveland and Michigan State University are examining the efficiency of this device and the amount of thrust a microwave discharge is likely to produce.

The comprehensive model developed in this thesis can be used in any application of an oxygen microwave discharge. The model is general enough that the many input parameters such as pressure, temperature and species concentrations can be varied until a desired output is obtained which maximizes the performance for a particular application. For example, a maximization of the overall momentum increase will determine the feasability of using an oxygen microwave discharge for spacecraft propulsion or maximization of the $O_2(^1\Delta)$ concentration will determine if threshold can be achieved in an $O_2(^1\Delta)$ - Iodine laser. The overall layout of the model is general enough that the chemical kinetics of the model can be modified so that the results of any gas exiting a discharge can be examined. For example, inclusion of nitrogen kinetics can be made to examine the processes of atmospheric plasmas.

Computer modeling can examine specific parameters and

processes which are difficult if not impossible to measure experimentally. Input conditions can be varied and a variety of experiments can be simulated efficiently and inexpensively, and then only a few specific experiments need to be made to check the performance of the model. In conclusion, theoretical modeling of plasmas can lead to a better understanding of the often elusive internal mechanisms of the plasma.

7.2 Recommendations for Future Work

The next step in the computer modeling of the chemical kinetics of an oxygen plasma is to include ion-electron reactions to the neutral kinetics model. (See Appendix E for a list of possible reactions.) The important kinetic mechanisms in the plasma itself can then be examined. However, information regarding the electron temperature and electron density becomes necessary. If argon and hydrogen are added to the oxygen plasma in trace amounts, it may be possible to measure the electron density and electron temperature using spectroscopic techniques (see Appendix D).

Another interesting modeling study is to examine other simple molecules such as nitrogen and hydrogen in similar neutral kinetic models and experiments. The similarities

between oxygen plasmas and other diatomic plasmas can then be assessed.

An ambitious project in the computer modeling of the neutral chemical kinetics of an oxygen plasma is to include two dimensional (r,z) variation in density and temperature, as well as radial and axial diffusion terms. Heat conduction and convection terms can then be included in the conservation of energy and momentum. More accurate assessments of the energy loss mechanisms can then be made. The major drawback to this recommendation is that the computer runs will become very expensive. The integrating routines EPISODE and LSODI involve matrix inversions and each added differential equation makes each step of the integrator more complex. Therefore, some simplifications may have to be made to a two dimensional model.

There are several experimental studies which can be made to check some of the predictions of the computer model. The placement of a thermocouple downstream of the discharge, past the point of total recombination, will yield the thermal equilibrium temperature of the gas. The magnitude of this temperature will indicate the degree of heat transfer outside of the discharge. Addition of argon to the oxygen plasma and measurement of the argon electronic temperature may lead to information regarding the neutral gas and electron temperatures, particularly if

an independent measurement of the electron temperature can be made, for example with electrical probes.

Another interesting experiment would be to use a well filtered microwave source and examine the oxygen atom concentration of plasmas generated in a specific electromagnetic mode. The predicted electromagnetic modes were not observed in this experiment due to the fact that the microwave oven is not a filtered source. With a filtered source, it may also be possible to sustain the discharge at much higher pressures. Titration measurements at pressures higher than 20 torr and lower than 1 torr can be compared to predictions of the computer model. The range of validity of the model can then be determined.

APPENDIX A

APPENDIX A

Suggested Rate Coefficients for the Neutral Kinetics of an Oxygen Discharge

Reaction	Forward Rate (mole, cc, sec)	Equilibrium Constant
1. $O + O_3 \rightarrow O_2 + O_2$	$1.3\times10^{13} e^{(-2.34\times10^{3}/T)}$	$1.4\times10^{2} T^{-0.57} e^{(4.7\times10^{4}/T)}$
2. $O + O_3 \rightarrow O_2(^1\Delta) + O_2$	0.0	
3. $O_2(^1\Delta) + O_3 \rightarrow 2O_2 + O$	$3.6\times10^{13} e^{(-2.85\times10^{3}/T)}$	$1.1\times10^{4} T^{-0.68} e^{(-1.4\times10^{3}/T)}$
4. $O_2(^1\Delta) + O_2 \rightarrow O_2 + O_2$	$1.36\times10^{4} T^{0.8}$	$1.5e^{(1.14\times10^{4}/T)}$
5. $O_2(^1\Delta) + O \rightarrow O + O_2$	$8.1\times10^{5} T^{0.8}$	$1.5e^{(1.14\times10^{4}/T)}$
6. $O + O + O \rightarrow O_2 + O$	$2.25\times10^{17} T^{-0.5}$	$2.3\times10^{-3} T^{0.36} e^{(6.0\times10^{4}/T)}$
7. $O + O + O_2 \rightarrow O_2 + O_2$	$6.25\times10^{17} T^{-0.5}$	$2.3\times10^{-3} T^{0.36} e^{(6.0\times10^{4}/T)}$
8. $O + O_2 + O_2 \rightarrow O_3 + O_2$	$3.0\times10^{13} e^{(4.47\times10^{2}/T)}$	$1.0\times10^{-5} T^{0.98} e^{(1.3\times10^{4}/T)}$

Appendix A continued.

Reaction	Forward Rate (mole,cc,sec)	Equilibrium Constant
9. $O + O_2 + O_3 \rightarrow O_3 + O_3$	$6.0 \times 10^{13} e^{(3.0 \times 10^2/T)}$	$1.0 \times 10^{-5} T^{0.98} e^{(1.3 \times 10^4/T)}$
10. $O \rightarrow \frac{1}{2} O_2$	5.0×10^{-4}	
11. $O_2(^1\Delta) \rightarrow O_2$	2.0×10^{-5}	

APPENDIX B

APPENDIX B

EQUILIBRIUM CONSTANT DETERMINATION

In the computer modeling of any system containing chemical kinetics, both the forward rate constant and the backward rate constant must be known. For example, in the reaction $A_1 + A_2 = B_1 + B_2$, the rate constants must be known to determine the time derivatives

$$\frac{dA_1}{dt} = [B_1][B_2]k_b - [A_1][A_2]k_f \qquad (B1)$$

Usually one of the rate constants can be found in the literature, or measured experimentally. The other rate constant can be determined from the equilibrium constant through the following expression

$$K_{eq} = k_f/k_b = \frac{[B_1]\,[B_2]}{[A_1]\,[A_2]} \qquad (B2)$$

The equilibrium constant can be determined by using the relation[88]

$$\ln K_{pr} = \frac{1}{RT} \sum_i \nu_{ri} H_i + \frac{1}{R} \sum_i \nu_{ri} S_i \qquad (B3)$$

where K_{pr} is related to K_{eq} by $K_{pr} = (RT)^{\nu_{ri}} K_{eq}$, H_i and S_i are the temperature dependent heats of formation and entropies, ν_{ri} is the difference in the stoichiometric coefficients ($\beta_{ri} - \alpha_{ri}$), R is the universal gas constant and T is the temperature. Once a list of K_{eq} vs T is generated, the functional form of K_{eq} can be determined by fitting an assumed functional form to the generated K_{eq}'s. The Arhhenius form of $AT^B e^{-C/T}$ is most often used. The constants A, B and C are the parameters to be fit. A kinetics program NEST[88] from the Aerospace Corporation uses three temperatures to generate three K_{eq}'s to determine A, B and C in a 3x3 matrix. However, small errors in equation (B3) can lead to large errors in A, B and C due to the exponential nature of the Arhhenius form, so it is more accurate to fit many points rather than three. Appendix A lists the equilibrium constants for several reactions using a 40 point fit. The value of $\ln(K_{eq})$ was calculated every 100 K starting at 100 K and ending at 4000 K. The enthalpies and entropies are listed every 100 K in the JANAF tables.[68]

The K_{eq} can be determined for reactions involving electronically excited species by first computing K_{eq} for

the reaction involving only ground state species and then using (B2) and assuming a Maxwellian distribution to determine the correction factor. For example, for the reaction $O_2(^1\Delta) + O_3 = 2O_2 + O$

$$K_{eq} = \frac{[O_2]^2 [O]}{[O_2(^1\Delta)][O_3]} \qquad \text{(B4)}$$

Multiplying and dividing by O_2 gives

$$K_{eq} = \frac{[O_2]^2 [O]}{[O_2][O_3]} \times \frac{[O_2]}{[O_2(^1\Delta)]} \qquad \text{(B5)}$$

but noting that the first product is just K_{eq} for $O_2 + O_3 = 2O_2 + O$

$$K_{eq} = K_{eq}(\text{ground}) \frac{[O_2]}{\frac{1}{[O_2(\Delta)]}} \qquad \text{(B6)}$$

Assuming a Maxwellian distribution where

$$\frac{O_2(^1\Delta)}{O_2} = \frac{g_{excited}}{g_{ground}} e^{-E/kT} \qquad \text{(B7)}$$

where E is the energy of the excited state and g is the degeneracy factor. Thus the equilibrium constant is now $K_{eq} = K_{eq}(\text{ground})e^{E/kT}$ or in other words $K_{eq} = AT^B e^{D/kT}$ where D = E - C, where A, B and C are the values found for the ground state equilibrium constant.

APPENDIX C

APPENDIX C

ACCURACY OF NITROGEN DIOXIDE TECHNIQUE

The use of NO_2 titration for determination of oxygen atom concentration is a widely used technique. However, there is some question as to the accuracy of this method. This titration technique requires that

$$O + NO_2 = NO + O_2 \qquad (C1)$$

is much faster than the reaction which produces the characteristic "green glow"

$$O + NO = NO_2 + h\nu \qquad (C2)$$

and much faster than any other mechanisms which could deplete the O atom concentration at the point of titration. Ideally, when the oxygen atom concentration exactly equals the nitrogen dioxide concentration, reaction (C1) completely depletes the O atom concentration, very quickly removing any atoms which might react with the much slower reaction (C2). Thus the "green glow" is extinguished at this point. However, if other reaction mechanisms such as

$$NO + O + O_2 = NO_2 + O_2 \qquad (C3)$$

$$O + O + M = O_2 + M \qquad (C4)$$

$$O = 1/2\ O_2 \ (wall) \qquad (C5)$$

deplete the O atom concentration at a comparable rate to that of reaction (C1) at the point of titration, the one to one correspondence between the NO_2 flowrate needed to extinguish the glow and the actual O atom flowrate cannot be made.

The depletion of oxygen atoms at any particular point downstream of the electrical discharge in the presence of NO_2 can be found by simultaneoulsy solving the following four differential equations:

$$\frac{d[O]}{dt} = -k_1[O][NO_2] - k_2[NO][O] - k_3[NO][O][O_2] - k_4[O][O][M] - k_5[O] \qquad (C6)$$

$$\frac{d[NO_2]}{dt} = -k_1[O][NO_2] + k_2[NO][O] + k_3[NO][O][O_2] \qquad (C7)$$

$$\frac{d[NO]}{dt} = k_1[O][NO_2] - k_2[NO][O] - k_3[NO][O][O_2] \qquad (C8)$$

$$\frac{d[O_2]}{dt} = k_4[O][O][M] + 1/2\, k_5[O] \qquad (C9)$$

In the above equations the k_i's represent the forward reaction rates and M of reaction (C4) is assumed to be either O or O_2. It is also assumed that the back rates are very small and can be neglected. Note that $d[O]/dt = d[NO_2]/dt$ if all terms in the right hand sides of equations (C6) and (C7) are very small compared with $k_1[O][NO_2]$.

The set of differential equations was solved using a gas temperature of 300 K and the following rates, also evaluated at 300 K:

Reaction	k_f (mole, cc, sec)	Reference
1	$1.95\times10^{13}\ \exp(-533/T)$	82
2	1.5×10^{7} (300 K)	83
3	$1.44\times10^{15}\ \exp(971/T)$	82
4a M=O	$2.25\times10^{17}\ T^{-0.5}$	Chapter 6
4b M=O_2	$6.25\times10^{17}\ T^{-0.5}$	"
5	$1.0\ T^{-0.5}$	"

Reaction (C2) was neglected and γ, the wall recombination coefficient for reaction (C5) was 5×10^{-4}. If titration is

valid at 300 K, it will also be valid at higher temperatures (as long as wall recombination is not large at the titration point), because reaction (C1) increases with temperature and reaction (C3) and (C4) decrease with temperature. (The wall effects were checked for T=1000 K and it was found that the wall reaction was always two orders of magnitude smaller than reaction (C1) regardless of where titration occurred.)

As can be seen by figures C1 and C2, reaction (C1) dominates the kinetic mechanisms at the titration endpoint especially for lower pressures and small amounts of atoms (indicated by a ratio of O_2/ O). The time for depletion of O atoms to 1% of its original value is in the millisecond range. However, it takes longer for the O atoms to become depleted by reaction (C1) when attempting to titrate large numbers of oxygen atoms. Thus, based on kinetic considerations alone, the titration technique should be most accurate near the exit of the discharge when the O_2/O ratio is small and less accurate downstream of the discharge where the O_2/O ratio is large.

The accuracy of NO_2 titration with respect to flowrate is difficult to ascertain. Clyne[74] points out that titration will overestimate the O atom concentration when the NO_2 flowrate is high because the time scale of the reactions at the titration endpoint and the time scale of

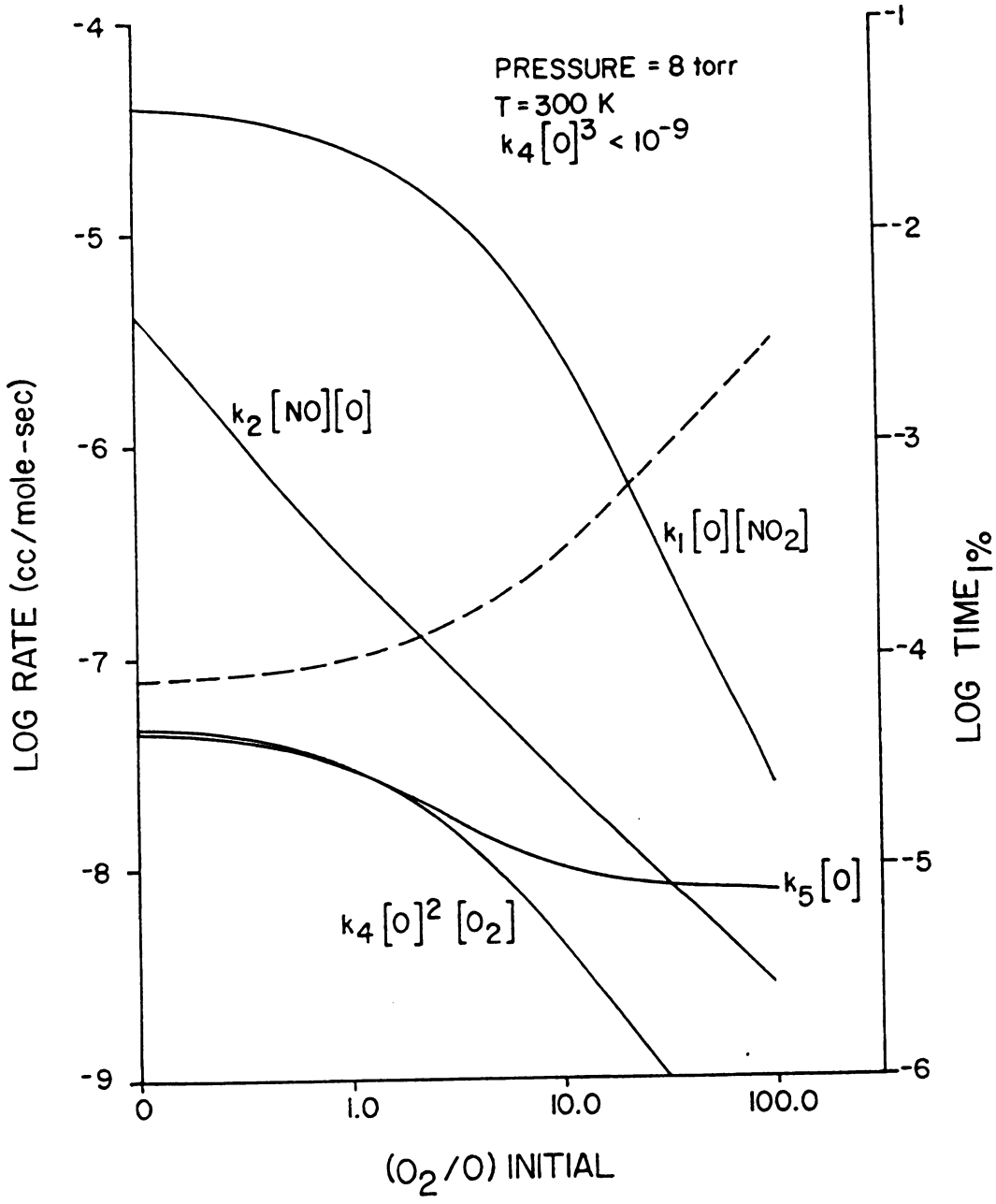

Figure C1 The net reaction rates as a function of initial O_2/O ratio. The dashed line indicates the time to deplete the O atom concentration to 1% of its initial concentration as a function of initial O_2/O ratio.

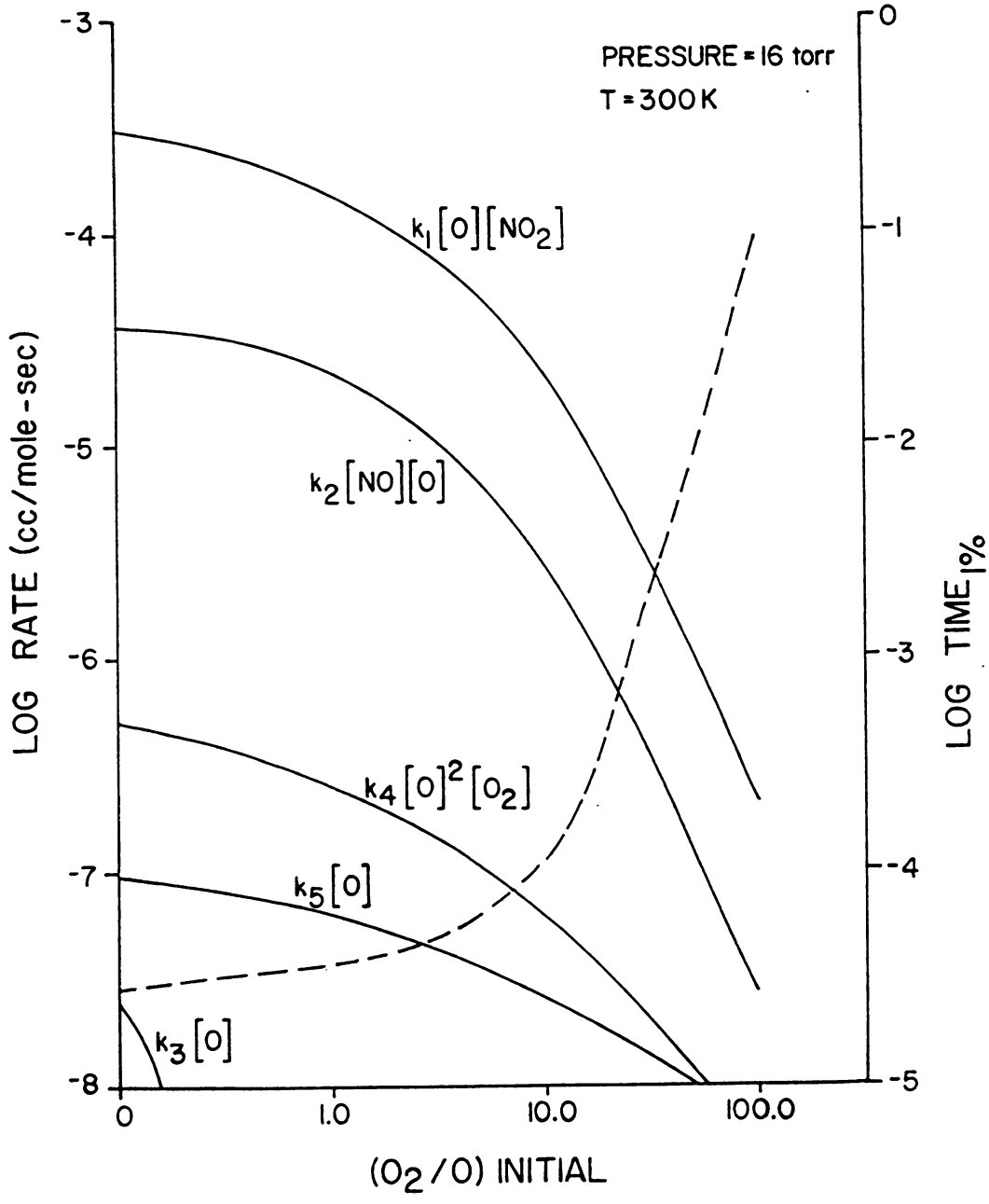

Figure C2 The net reaction rates as a function of intial O_2/O ratio. The dashed line indicates the time to deplete the O atom concentration to 1% of its initial concentration as a function of initial O_2/O ratio.

the system will become equal. Clyne also comments that NO_2 titration will not be accurate when the concentration is low because, as seen in Figures C1 and C2, other mechanisms become important.

Mearns and Morris[89] on the other hand, conclude that fast flowrates of initial O_2 give more accurate titration measurements than slow flowrates. If the NO_2 flowrate is known to within a fixed uncertainty, larger flowrates will have a small fractional error. However, for the experiment described in this paper, the flowrate of NO_2 was not measured with a flowmeter but by observing the increase in pressure, with respect to time, of the NO_2. The pressure increase was monitored with a Heise gauge and a stop watch. For very high titrant flowrates, such as those needed near the exit of the discharge where the O atom concentration was highest, the pressure increase was so rapid, it was difficult to measure the instantaneous pressure. Thus, the accuracy of measuring O atoms based upon flowrate considerations appears to improve downstream where slower flowrates of NO_2 are used, but not so far downstream that the O atom concentration is too small.

In conclusion, the accuracy of NO_2 titration is dictated by 1) the O atom concentration, 2) the pressure and, 3) both NO_2 and initial O_2 flowrates. If the oxygen atom concentration is low, or the pressure high, kinetic

mechanisms other than reaction (Cl) can be important and there will no longer be a one-to-one correspondence between the NO_2 concentration needed to extinguish the glow and the oxygen atom concentration. This effect can also be present for small initial molecular oxygen flowrates. If the initial molecular flowrate is high however, the time scale of the flowing system approaches the time scale of the kinetics at the titration endpoint. Thus, it is best to titrate at pressures lower than 16 torr for "medium" initial O_2 flowrates. Also, it is best not to titrate too closely to the exit of the discharge where very fast NO_2 flowrates are needed, nor too far from the discharge where the oxygen atom concentrations are small. The experiment described here was performed with these considerations in mind.

APPENDIX D

APPENDIX D

SPECTROSCOPIC MEASUREMENTS

D.1 Introduction

To correctly model the kinetic processes of a microwave initiated plasma, several parameters such as electron density, electron temperature, gas temperature and species concentrations must be known. There are many diagnostic techniques commonly used to determine these important parameters but in general they are difficult to perform and the technique can perturb the plasma. Emission spectroscopy is a valuable and effective diagnostic tool because it does not distort the electric or magnetic fields of the plasma and many useful plasma parameters can be determined from the same experimental configuration. Emission spectroscopy has been used for many years and there are many excellent references describing both the applications and limitations of the method, as well as suggesting experimental configurations.[1,90-96]

In this appendix, three experiments are described which use emission spectroscopy to identify species and to determine three important plasma parameters; the average

electron density, the electron temperature, and the average wall temperature.

D.2 Species Identification

Emission spectra of oxygen and argon plasmas were observed for the experiments described in the next three sections. In oxygen, the only lines observed at pressures of 2 torr and above were atomic neutral lines as well as two hydrogen lines H_β (4861Å) and H_α (6563Å). The most prominent lines are listed in Table D1. At pressures below 2 torr, a molecular spectrum was observed. This molecular spectrum was identified as the electronic transition $^4\Sigma - {}^4\Pi$ of O_2^+. Many rotational branches of several vibrational bands were observed. Due to the complexity of electronic molecular spectra, only a few rotational lines were identified. (See Section D.5)

Emission spectra of several argon plasmas were also collected. As in the case of oxygen, the only lines observed were neutral atomic transitions, (see Table D1) as well as H_α, H_β and an oxygen atom triplet.

At no time were any atomic ions observed in either the argon or oxygen plasmas. As will be explained in the next section, the electron density was between 10^{13} and 10^{14} electrons/cc, compared to neutral densities of 10^{16} to

Table D.1 List of Observed Neutral Lines in O_2 and Ar Plasmas

Oxygen Atom Lines:	4368 Å	6046 Å
	5022 Å	6157 Å
	5329 Å	6455 Å
	5437 Å	7157 Å
	5577 Å	7254 Å
Argon Atom Lines:	4164 Å	7948 Å
	4200 Å	8006 Å
	6965 Å	8015 Å
	7067 Å	8104 Å
	7272 Å	8115 Å
	7383 Å	8264 Å
	7504 Å	8408 Å
	7515 Å	8425 Å
	7636 Å	8521 Å
	7724 Å	

10^{18}. Therefore, the ion density is between 10^{-3} and 10^{-4} times smaller than the neutral density, and it would be expected that the ion emission would be very low for this case.

D.3 Stark Broadening

D.3.1 Introduction

By definition, a plasma contains both free electrons and ions even though the majority of a weakly ionized gas is composed of neutral species. The ions and electrons create localized electric fields around the neutral species. There is a coupling between the energy of these localized electric fields and the energy of the atoms and molecules, depending upon the orbital angular momentum of the atom or molecule, which causes a splitting of each line emitted by the radiating atom or molecule. This splitting of each line by an electric field is called the Stark effect. (See Schiff[97] or Merzbacher[98].) The spacing of each component of each emitted line depends upon the magnitude of the applied electric field. In a plasma however, the ions are at different distances from each atom or molecule, so the applied electric field seen by each atom and molecule will vary. An observed emitted line from a plasma will appear broader than normal due to the fact

that the line is composed of many lines, each of which is split by different amounts due to the Stark effect. Therefore Stark broadening is a statistical effect which depends upon the number of ions and electrons.

The dependence of the width of a Stark broadened line on electron density can be thought of in this simple way. If r_o is the radius of a sphere containing one ion and n_i is the number of ions per unit volume, $\vec{E}$ is the electric field strength and $\Delta\lambda_S$ is the full width at half height of the Stark broadened line, then

$$n_e = \frac{1 \text{ (ion)}}{(4/3\pi r_o^3)} \qquad \text{(D1)}$$

Therefore

$$r = \frac{3}{(4\pi n_e)}^{1/3} \qquad \text{(D2)}$$

From Coulombs law, where $\vec{E}$ is the electric field strength

$$\vec{E} \propto \frac{1}{r_o^2} \tag{D3}$$

So

$$\vec{E} \propto \left(\frac{4\pi n_e}{3} \right)^{2/3} \tag{D4}$$

From quantum mechanics (see Schiff[97] or Mertzbacher[98]) $\Delta\lambda \propto \vec{E}$, therefore

$$\Delta\lambda \propto n_e^{2/3} \tag{D5}$$

The theory of Stark broadening is very complicated. In depth discussions of the theory of Stark broadening can be found in References 90, 91, 93 and 94. A comprehensive literature review of Stark broadening experiments in several elements can be found in reference 99. Due to the simple nature of hydrogen, Stark broadening theory is most accurate for the hydrogen emissions lines. The second line of the Balmer series, denoted H_β , is particularly useful as an indicator of electron density because it is very sensitive to Stark broadening, which is helpful for low

electron densities, and because it occurs in the visible region of the spectrum at 4861Å.

Griem[91] suggests that the electron density can be written as

$$N_e = C(N_e, T_e)\, \Delta\lambda_S^{3/2} \qquad (D6)$$

where $\Delta\lambda_S$ is the full width at half height (fwhh) of the Stark broadened component of the emitted line and C is a coefficient which is weakly dependent upon the electron density (N_e) and the electron temperature (T_e). The values for C to be used for the H_β line are tabulated by Griem[91] and summarized in Table D.2.

TABLE D.2 Values for $C(N_e, T_e)$ for H_β

$T_{electron}$ Kelvin	C $N_e=10^{14}$	C $N_e=10^{15}$
5000	3.84×10^{14}	3.68×10^{14}
10000	3.80×10^{14}	3.58×10^{14}
20000	3.72×10^{14}	3.55×10^{14}
40000	3.76×10^{14}	3.53×10^{14}

D.3.2 Experimental Apparatus

D.3.2.1 Reactor Flow System

The microwave plasma flow system is shown in Figure D1 and is very similar to the flow system in Chapter 5. The plasma was contained in a 6 mm O.D. (4 mm I.D.) quartz tube situated coaxially with a cylindrical microwave cavity. The gas control system consisted of high purity argon and hydrogen sources, flowmeters, a back pressure monitor and several needle and bellows valves. A constant back pressure of 1400 torr was maintained up to a metering valve. Downstream from the metering valve, the gases entered the containment tube via 6 mm copper and plastic tubing and were exhausted to a 58 CFM vacuum pump via 6 mm plastic tubing and 50 mm pyrex tubing. The plasma pressure was controlled by a bellows valve located after the containment tube and the pressure was monitored with a Heise gauge. Discharges with volumetric flowrates of 0 and 5 ml/sec with pressures ranging from 50 to 1000 torr were investigated.

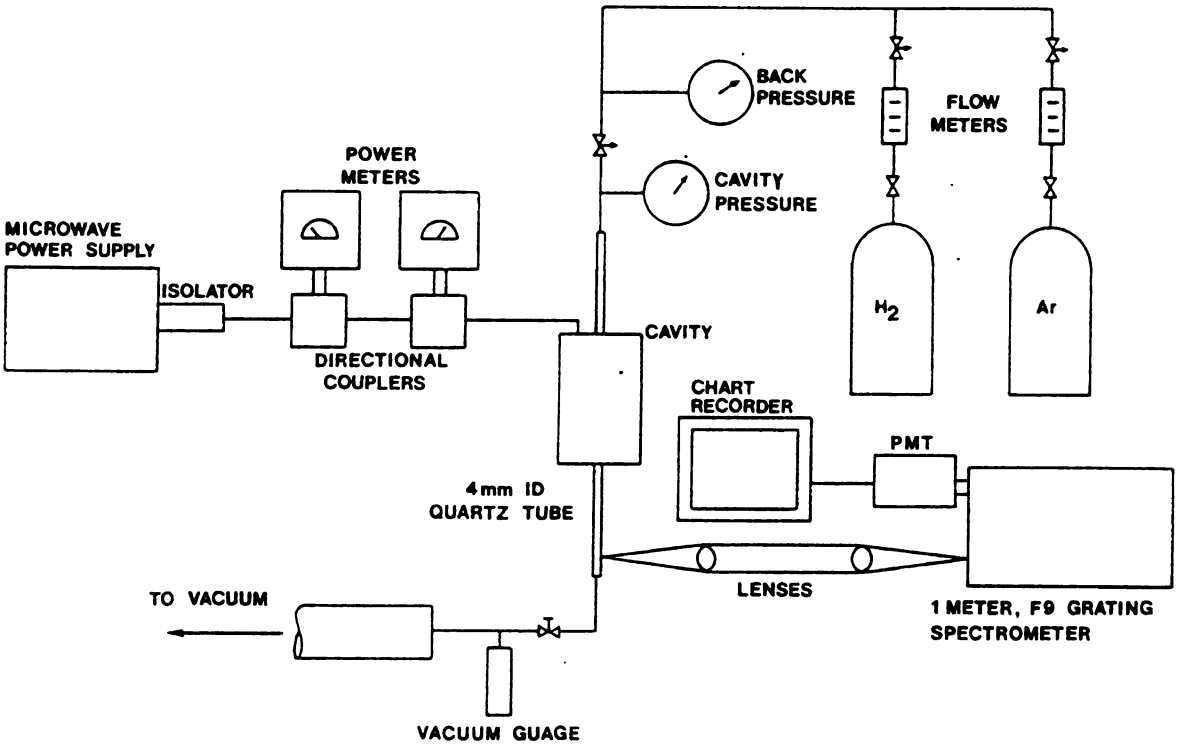

Figure D1 Experimental Apparatus

D.3.2.2 Microwave System

A 2.45 GHz filtered, variable power supply capable of delivering 130 watts of continuous power was used as a microwave power source. The magnetron was protected from reflected power by an isolator. The microwaves entered a surface wave launcher[100,101] through a directional coupler, so that incident and reflected power could be monitored simultaneously. The power absorbed by the plasma was assumed to be incident power minus reflected power times 70% to account for losses in the coaxial cable connecting the output of the directional coupler to the microwave cavity.[102] The isolator and the small coaxial cable connecting the probe (a loop) to the large coaxial cable were air cooled. The inside of the cavity was also air cooled through a screen viewing port.

The plasma was contained in a quartz tube coaxial with the 2.54 cm O.D. cylindrical copper surface wave launcher. The cavity and quartz tube were situated vertically so that the length of the plasma was centered along the length of the entrance slit to the spectrometer. The position of the probe, the length of the cavity and the position of the center conductor were varied until minimum reflected power occurred and until the plasma looked similar to those used in references 100 and 102.

D.3.2.3 Optical System

The light emitted from the plasma was gathered with two 3.7 cm diameter lenses with focal lengths of 25 cm. The first lens was placed 25 cm from the discharge and the second lens was placed 25 cm from the entrance slit to the spectrometer leaving 50 cm between the lenses. At the exit slit of a grating spectrometer (f9, 1 meter, Czerny Turner) was a high quantum efficiency photomultiplier tube (PMT). The output of the PMT was illustrated on a digital pico-ammeter and a strip chart recorder. The spectrometer, lenses and microwave cavity were aligned using a He-Ne laser situated at the exit slit of the spectrometer.

D.3.3 Results

Small amounts of hydrogen were added to the argon in an attempt to improve the signal to noise ratio of the H_β line. Due to limitations in the size of the flowtubes, the hydrogen could not be made any smaller than 2% of the incoming argon. At 38 torr and 5% hydrogen, the plasma length was shortened to 20% of the original length, without any hydrogen. Also, the plasma was not sustained at as high a pressure with the hydrogen as without the hydrogen (100 torr vs well over an atmosphere). (See Figure D2.)

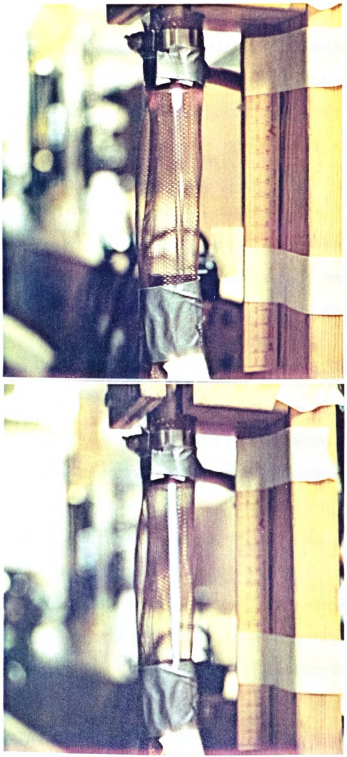

Figure D2. The top photo shows an argon plasma at 38 torr with 5% hydrogen added and the second photo shows a pure argon plasma at 38 torr.

Since this small amount of hydrogen affected the plasma, the density measurements were made without additional hydrogen. There was enough residual hydrogen in the argon bottle and the flow system, such that the H_β could be observed.

The full width at half height (fwhh) of H_β was measured for several pressures at a flowrate of 5 ml/sec and at zero flowrate. The gas temperature was assumed to be 1000 K and the Doppler profile was calculated. The Doppler contribution was assumed to be the only Gaussian contribution to the line and was "deconvoluted" from the measured line width using tables of Voigt profiles[103] (see Table D.3) The Doppler profile only accounted for a few percent of the fwhh. The remaining Lorentzian half width was assumed to be due to Stark broadening and instrument broadening. The instrument broadening was calculated by measuring the width of $Ar_{4200\ \mathring{A}}$ which has negligible Doppler and Stark broadening. The insturment broadening was found to be $0.22\mathring{A} \pm 0.02\mathring{A}$. The instrument broadening contribution was "subtracted" from the Lorentzian profile to get the Stark broadened fwhh. The electron density was then calculated using equation D6 and Table D2 assuming T_e = 10000; see Figure D3 for a sample line and Figure D4 for electron density results. The uncertainty in T_e accounts for an error of less than 1%.

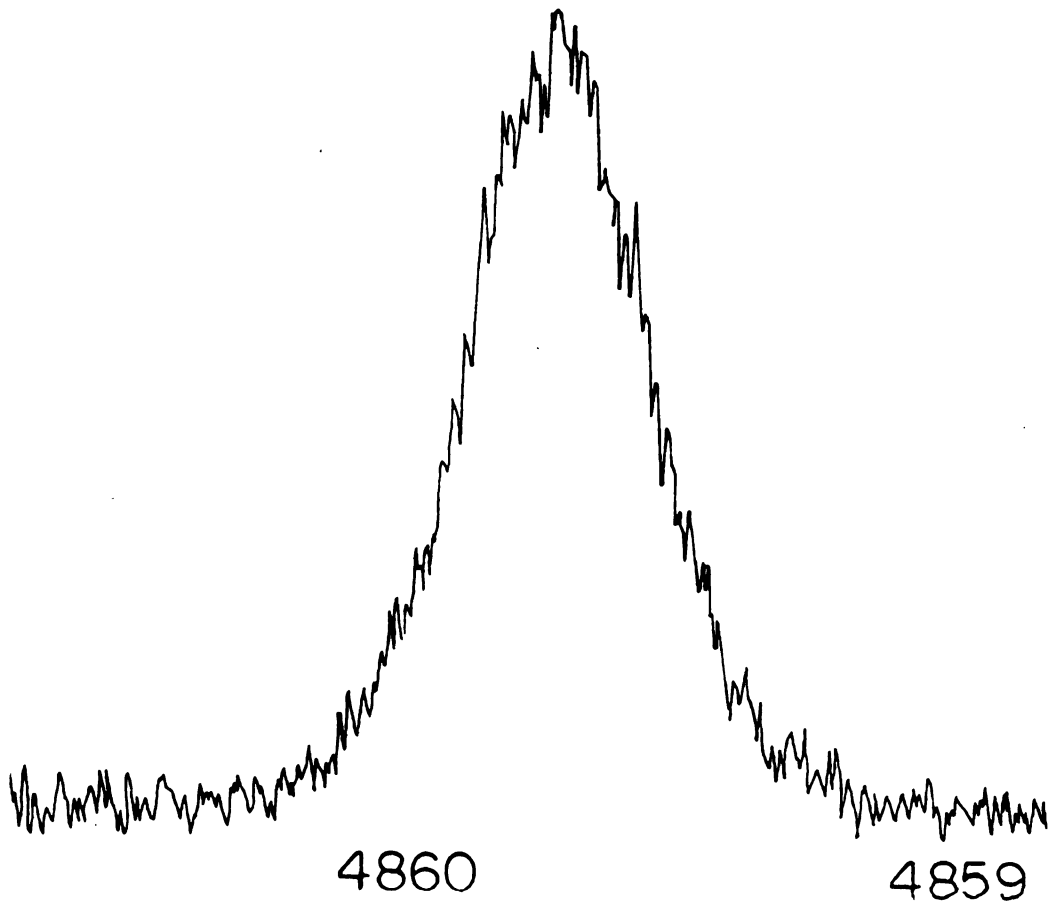

Figure D3 The line shape of H_β (4861Å).

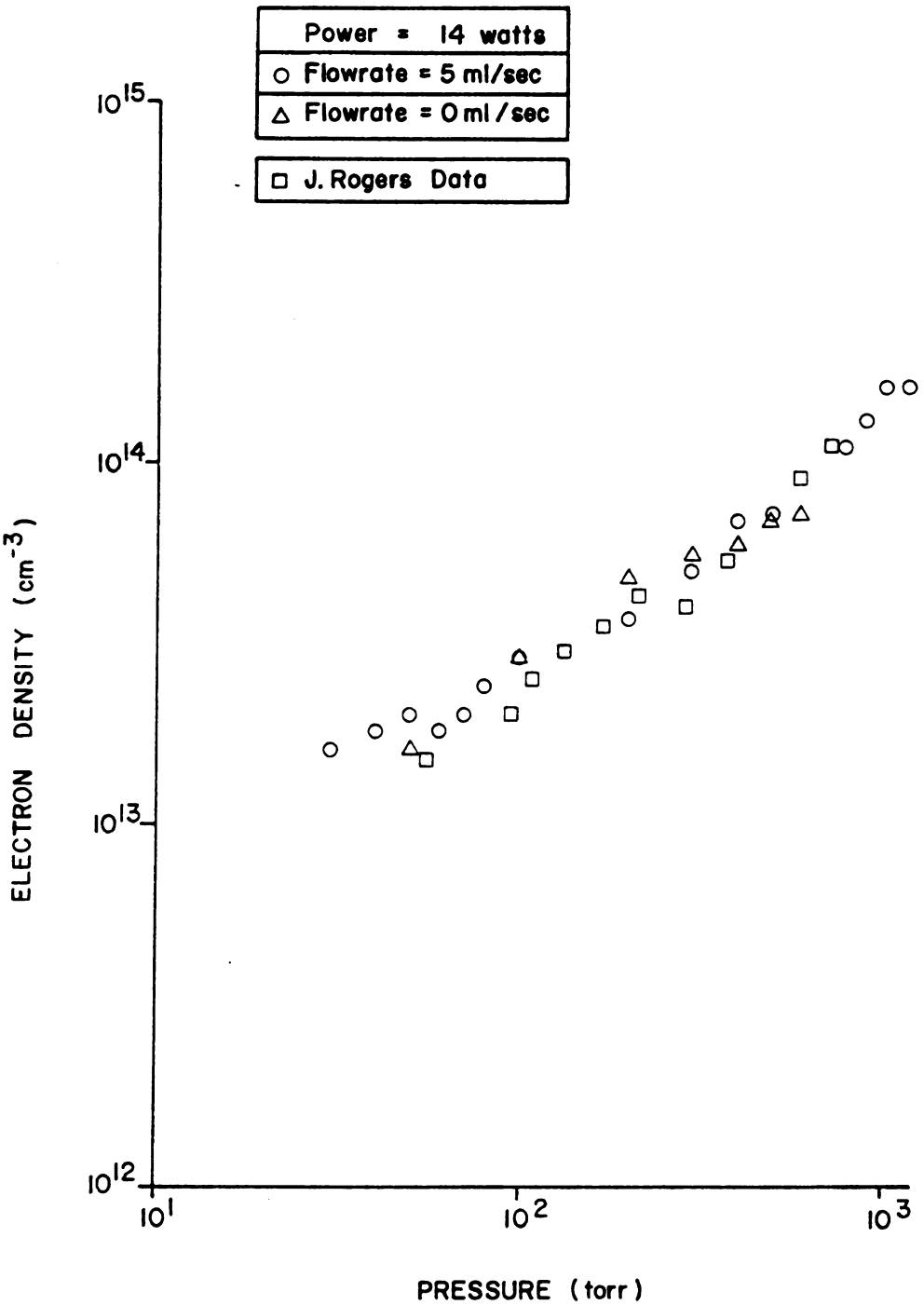

Figure D4 The electron density as a function of pressure.

Table D.3 The Half Width of Voigt Profiles[101]

Lorentzian	Doppler
Observed	Observed
0.993	0.083
0.972	0.162
0.941	0.235
0.904	0.301
0.886	0.327
0.863	0.359
0.794	0.441
0.742	0.494
0.672	0.559
0.655	0.574
0.637	0.589
0.618	0.605
0.597	0.622
0.575	0.639
0.552	0.656
0.527	0.675
0.500	0.694
0.472	0.715
0.442	0.736
0.410	0.758
0.375	0.789
0.338	0.804
0.299	0.829
0.257	0.855
0.212	0.882
0.164	0.910
0.113	0.939

A black and white photograph of the plasma was taken for each density measurement. (See Figure D5.) A ruler was placed next to the plasma so that the scale of each picture would be known. The projected area of the plasma was measured using an electronic "digitizer". The average

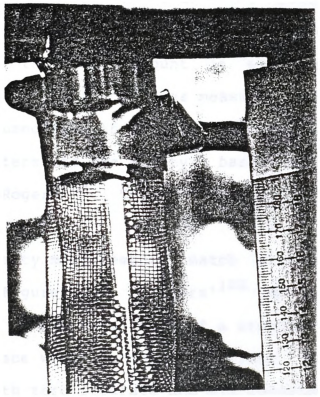

Figure D5 An example of the photographs used to determine the volume of the plasma.

radius of the plasma was found by assuming that the projected area of the plasma could be represented by a rectangle of area 2rL where r is the average radius and L is the length of the plasma, which was also measured. The volume of the plasma was assumed to be cylindrical and approximately equal to $\pi r^2 L$. The power density was estimated by assuming that the plasma extended into the cavity by the same amount it extended outside the cavity.[102] The input power was measured with power meters. It was assumed that there was a 30% drop in power between the power meters and the cavity, based upon measurements made by J. Rogers[102]. Typical results are shown in Figure D6.

The density measurements match previous data quite well (see Figure D4). Rogers'[100] data were taken from measurements of the wavelength of a standing wave produced by two surface wave launchers in series. His measurements were made with zero flowrate and his containment tube was horizontal. The measurements reported here were made with one surface wave launcher and the containment tube was in a vertical position. In spite of these differences, the data agree extremely well. Note that there is an increase in electron density with pressure and that flowrate did not affect the electron density.

A comparison of measured power density versus pressure

for this work and Reference 100, shows similar trends, (see Figure D6). However, Rogers power densities were consistently between one and one and one half orders of magnitude larger than the power density of this experiment. There could be two causes for this. The first is that there is an uncertainty in determination of the extension of the plasma into the reactor cavity. Therefore, the assumption that the plasma extended into the cavity an equal amount that it extended outside the cavity, may underestimate the power density. The other reason is that the heat transfer losses of this and Rogers' experiment were different due to the fact that this experiment was vertical where natural convection is important and Rogers' experiment was horizontal. Reference 100 (p. 57) shows that vertical plasmas have lower power densities than horizontal plasmas.

D.3.4 Error Discussion

There were several sources of errors in this experiment.

1. The signal to noise was very low with the worst ratio being 5:1.
2. At higher pressures, the signal was weak, so the most sensitive scale of the PMT had to be used. The

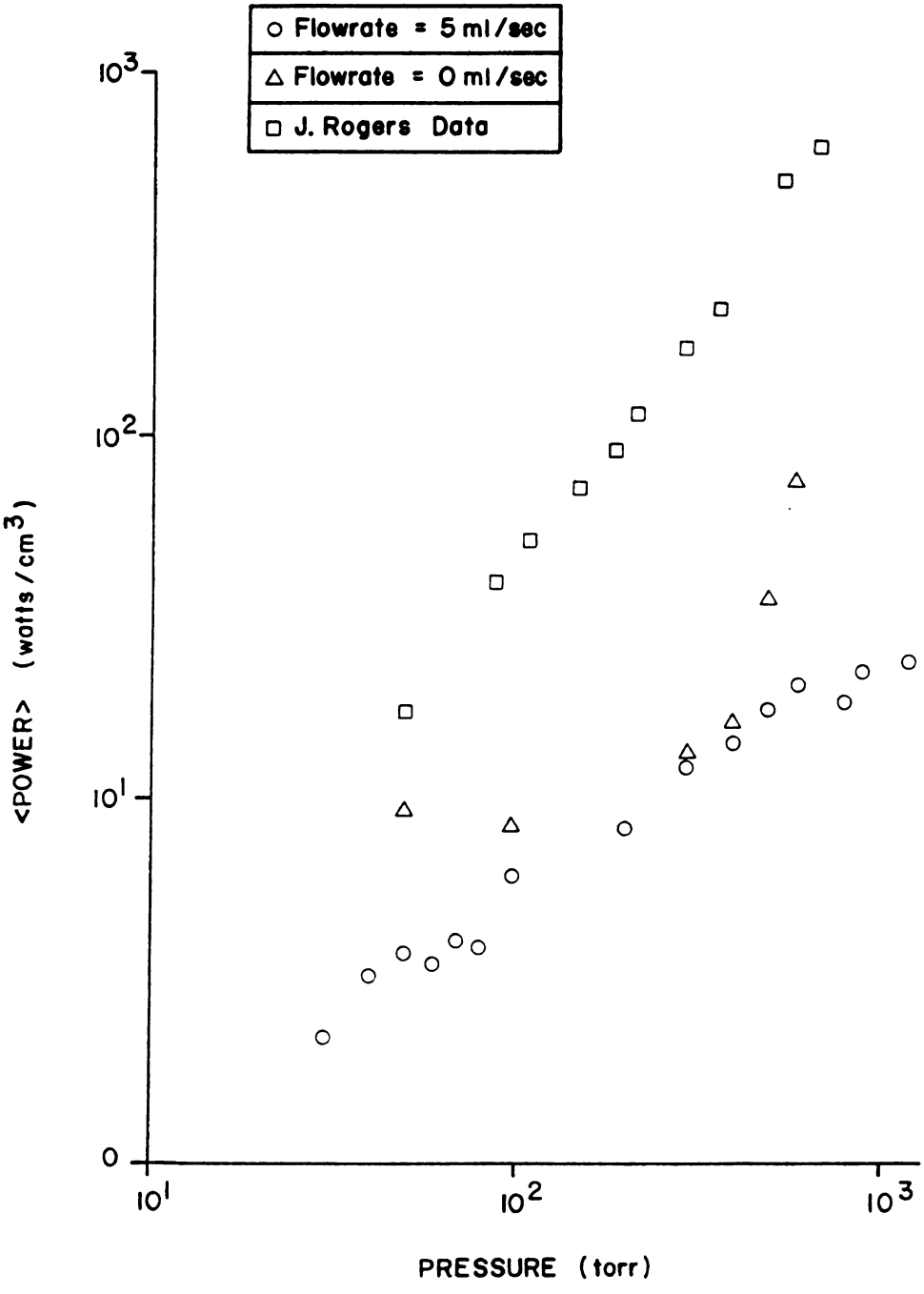

Figure D6 The power density as a function of pressure.

signal tended to be very jagged and it was difficult to determine the fwhh.

3. The resolution of the spectrometer was low, due to the fact that the slits had to be opened to increase the signal. In the worst case, the instrument function accounted for 60% of the Lorentzian line function.
4. The electron temperature was only approximately known. This uncertainty will affect the Stark broadening formula by at most one percent.
5. The gas temperature was only approximately known, so the Doppler contribution was also only approximately known. At these electron densities it could account for a few percent error.
6. The plasma was not necessarily stable from one measurement to the next. The power supply occasionally varied, causing the plasma to lengthen or contract. The plasma would occasionally flicker resulting in a slightly different plasma position.

There are also errors in the power density due to the way both the power and plasma volume were measured.

1. The boundary of the plasma was not always sharp and clearly defined. Therefore it was difficult to measure the projected area.
2. The assumption that the projected area of the plasma

is rectangular and the volume of the plasma is cylindrical may not be accurate.

3. The plasma volume contained in the cavity was not known.
4. The assumption that the input power is 70% of the power measured by the power meters may not be as accurate for this experiment as it was for Rogers' experiment.

With these errors in mind, there are several recommendations for improving this experiment.

D.3.5 Recommendations for Electron Density Measurements

The most obvious recommendation is to enhance the H_β signal, although as mentioned this has proven to be very difficult. It may be possible to enhance the H_β signal without adversely affecting the plasma by adding small amounts of hydrogen to a nitrogen plasma. However, it takes more power to sustain a plasma in a diatomic gas, so a more powerful power supply will have to be used.

If the signal of the H_β could be enhanced, a Fabry-Perot etalon could be used, and the resolution could be improved.[105] Speer er al.[106] and Kreye[107] have shown that a Fabry-Perot etalon system improves the resolution of

emitted plasma lines. In particular, Speer showed that grating spectrometers tend to overestimate the linewidth leading to overestimated electron densities. Thus it is important to improve the resolution to make sure that the electron density is not overestimated.

Ideally the plasma should be initiated using two surface wave launchers, as in Rogers' experiment. Then the electromagnetic and the spectroscopic methods of electron density determination could be compared. Also, experiments performed with vertical and horizontal plasmas could help answer the questions of heat transfer and its effect on power density. If an accurate method for determining electron and gas temperature could be found, the electron density could be known with even greater precision and fundamental questions about plasmas might be answered.

D.4 Electron Temperature

D.4.1. Introduction

A plasma is in thermodynamic equilibrium if there exists detailed balancing for every (collisional) interaction process[92] and if the collisions take place with "sufficient rapidity that the distribution (of populataion densities) responds instantaneously to any change in plasma conditions."[93] When any gas is in

equilibrium, "the populations of different energy states corresponding to internal degrees of freedom are given by Maxwell-Boltzmann distributions".[95]

$$n_i = n_o \frac{g_i}{Z} e^{-E_i/kT} \tag{D7}$$

where n_i is the density of state i (atoms/cc), g_i is the statistical weight of the state i, T is the temperature, k is Boltzmann's constant, Z is the partition function

$$Z = \sum_i g_i e^{-E_i/kT} \tag{D8}$$

and E_i is the energy of the state i

$$E_i = hc/\lambda_i \tag{D9}$$

where h is Planck's constant, c is the speed of light and λ_i is the wavelength of the transition i - j. When self - absorption is negligible, the integrated radiance of an atomic line is given by[95]

$$N_{ij} = \frac{c}{4\pi} L\, n_i A_{ij} \frac{h}{\lambda_{ij}} \quad \frac{\text{erg}}{\text{sec-cm}^2\text{-steradians}} \qquad \text{(D10)}$$

where A_{ij} is the Einstein coefficient for spontaneous emission and L is the path length. Plugging (D7) into (D10)[96] yields

$$N_{ij} = 1.582\times10^{-20} \frac{g_i A_{ij}}{Z\,\lambda_{ij}} n_o L\, e^{-E_i/kT} \quad \frac{\text{Watts}}{\text{cm}^2\text{-steradians}} \qquad \text{(D11)}$$

The temperature corresponding to the equilibrium distribution of the electronically excited states of an atom can be determined by measuring the relative populations of two or more electronic states from a neutral atom. Taking the natural logarithm of (D11) gives

$$\ln \frac{N_{ij}\lambda_{ij}}{g_i A_{ij}} = \ln \frac{Lhcn_o}{4\pi Z} - \frac{E_i}{kT} \qquad \text{(D12)}$$

If $\ln(N\lambda/gA)$ is plotted against E/k, then the negative inverse of the slope will be the temperature and the constant $\ln(Lhcn_o/4\pi Z)$ will be the y intercept.

There are two disadvantages to measuring the

temperature with this method.[95] The first is that this method is critically dependent upon the accuracy of the line intensity measurements, particularly if the energy spacing between the lines is small ($E(1) - E(2) < 0.4$ eV) as it usually is for lines used in this method. The second is that this method is very sensitive to errors in the transition probabilities. These unfortunately are large because, for example in argon, they are only known to within at most 25%.[104]

D.4.2 Experiment

The experimental apparatus used to measure the temperature representing the distribution of the atomic electronic states was like that of Chapter V with a few exceptions. The gas employed for the temperature measurements was argon and not oxygen and the power supply was the filtered 100 Watt source described in Secion D.2. The optical apparatus was identical to Section D.2.2.3. The photomultiplier tube (PMT) was calibrated with a 45 Watt quartz halogen tungsten filament lamp which had been calibrated aginst a National Bureau of Standard's source.

D.4.3. Results

The accuracy of the temperature determination from line intensities was checked by measuring the ratio of intensities of two lines which originated from the same upper state. The ratio of two line intensities is given by

$$\ln \frac{N(1)}{N(2)} = \ln \frac{g(1)A(1)\lambda(2)}{g(2)A(2)\lambda(1)} - \frac{(E(1) - E(2))}{kT} \qquad (D13)$$

When E(1) = E(2), then the ratio of the two lines will be a constant

$$\frac{N(1)}{N(2)} = \frac{g(1)A(1)\lambda(2)}{g(2)A(2)\lambda(1)} \qquad (D14)$$

Two pairs of lines (see Table D4) were measured to determine if the ratio of areas was equal to a constant. See Figure D7 for an example of an emission line. The values were corrected for the non-linearity of the spectral response of the PMT. For the 7272 Å - 6965 Å pair, the measured area ratio was 0.26 and the calculated value was 0.29 representing a 10% difference and for the 7383 Å -7067 Å pair, the measured area ratio was 2.14 and the calculated value was 2.11, representing a 1.4% difference. Under

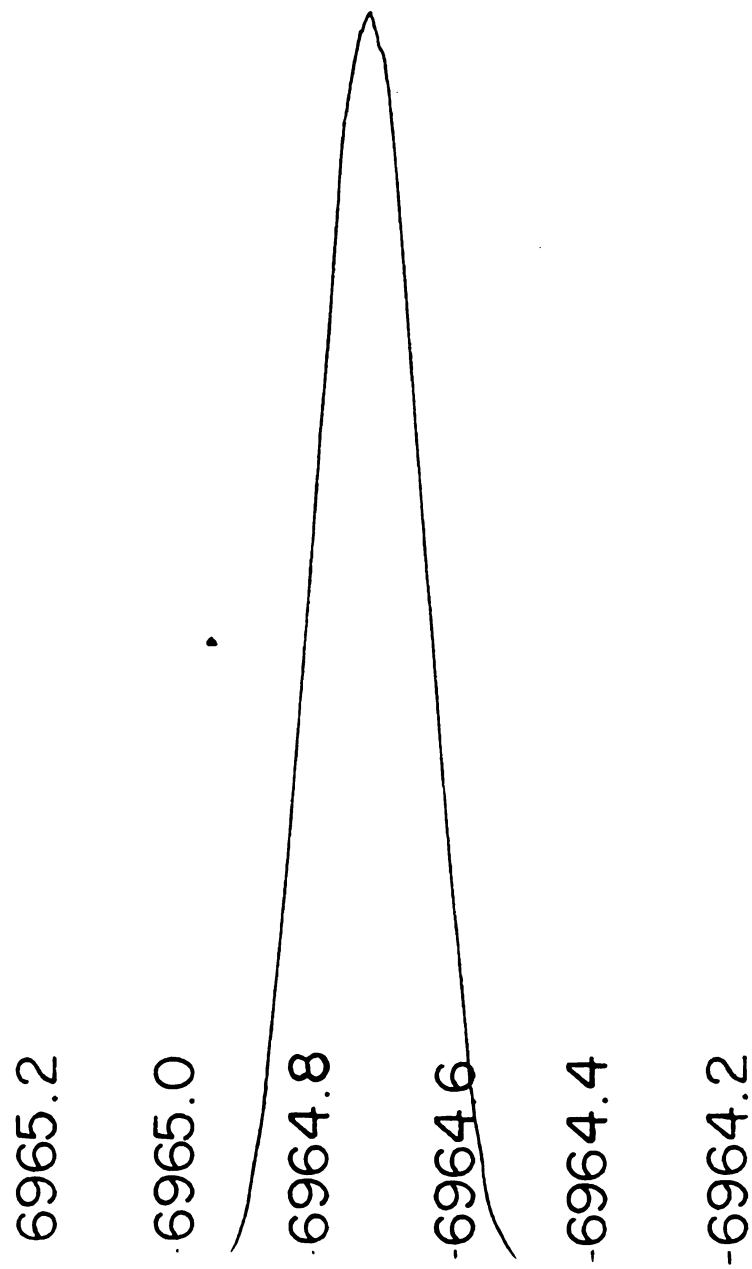

Figure D7 An example of an argon emission line.

Table D.4 Emission Lines Used to Check Experimental Method

$\overset{\circ}{(A)}$	$E_i(cm^{-1})$	g_i	$A_{ij}(cm^{-1})x10^8$
7272.93	107496	3	0.02
6965.43	107496	3	0.067
7383.98	107290	5	0.087
7067.22	107290	5	0.0395

certain circumstances, it is necessary to approximate the intensity ratio by the ratio of the line heights (see Section D.5.3). This approximation was also checked and the first pair had a height ratio of 0.27 representing a 5% difference from the calculated value and the second pair had a height ratio of 2.04, representing a 4% difference from the calculated value. The area and height measurements could be reproduced to within 10% of previous measurements. Thus, within the limits of the experiment, the line intensity technique was valid.

It is very difficult to find emission lines which have large energy spacings, which occur in the same region of the spectrum and have similar intensities such that they can be viewed on the same PMT amplification scale. Five lines were found to be suitable for an argon plasma at 6

torr. The wavelengths are given in Table D5.[104]

Figure D8 shows 5 sets of data taken at 6 torr. Each straight line represents data taken at specific spectrometer slit height and width settings as well as specific PMT settings. The average temperature of 7380 K ± 840 K was found by averaging the temperatures of the five sets of measurements.

If the electronic states are in equilibrium with the free electron gas, then the electronic temperature is the same as the electron temperature. If on the other hand, the electronic states are in equilibrium with the ground state, then the electronic temperature is the gas temperature. The equilibrium of the electronic state depends upon the collisional processes. The electronic states are in equilibrium with the electron gas if the collisional excitation, represented by

$$Ar + e \quad --- \quad Ar^* + e \qquad (D15)$$

where Ar* is the electronically excited state, is the dominating mechanism. The electronic states are in equilibrium with the gas (ground state) if the deactivation process

$$Ar + Ar^* \text{ --- } Ar + Ar \qquad (D16)$$

Table D.5 Lines used in Temperature Determination

Wavelength (Å)	E_i (cm^{-1})	g_i	A_{ij} (sec^{-1}) x 10^8
7724.21	107496	3	0.127 ± 0.032
7723.76	106087	4	0.057 ± 0.014
7635.11	106238	5	0.274 ± 0.069
7514.65	107054	1	0.430 ± 0.108
7503.87	108723	1	0.472 ± 0.118

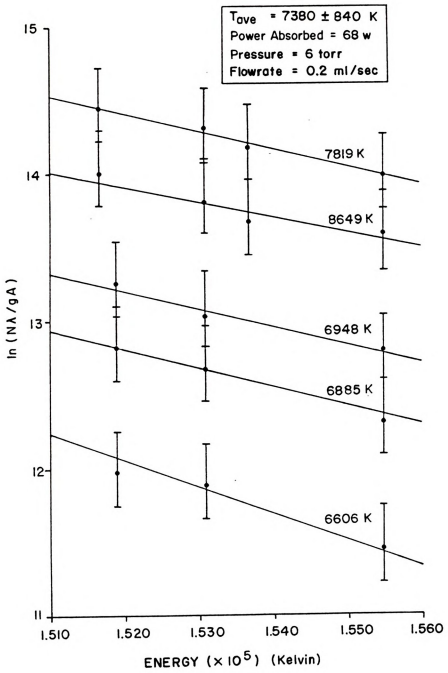

Figure D8 Temperature determination from ratios of line intensities.

is the dominating process. Further kinetic studies of argon need to be made to determine under what conditions the electronic temperature represents the electron temperature.

In a similar experiment where the quartz tube was situated vertically, Rogers'[100] (p. 99) found that the electron temperature was between 5000 and 7000 K for tubes of 1.2cm and 2.5 cm regardless of pressure. Note that the temperature measured here for a tube of 1.9 cm diameter is close to this measured range. Rogers' also found that for smaller tubes (1.5 mm and 4.0 mm) the electron temperature may increase with pressure, although his data is inconclusive.

Moison et al.[108] on the other hand, measured an excitation temperature of 3500 K for plasmas contained in 1 to 2 mm quartz tubes at atmospheric pressure and 70 Watts absorbed power. He used six lines between 4251 Å and 4345 Å to determine the electronic temperature. (These lines were too weak to detect with enough accuracy to be used in this experiment.) Moison claims that his plasma was not in thermodynamic equilibrium because his temperatures were much lower than the 7000 K required for equilibrium at an electron density of $3 \times 10^{14} cm^{-3}$ (which he measures using Stark broadening) according to the Saha equation.

Bloyet et al.[109] measures the electronic excitation

temperature in a 1 mm quartz tube at an input power of 50 Watts while varying pressure (1-2 torr) and flowrate (0 and 0.5 ml/sec). They find that there does not appear to be any correlation between pressure or flowrate and electron temperature and electron density. They report electron temperatures between 5500 K and 6500 K and electron densities between 5.3 and 8.5 x $10^{14}cm^{-3}$.

D.4.4. Recommendations for Electronic Temperatures

An analysis of the rates of the important collisional processes must be made to determine which reaction mechanisms dominate, and whether the assumption that the electronic temperature is the temperature of the electron gas is valid. Examination of the collisional rates as a function of pressure should lead to predictions of the electronic temperatures dependence on pressure. For example, the question, "do the electron collisional processes dominate at all pressures, or is there a mixture of de-excitation as well as excitation processes occurring at high pressures?" needs to be answered.

The transition rates and energies of all of the observed spectral lines of the argon plasma of this experiment need to be examined to determine which lines are most suitable for determining the electronic temperatures.

The lines need to be far apart in energy spacing and their area ratio must be sensitive to electron temperature especially at high temperatures so that small errors in the area measurements do not lead to large electron temperature errors.

If suitable lines are found, experiments need to be performed at various pressures. Measurements of plasmas in different size tubes need to be performed to compare with Rogers'[100] data. The effect of absorbed power and gas flowrate should also be examined.

D.5 Rotational Temperature of Oxygen

D.5.1. Introduction

In a plasma, there are many types of equilibrium distributions. Translational equilibrium is attained after only a few molecular collisions, and rotational equilibrium is attained soon afterwards, but vibrational and electronic relaxation may take much longer.[1] The rotational temperature may be a close approximation to the thermal temperature whereas the vibrational temperature and especially electronic temperature (see Section D.4) may be "indicative" of excitation mechanisms.

The intensity of an emitted rotational line of level J' of the lowest vibrational state is proportional to[95, 96, 110]

$$N_J \propto (J'+J'') \, e^{-BJ'(J'+1)hc/kT} \qquad (D17)$$

where J" is the lower rotational state, B is the rotational constant (cm^{-1}), h is Planck's constant, c is the speed of light, k is Boltzmann's constant and T is the rotational temperature. Taking the natural logarithm of (D17) gives

$$\ln \frac{N_J}{J'+J''+1} \propto - \frac{BJ'(J'+1)hc}{kT} \qquad (D18)$$

If a plot is made of $\ln(N/J''+J''+1)$ versus $-BJ'(J'+1)hc/k$, the slope will be the inverse of the rotational temperature.

D.5.2. Experiment

Emission spectra of oxygen were observed in the experiment described in Chapter V. The image of the plasma was produced at the slits of the spectrometer using one 16 cm focal length lens[76] placed 32 cm from the plasma and 32 cm from the entrance slit of the spectrometer. At pressures above 2 torr, emissison lines due to neutral atomic oxygen and neutral atomic hydrogen were observed. At pressures below 2 torr, the plasma turned from a dull

violet color to a very bright white. When a spectral scan of the visible region was made at pressures below 2 torr, it was discovered that the white light was due to molecular emission spectra. The molecular spectrum was identified by comparison of spectra measured by others[111-121] and was found to be the first negative band of oxygen denoted $O_2^+(^4\Sigma - {}^4\Pi)$.

D.5.3. Results

Since the first negative band of oxygen is an electronic transition, there is coupling which occurs between the electronic and rotational angular momentum, which results in many branches (Figure D9) associated with each vibrational transition of the electronic transition. Each vibrational branch contains many rotational lines. Unfortunately, the vibrational bands tend to be very close to one another, (see Table D6), so that in a range of 150 Å, there is the possibility of observing several vibrational transitions associated with this one electronic transition, any of which contains 27 to 48 P, Q or R branches, with several rotational lines contained in each branch.[111] Needless to say, the spectrum of the first negative band of oxygen is very complicated. (See Figure D10)

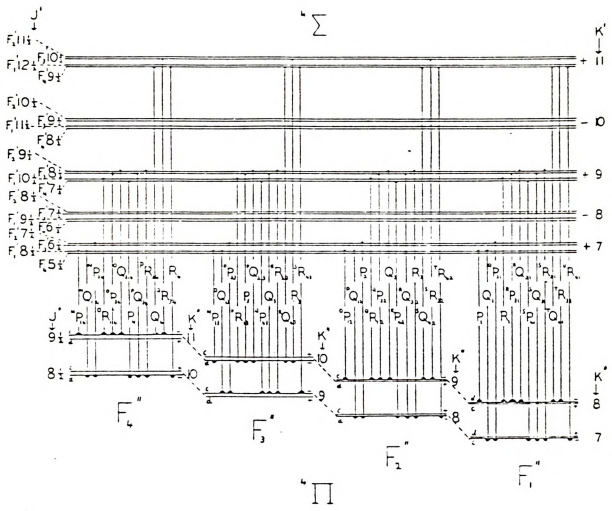

Figure D9 Structure of the rotational levels for the first negative band of oxygen.[115]

Table D.6 Band Heads of the First Negative System of O_2^+ [121]

Wavelength (Å)	Intensity	v'-v"
7150		2 - 5
6856.3		0 - 2
6770		1 - 3
6684		2 - 4
6419.2	10	0 - 1
6351.1	10	1 - 2
6291.9	6	2 - 3
6232.7	3	3 - 4
6117.2	3	4 - 5
6026.4	10	0 - 0
5973.5	10	1 - 1
5925.7	9	2 - 2
5883.5	8	3 - 3
5847.4	2	4 - 4
5814.4	1	5 - 5
5631.9	10	1 - 0
5597.6	10	2 - 1
5566.7	6	3 - 2
5540.8	2	4 - 3
5520.9	2	5 - 4
5295.7	9	2 - 0
5274.7	10	3 - 1
5259.2	6	4 - 2
5251.2	10	5 - 3
5241.0	8	6 - 4

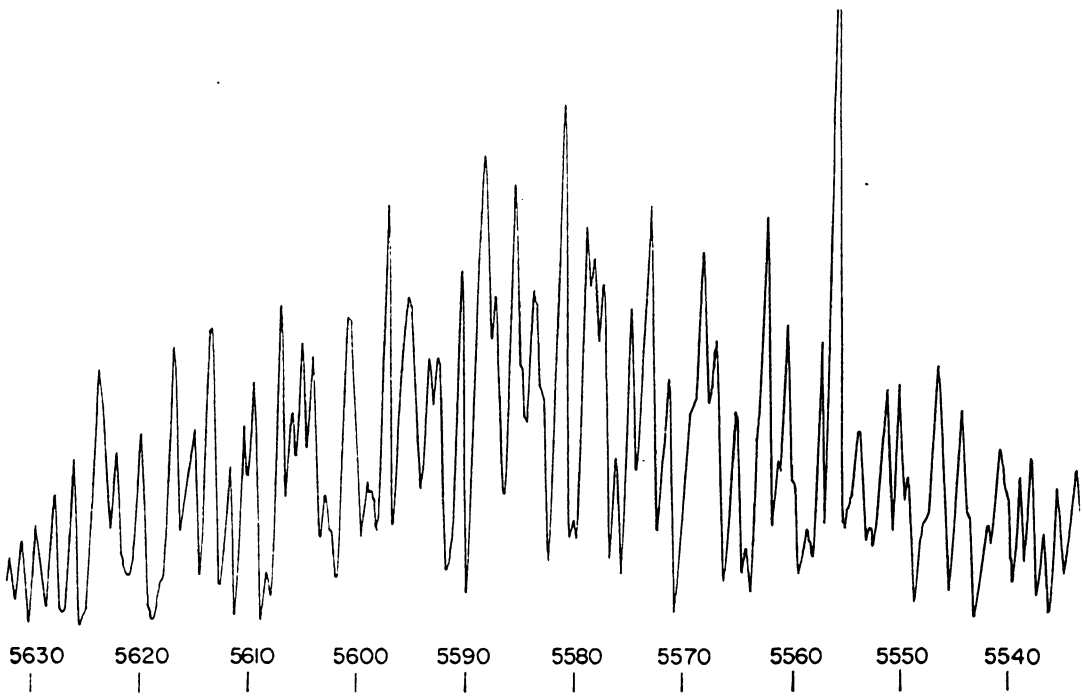

Figure D10 An example of O_2^+ first negative band spectra.

Three of the strongest vibrational bands ((0,0), (0,1) and (1,0)) were analyzed with an approximated resolution of 0.5 Å. Since the Q4 branch occurred at the beginning of each vibrational band and was reasonably strong in intensity, it was the easiest to identify. In each of the three vibrational cases, only the first seven lines of the Q4 branch were identified, because the lines of the other branches were superimposed on the higher rotational lines of Q4.

Due to the complexity of the spectrum, it was impossible to distinguish the area of any one line from the next. Therefore, only the height of each rotational line was measured. The relative heights approximate the relative areas for this apparatus, as discussed in Section D.4.3. The first seven lines of the Q4 branch in three vibrational bands have been plotted in Figure D11. The data points do form a straight line as predicted and result in an average temperature of 320 K.

The rotational temperature may or may not represent the average gas temperature. Oldenberg[123] discusses the criteria for the rotational temperature to represent the gas temperature. He indicates that when the rotational temperature does not match the gas temperature, a straight line is not obtained when the logarithm of the intensities is plotted against the energy, and the rotational

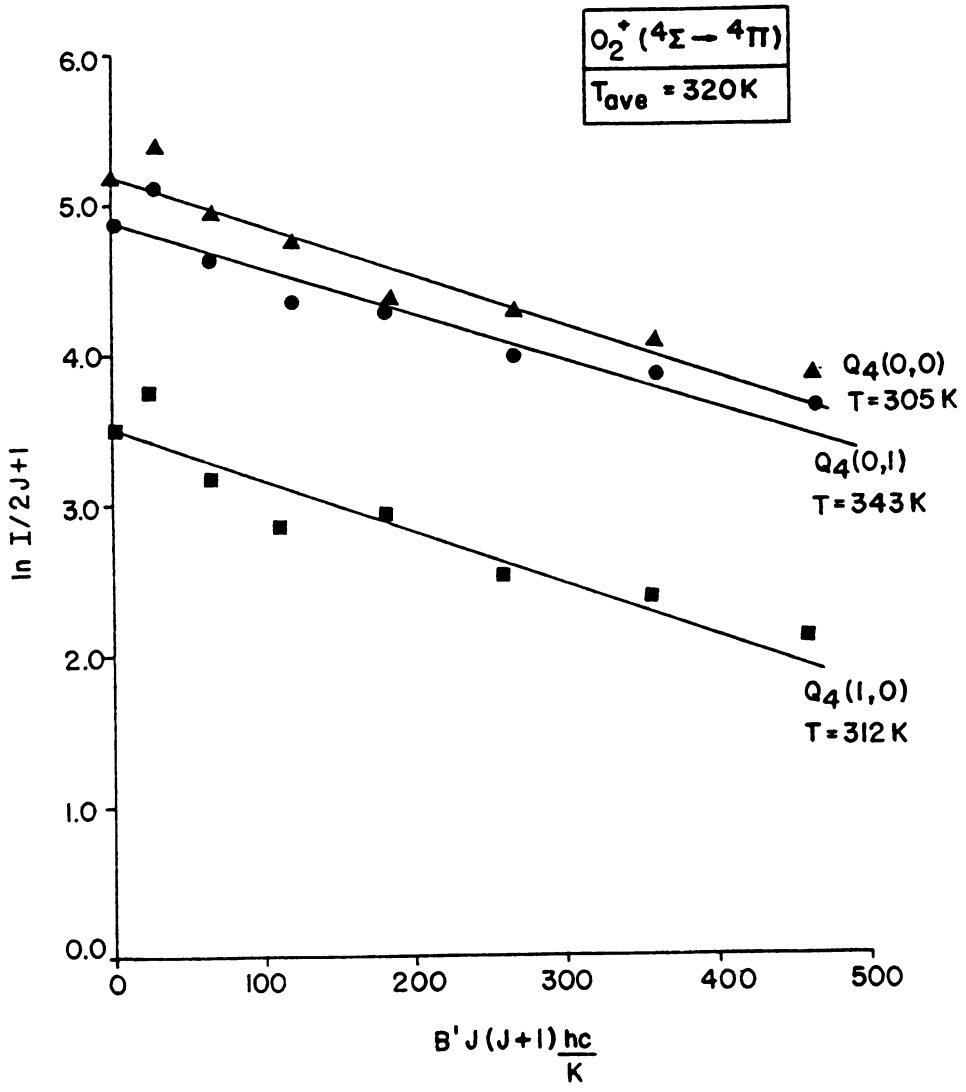

Figure D11 The inverse of the slope of the natural logarithm of the intensity versus the energy of the upper state is the rotational temperature.

temperature tends to result in an overestimation of the gas temperature. Since a fairly straight line is obtained, this rotational temperature is probably the gas temperature of O_2^+, although not necessarily that of the O atoms or the gas as a whole.

In Chapter II, it was found from computer modeling of the neutral kinetics that wall recombination is the dominant mechanism at 2 torr and below, whereas two and three body recombination are the dominant mechanisms at higher pressures. Thus the O_2^+ is probably due to recombination of O and O^+ at the wall. The computer model predicted temperatures of 1000 K to 2000 K for the overall gas temperature. But since the plasma containment tube was cooled with a fairly strong air flow around the outside of the tube, the tube wall is considerably cooler than the contents of the interior of the plasma. If O_2^+ is formed at the wall, the rotational temperature would be expected to represent the wall temperature which would be much lower than 1000 K. For this experiment, a rotational temperature of 320 K is consistent with an expected wall temperature.

Bozoky and Schmid[112] observed rotational spectra in a similar experiment of a high frequency radio discharge. The authors concluded that the rotational temperature was low because they were not able to discern the rotational development of the vibrational band heads, i.e. their

resolution was not good enough to separate the rotational lines.

D.5.4. Recommendations for Rotational Temperatures

An important recommendation for this experiment is the vary and record the flowrate of the air that cools the quartz plasma containment tube. The wall of the tube heats up dramatically for low and no flowrates because glowing hot spots and melting have been observed. If the rotational temperature of the O_2^+ represents the wall temperature, then it would be expected that the rotational temperature would rise as the cooling flowrate is reduced.

D.6 Conclusions

Emission spectroscopy measurements of argon and oxygen plasmas give results consistent with electromagnetic measurements and with chemical modeling results. The electron temperature of an argon plasma at 6 torr was found to be 7380 K. The electron density of an argon plasma was measured from Stark broadening and was found to be in the range of 10^{-13} to 10^{-14} electrons/cc which match surface wave measurements for a pressure range of 50 to 1000 torr. Rotational temperature measurements of O_2^+ indicate the

temperature of a cooled containment tube wall to be slightly above room temperature at 320 K.

APPENDIX E

APPENDIX E

RATE COEFFICIENTS FOR CHARGED COLLISIONAL PARTNERS IN OXYGEN DISSOCIATION

	Reaction	Rate Coefficient (cc,sec,mole)	Ref.
1.	$O(^1D) + e \rightarrow O + e$	9×10^{14}	17
2.	$O_2 + e \rightarrow O_2^+ + 2e$	$\sigma(E)$*	124
3.	$O_2 + e \rightarrow O^- + O$	6×10^{7}	17
4.	$O + e \rightarrow O^+ + 2e$	$\sigma(E)$	127
5.	$O_2 + e \rightarrow O^+ + O + 2e$	$\sigma(E)$	126
6.	$O_2 + e \rightarrow O^+ + O^- + 2e$	$\sigma(E)$	125
7.	$O + e \rightarrow O^- + h\nu$	7.8×10^{8}	17
8.	$O_2 + e \rightarrow O_2^- + h\nu$	1.2×10^{5}	17
9.	$O_3 + e \rightarrow O_3^- + h\nu$	6.0×10^{6}	17
10.	$O_2 + e \rightarrow O_2(^1\Delta) + e$	2.9×10^{14}	12
11.	$O_2 + e \rightarrow 2O + e$	1.4×10^{14}	12
12.	$O_2 + e \rightarrow O_2(^1\Sigma) + e$	6.6×10^{13}	12
13.	$O_2^- + O_2(^1\Delta) \rightarrow 2O_2 + e$	1.2×10^{14}	135,17
14.	$O^- + O_2(^1\Delta) \rightarrow O_2^- + O$	6.0×10^{13}	17
15.	$O^- + O_2(^1\Delta) \rightarrow O_3 + e$	1.8×10^{14}	135,17
16.	$O^+ + O_2 \rightarrow O + O_2^+$	2.4×10^{13} 1.2×10^{13}	128 17
17.	$O_2^- + O \rightarrow O_2 + O^-$	$\sigma(E)$ 3×10^{13} 6×10^{13}	129,131 133 17

* $\sigma(E)$ indicates cross sectional data as a function of energy

Reaction	Rate Coefficient (cc,sec,mole)	Ref.
18. $O^- + O_3 \rightarrow O_3^- + O$	3.2×10^{14}	134,17
19. $O_2^- + O_3 \rightarrow O_2 + O_3^-$	2.4×10^{14}	134,17
20. $O^+ + O \rightarrow O_2^+ + h\nu$	6.0×10^{6}	137
21. $O^- + O_2 \rightarrow O_3^- + h\nu$	6.0×10^{6}	133
22. $O^- + O_2 + O_2 \rightarrow O_3^- + O_2$	$\sigma(E)$ 4.0×10^{17}	129,131
23. $O_3^- + O \rightarrow O_2^- + O_2$	6×10^{12}	17
24. $O^+ + O + M \rightarrow O_2^+ + M$	3.6×10^{17}	17
25. $O^- + O \rightarrow O_2 + e$	1.8×10^{15} 8.4×10^{13} 1.2×10^{14}	133 134 17
26. $O_2 + e \rightarrow O^- + O$	6.0×10^{7}	17
27. $O^- + O_2 \rightarrow O + e + O_2$	1.4×10^{15}	17
28. $O + O_2^- \rightarrow O_3 + e$	2.0×10^{14}	134,135,17
29. $O_2^- + O_2 \rightarrow 2O_2 + e$	1.6×10^{14}	17
30. $O_2 + O_2 + e \rightarrow O_2^- + O_2$	5.1×10^{18}	17
31. $O_2 + e + O \rightarrow O_2^- + O$	3.6×10^{16}	17
32. $O^- + O_2 \rightarrow O_3 + e$	$\sigma(E)$ 3.0×10^{9}	130 17
33. $O_3 + e \rightarrow O^- + O_2$	5.4×10^{12}	17
34. $O^- + O_3 \rightarrow 2O_2 + e$	3.2×10^{14}	17
35. $O_3^- + O \rightarrow 2O_2 + e$	6.0×10^{12}	17
36. $O_2^+ + e \rightarrow 2O$	1.3×10^{17}	15
37. $O^+ + e + M \rightarrow O + M$	3.6×10^{21}	137
38. $O_2^+ + e + M \rightarrow O_2 + M$	3.6×10^{21}	137

Reaction	Rate Coefficient (cc,sec,mole)	Ref.
39. $O^+ + e \rightarrow O + h\nu$	2.1×10^{12}	17
40. $O_2^+ + e \rightarrow O_2 + h\nu$	2.4×10^{12}	17
41. $O_2^+ + O_2^- \rightarrow O_2 + 2O$	6.0×10^{16}	137
42. $O_2^+ + O_2^- \rightarrow O_2 + O_2(^1\Delta)$	6.0×10^{15}	137
43. $O^+ + O^- \rightarrow 2O$	$\sigma(E)$ 1.6×10^{16}	132 17
44. $O_2^+ + O^- \rightarrow O_2 + O$	5.8×10^{16}	17
45. $O_2^- + O^+ \rightarrow O_2 + O$	2.5×10^{17}	17
46. $O^- + O^+ + M \rightarrow O_2 + M$	7.3×10^{22}	137
47. $O^- + O_2^+ + M \rightarrow O_3 + M$	7.3×10^{22}	137
48. $O_2^- + O^+ + M \rightarrow O_3 + M$	7.3×10^{22}	137
49. $O_2^- + O_2^+ + M \rightarrow 2O_2 + M$	7.3×10^{22}	137
50. $O_2^- + O_2^+ \rightarrow 2O_2$	1.2×10^{17}	137
51. $O_3^- + O^+ \rightarrow O_3 + O$	1.2×10^{17}	137
52. $O_3^- + O_2^+ \rightarrow O_3 + O_2$	1.2×10^{17}	137
53. $O_3^- + O_2^+ \rightarrow O_3 + 2O$	1.2×10^{17}	137
54. $O_2^+ + O \rightarrow O^+ + O_2$	$\sigma(E)$	136
55. $O_2(^1\Delta) + e \rightarrow O_2 + e$	6.0×10^{12}	17

LIST OF REFERENCES

LIST OF REFERENCES

1. G. Marr, Plasma Spectroscopy (Amsterdam: Elsevier Publishing Co., 1968).

2. N. Krall and A. Trivelpiece, Principles of Plasma Physics (New York: McGraw Hill, 1973).

3. Properties and Applications of Low Temperature Plasmas, International Union of Pure and Applied Chemistry (New York: Plenum Press, 1966) Volume 13, no. 3.

4. R. Baddour and R. Timmins, Application of Plasmas to Chemical Processing (Cambridge: MIT Press, 1967).

5. J. Hollahan and A. Bell, Techniques and Applications of Plasma Chemistry (New York: John Wiley and Sons, 1974).

6. F. McTaggart, Plasma Chemistry in Electrical Discharges (Amsterdam: Elsevier Publishing Co., 1967).

7. J. Asmussen, R. Mallavarpu, J. Hamann and H. Park, "The Design of a Microwave Plasma Cavity," Proc. IEEE 62 , 109,1974

8. C. Hawkins and S. Nakanishi, "Free Radical Propulsion Concept," NASA memo 81770, Lewis Research Center 1981.

9. A. Bell and K. Kwong, "Dissociation of Oxygen in a Radiofrequency Electrical Discharge," AIChE 18 ,990 (1972).

10. A. Mearns and A. Morris, "Oxidation Reactions in a Microwave Discharge: Factors Affecting Efficiency of Oxygen Atom Production," Chem. Eng. Prog. Ser. No. 112 , 37 (1971).

11. P. Francis, "The Production of Oxygen Atoms in a Microwave Discharge and the Recombination Kinetics in a Gas Flow System," J. Appl. Phys. 2 , 1717 (1969).

12. J. Bonnet, G. Fournier, D. Pigache and M. Lecuiller, "Kinetics of Species Produced by an Electron Beam Controlled Discharge in Oxygen at

Atmospheric Pressure," J. Phys. Letts. 41 , 477 (1980).

13. P. Kocian, "Note on the Dissociation of Oxygen in a Low Pressure Discharge Plasma," Phys. Letts. 73A , 17 (1979).

14. R. Wayne, "Singlet Molecular Oxygen", Ed. J. Pitts, G. Hammond, and A. Noyes , "Adv. In Photochemistry" 7 311 (1969) (New York: Interscience Pub., 1969)

15. J. Dettmer, "Discharge Processes in the Oxygen Plasma," Ph.D Thesis (1978)

16. R. Kerber, A. MacKnight and R. Franklin, "Possible High Energy Laser at 1.27 Microns," Appl. Optics 17 , 3276 (1978).

17. M. Bortner and T. Bauer, Defense Nuclear Agency Reaction Rate Handbook , (National Technical Information Service, U. S. Department of Commerce, March 1972).

18. H. Johnston, "Gas Phase Reaction Kinetics of Neutral Oxygen Species," National Standard Reference Data Series, National Bureau of Standards, NSRDS - NBS 20 (1968), C13:48:20.

19. R. Hampson and D. Garvin, "Reaction Rate anad Photochemical Data for Atmospheric Chemistry," (National Bureau of Standards, 1977) C13.10:513

20. K. Schofield, "Evaluated Chemical Kinetic Rate Constants for Various Gas Phase Reactions," J. Phys. and Chem. Ref. Data 2 , No. 1., 25 (1973).

21. K. Schofield, "An Evaluation of Kinetic Rate Data for Reactions of Neutrals of Atmospheric Interest," Planet. Space Sci. 15 , 643, (1967).

22. D. Baulch, R. Cox, R. Hampson, J. Kerr, J. Troe, and R. Watson, "Evaluated Kinetic and Photochemical Date for Atmospheric Chemistry," J. Phys. and Chem. Ref. Data 9 , 295 (1980)

23. "Chemical Kinetic and Photochemical Data for Use in Stratospheric Modelling," (Jet Propulsion Laboratory, 1981), JPL Publication 81-3.

24. I. Clark, I. Jones and R. Wayne, "The Kinetics of

the Reaction Between $O_2(^1\Delta)$ and Ozone,", Proc. R. Soc. London Ser. A 317 , 407 (1970).

25. D. Davis, W. Wong, J. Lephardt, "A Laser Flash Photolysis - Resonance Fluorescence Kinetic Study: Reaction of $O(^3P)$ with O_3," Chem. Phys. Lett. 22 , 273 (1973).

26. S. Benson and A. Axworthy, "Reconsideration of the Rate Constants From the Thermal Decomposition of Ozone," J. Chem. Phys. 42 , 2614 (1965).

27. L. Phillips and J. Schiff, "Mass Spectrometric Studies of Atom Reactions. I. Reactions in the Atomic Nitrogen - Ozone System," J. Chem. Phys. 36, 1509 (1962).

28. D. Krezenski, R. Simonaites, J. Heicklen, "The Reactions of $O(^3P)$ with Ozone and Carbonyl Sulfide," Int. J. Chem. Kinetics 3 , 467, (1971).

29. D. Biendekapp and E. Bair, "Ozone Ultraviolet Photolysis. I. The Effect of Molecular Oxygen," J. Chem. Phys. 52 , 6119 (1970).

30. D. Biendekapp, L. Hartshorn and E. Bair, "The $O(^1D)$ and H_2O Reaction," Chem. Phys. Lett. 5 , 379 (1970).

31. D. Snelling and E. Bair, "Nonadiabatic Decomposition of N_2O in the Deactivation of $O(^1D)$ by N_2," J. Chem. Phys. 47 ,228 (1967).

32. R. Heidner, D. Husain and J. Wiesenfeld, "Kinetic Study of Electronically Excited Oxygen Atoms, $O(2^1D_2)$, by Time - Resolved Atomic Absorption Spectroscopy in the Vacuum Ultra - Violet (λ=115.2 nm, $O(3^1D_2 - 2^1D_2)$)," Chem. Phys. Lett. 16 , 530 (1972) and "Kinetic investigation of Electronically Excited Oxygen Atoms, $O(^1D)$ by Time Resolved Attenuation of Atomic Resonance Radiation in the Vacuum Ultra Violet," Chem. Soc. Farad. II 69 , 927,1973.

33. R. Gilpen, H. Schiff and K. Welge, "Photo Dissociation of O_3 in the Hartley Band. Reactions of $O(^1D)$ and $O_2(^1\Delta_3)$ with O_3 and O_2," J. Chem. Phys. 55 , 1087 (1971).

34. R. Young, G. Black and T. Slanger, "Reaction and Deactivation of $O(^1D)$," J. Chem. Phys. 49 , 4758

(1968).

35. J. Noxon, "Optical Emission from O (^{1}D) and $O_2(b^1\Sigma)$ in Ultraviolet Photolysis of O_2 and CO_2," J. Chem. Phys. 52, 1852 (1970).

36. G. Streit, C. Howard, A. Schmeltekopf, J. Davidson and H. Schiff, "Temperature Dependence of O(^{1}D) Rate Constants for Reactions with O_2, N_2, CO_2, O_3, and H_2O," J. Chem. Phys. 65, 4761 (1967).

37. I. Izod and R. Wayne, "The Formation, Reaction and Deactivation of $O_2(^1\Sigma)$," Proc. Royal. Soc. A308, 81 (1968).

38. S. Filseth, A. Zia and K. Welge, "Flash Photolytic Production, Reactive Lifetime and Collisional Quenching of $O_2(b^1\Sigma, v'=0)$," J. Chem. Phys. 52, 5502 (1970).

39. D. Snelling, "The Ultraviolet Flash Photolysis of Ozone and the Reactions of O(^{1}D) and $O_2(^1\Sigma)$," Can. J. Chem. 52, 257 (1974).

40. F. Stuhl and K. Welge, "Deactivation of O(^{1}S) and $O_2(b^1\Sigma)$," Can. J. Chem. 47, 1870 (1969).

41. K. Becker, W. Groth and U. Schurath, "The Quenching of Metastable $O_2(^1\Delta)$ and $O_2(^1\Sigma)$ Molecules," Chem. Phys. Lett. 8, 259 (1971).

42. R. Wayne and T. Pitts, "Rate Constant for the Reaction $O_2(^1\Delta) + O_3 = 2O_2 + O$," J. Chem. Phys. 50, 3644 (1969).

43. K. Becker, W. Groth and U. Schurath, "Reaction of $O_2(^1\Delta)$ and Ozone." Chem. Phys. Letts 14, 489 (1972).

44. R. McNeal and G. Cook, "Photoionization of Electronically Excited Oxygen : Rate of the Reaction $O_2(a^1\Delta) + O_3 = 2O_2 + O$," J. Chem. Phys. 47, 5385 (1967).

45. F. Findley and D. Snelling, "Temperature Dependence of the Rate Constant for the Reaction $O_2(^1\Delta) + O_3 = 2O_2 + O$," J. Chem. Phys. 54, 2750 (1971).

46. S. Arnold and E. Ogryzlo, "Some Reactions Forming $O_2(^1\Delta)$ in the Upper Atmosphere," Can. J. Phys. 45

, 2053 (1967).

47. R. Derwent and B. Thrush, "Measurements on $O_2(^1$) and $O_2(^1$) in Discharge Flow System," Trans. Farad. Soc. 67 , 2036 (1971).

48. F. Findley and D. Snelling, "Collisional Deactivation of $O_2(^1\Delta)$," J. Chem. Phys. 55 , 545 (1971).

49. F. Findley, C. Fortin and D. Snelling, "Deactivation of $O_2(^1\Delta)$," Chem. Phys. Lett. 3 , 204 (1969).

50. I. Clark and R. Wayne, "The Reaction of $O_2(^1\Delta)$ with Atomic Nitrogen and with Atomic Oxygen," Chem. Phys. Lett. 3 , 405 (1969).

51. R. Steer, R. Ackerman and J. Pitts, "Singlet Oxygen in the Environmental Sciences. V. Rates of Deactivation of $O_2(^1\Delta)$ by Oxygen and Nitrogen," J. Chem. Phys. 51 , 843 (1969).

52. T. Kenshea Tech. Report AFCRL 067-0221, April 1967

53. M. Camac and A. Vaughan, "O_2 Dissociation Rates in O_2 - Ar Mixtures," J. Chem. Phys. 34 , 460 (1961) as cited by 20.

54. J. Rink, H. Knight and R. Duff, "Shock Tube Determination of Dissociation of Rates of Oxygen," J. Chem. Phys. 34 , 1942 (1961), and J. Chem. Phys. 36 , 572 (1962).

55. J.Wilson , "An Experiment to Measure the Recombination Rate of Oxygen," Fluid Mech. 15 , 497 (1963).

56. K. Wray, "Shock Tube Study of the Recombination of O Atoms by Ar Catalysts at High Temperatures," J. Chem. Phys. 38 , 1518 (1963) as cited by 20 and "Shock Tube Study of the Coupling of the O_2 - Ar Rates of Dissociation and Vibrational Relaxation," J. Chem. Phys. 37 , 1254 (1962).

57. J. Kiefer and R. Lutz, "Recombination of Oxygen Atoms at High Temperatures as Measured by Shock Tube Densitometry," J. Chem. Phys. 42 , 1709 (1965) as cited by 20.

58. F. Kaufman and J. Kelso, "Rate Constant of the

Reaction $O + 2O_2 = O_3 + O_2$," Dis. Farad. Soc. 37 , 26 (1964).

59. M. Sauer and L. Dorfman, "Pulse Radiolysis of Gaseous Argon - Oxygen Solutions. Rate Constant for the Ozone Formation Reaction," J. Am. Chem. Soc. 87 , 3801 (1965).

60. F. Kaufman and J. Kelso, "M Effect in the Gas - Phase Recombinatin of O with O_2," J. Chem. Phys. 46, 4541 (1967).

61. I. Arnold and R. Comes, "Temperature Dependence of the Reactions $O(^3P) + O_3 + 2O_2$ and $O(^3P) + O_2 + M = O_3 + M$," Chem. Phys. 42, 231 (1979).

62. S. Benson and A. Axworthy, "Mechanisms of the Gas Phase, Thermal Decomposition of Ozone," J. Chem. Phys. 26 , 1718 (1957) as cited by 20.

63. J. Zaslowsky, H. Urback, F. Leighton, R. Wnuk and J. Wojtowicz, "The Kinetics of the Homogenouos Gas Phase Thermal Decomposition of Ozone," J. Am. Chem. Soc. 82 , 2682 (1960).

64. P. Williams and M. Mulcahy, "The Effects of Various Coatings on the Recombination Coefficient of Oxygen Atoms at Glass Surfaces," Aust. J. Chem. 19 , 2163 (1966).

65. J. Greaves and J. Linnett, "Recombination of Atoms at Surfaces," Trans. Farad. Soc. 54 , 1355 (1961).

66. J. Linnett and D. Marsden, "The Kinetics of Recombination of Oxygen Atoms at a Glass Surface," Proc. Roy. Soc. A234 , 489 (1956).

67. R. Heidner and C. Gardner, "$O_2(^1\Delta)$ - I Atom Kinetic Studies," SD-TR-79-6, Aerospace Corp, (1979).

68. Joint Army Navy Air Force Thermodynamic Tables, Dow Chemical Co. Midland, Michigan.

69. W. Jones and N. Davidson, "The Thermal Decomposition of Ozone in a Shock Tube Study," J. Am. Chem. Soc. 84 , 2868 (1962).

70. L. Bader and E. Ogryzlo, "Reactions of $O_2(^1\Delta)$ and $O_2(^1\Sigma)$," Disc. Farad. Soc. 37 , 46 (1964).

71. M. Clyne, "Reactions of Atoms and Free Radicals Studied in Discharge Flow Systems", Editor B. Levitt, Physical Chemistry of Fast Kinetics, Vol. I. "Gas Phase Reactions of Small Molecules", (London: Plenum Press, 1973).

72. R. Wayne, "Reactions of Excited Species in the Photolysis of Ozone," Trans. Farad. Soc. 68 , 172 (1972).

73. D. Matthews, "Interferometric Measurements in the Shock Tube of the Dissociation Rate in Oxygen," Phys. of Fluids 2 , 170 (1959).

74. M. Clyne, D. McKenney and B. Thrush, "Rate of Combination of Oxygen Atoms with Oxygen Molecules," Trans. Farad. Soc. 61 2701 (1965).

75. G. Black and T. Slanger, "Production of $O_2(^1\Delta)$ by Oxygen Atom Recombination on a Pyrex Surface," J. Chem. Phys. 74 , 6517 (1981).

76. J. Hinkle, M.S. Thesis

77. S. Penner, Chemical Reactions in Flow Systems (Butterworth Scientific Pub: London, 1955).

78. J. Hirschfelder, C. Curtis and R. Bird, Molecular Theory of Gases and Liquids (John Wiley and Sons, 1954).

79. W. Vincenti and C. Kruger, Introduction to Physical Gas Dynamics , (John Wiley: New York, 1965)

80. A. Hindemarsh, Lawrence Livermore Laboratories

81. S. Mertz, M. Hawley and J. Asmussen, "An Experimental Study of Reactions of CO and H_2 in a Continuous Flow Microwave Discharge Region," IEEE - Trans. on Plasma Sci. PS - 2(4) , 297 (1974).

82. F. Klein and J. Herron, "Mass Spectrometric Study of the Reactions of O Atoms with NO and NO_2, " J. Chem. Phys. 41 , 1285 (1964).

83. F. Kaufman, "The Air Afterglow and its Uses in the Study of Some Reactions of Atomic Oxygen," Proc. Roy. Soc. London A247 , 123 (1958).

84. T. Morin, R. Chapman, J. Filpus, M. Hawley, R.

Kerber, J. Asumssun, and S. Nakanishi, "Measurements of Energy Distribution Thrust for Microwave Plasma Coupling of Electrical Energy to Hydrogen for Propulsion," to be published

85. G. Fournier, J. Bonnett and D. Pigache, "Comparison of the Macroscopic Properties of Field - Accelerated Electrons in Dry Air and in Pure Oxygen," J. Phys. Lett. 41 , L173 (1980).

86. R. McCarthy, "Chemical Synthesis from Free Radicals Produced in Microwave Fields," J. Chem. Phys. 22 , 1360 (1954).

87. J. Battey, "Design Criteria for Uniform Reaction Rates in an Oxygen Plasma," IEEE Trans. on Electron Devises, 24, 140 (1977).

88. E. Turner, G. Emanuel and R. Wilkens, "The NEST Chemistry Computer Program," Volume I, SAMSO-TR-70-311, Aerospace Co (1970).

89. A. Mearns and A. Morris, "Use of the Nitrogen Dioxide Technique for Oxygen Atom Determination at Pressures Above 2 Torr," J. Phys. Chem. 74 , 3999 (1970).

90. H. Griem, Plasma Spectroscopy (New York: McGraw Hill, 1964).

91. H. Griem, Spectral Line Broadening by Plasmas (New York: Academic Press, 1974).

92. W. Lochte - Holtgreven, Plasma Diagnostics (Amsterdam: North Holland Pub., 1968).

93. R. Huddlestone and S. Leonard, Plasma Diagnostic Techniques (New York: Academic Press, 1965).

94. D. Bates and B. Bederson, Advances in Atomic and Molecular Physics, Volume 2 (New York: Academic Press, 1975).

95. R. Tourin Spectroscopic Gas Temperature Measurements (Amsterdam: Elsevier Publishing Co., 1966).

96. G. Herzberg, Spectra of Diatomic Molecules (New York: Van Nostrand, 1950).

97. L. Schiff, Quantum Mechanics (New York: McGraw Hill,

1955).

98. E. Merzbacher, Quantum Mechanics (New York: John Wiley and Sons, 1961).

99. N. Konjevic and J. Roberts, "A Critical Review of the Stark Widths and Shifts of Spectral Lines from Non - Hydrogenic Atoms," J. Phys. Chem. Ref. Data 5 , no. 2,209 (1976).

100. J. Rogers, "Properties of Steady State, High Pressure Argon Microwave Discharges," Ph.D thesis (1982).

101. J. Rogers and J. Asmussen, "Standing Waves Along a Microwave Generated Surface Wave Plasma," IEEE Trans. on Plasma Sci. PS-10 , 1, 11 (1982).

102. J. Rogers, private communication

103. J. Davies and J. Vaughan, "A New Tabulation of the Voigt Profile," J. of Astrophys. 137 , 1302 (1963).

104. W. Wiese, M. Smith and B. Miles, "Atomic Transition Probabilities Vol. II, Sodium thru Calcium," NSRDS - NBS (1969) C13:48,22

105. M. Abroyan, Y. Kagan, N. Kolokolov and B. Lavrov, "Spectroscopic Determination of Electron Concentration in the Arc of a Duoplasmatron Ion Source," Opt. Spectrosc. 36 no. 4, 375 (1974).

106. D. Speer, S. Laven, A. Karp and M. Stockton, "Etalon - Spectrograph system for Improved Resolution over a Wide Spectral Range," App. Optics 19 , 2757 (1980).

107. W. Kreye, "Use of a Fabry - Perot/Monochrometer System for Enhancement of the Spectral Line to Noise Power Ratio from Line and Continuum Sources," J. Opt. Soc. of Am. 65 , 1427 (1975).

108. J. Hubert, M. Moisan and A. Ricard, "A New Microwave Plasma at Atmospheric Pressure," Spect. Acta 33B , 1 (1979).

109. E. Bloyet, P. Leprince, J. Marec, J. Mermet, M. Pouey and P. Randon, "Microwave Plasma Torch - Spectroscopic Measurements," VII Gas Discharges, (London, 1982).

110. A. Gaydon, Spectroscopy of Flames , (New York: Halsted Press, 1974)

111. T. Nevin, "Rotational Analysis of the 1st Negative Band Spectrum of Oxygen," Phil. Tran. Roy. Soc. A237 , 471 (1938).

112. L. Bozoky anad R. Schmid, "Additional First Negative Oxygen Bands," Phys. Rev. 48 , 465 (1935).

113. R. Mulliken and D. Steven, "New O_2^+ Bands. Dissociation Energy of O_2^+ and Ionization Potential of O_2, "Phys. Rev. 44 , 720 (1933).

114. D. Albritton, A. Schmeltekopf and W. Harrop, "An Analysis of the O_2^+ First Negative Band System," J. Molec. Spec. 67 , 157 (1977).

115. T. Nevin and T. Murphy, "Analysis of the (0,3) Band of the First Negative System of the O_2^+ Molecule," Proc. Roy. Irish Acad. A46 , 169 (1941).

116. T. Nevin, "Rotational Analysis of the First Negative Band Spectrum of Oxygen II," Proc. Roy. Soc. A174 , 371 (1940).

117. J. Hansen, M. Graff, J. Moseley and P. Cosby, "Predissociation Spectroscopy of O_2^+ $^4\Sigma$(v"=6-11) -- $^4\Pi$(v'=5-9)," J. Chem. Phys. 74, 2195 (1981).

118. M. Dufay, J. Desesquelles, M. Druetta, and M. Eidelsberg, "Etude de L'Excitation de L'Azote et de L'Oxygene par Chocs Protoniques," Ann. Geophy. 22 , 614 (1966).

119. S. Weniger, "Etude du Spectre de la Molecule D'Oxygene Ionisee dans le Proche Infra-Rouge," J. de. Phys. et Radium 23 , 225 (1962).

120. P.Cosby, J. Ozenne and J. Moseley, "High Resolution Photofragment Spectroscopy of the O_2^+ $^4\Sigma$ (v'=3,4,5) -- $^4\Pi$(v'=3,4,5) First Negative System Using Coaxial Dye-Laser and Velocity Tuned Ion Beams," J. Molec. Spec. 79 , 203 (1980).

121. P. Krupenie, "The Spectrum of Molecular Oxygen," J. Phys. and Chem. Ref. Data 1 , 423 (1972).

122. A. Mitchell and M. Zemansky, Resonance Radiation and Excited Atoms , (Cambridge: University Press, 1934).

123. O. Oldenberg, "On Adnormal Rotation of Molecules," Phys. Rev. 46 , 210, 1934.

124. D. Rapp and D. Briglia, "Total Cross Sections for Ionization and Attachment in Gases by Electron Impact I. Positive Ionization," J. Chem. Phys. 43 , 1464, 1965.

125. D. Rapp and D. Briglia, "Total Cross Sections for Ionization and Attachment in Gases by Electron Impact II. Negative Ion Formation," J. Chem. Phys. 43 , 1480, 1965.

126. D. Rapp, P. Englander-Golden and D. Briglia, "Cross Sections for Dissociative Ionization by Electron Impact," J. Chem. Phys. 42 , 4081, 1965.

127. E. Rothe, L. Marion, R. Neynaber and S. Trujillo, "Electron Impact Ionization of Atomic Hydrogen and Atomic Oxygen," Phys. Rev. 125 ,582, 1961.

128. F. Fehsenfel, P. Golden, A. Schmeltekopf and E. Ferguson, "Laboratory Measurement of the Rate of the Reaction $O^+ + O_2 = O_2^+ + O$ at Thermal Energy," Planet. Space Sci. 13 , 579, 1965.

129. R. Snuggs, D. Volz, I. Gatland and J. Schummers, "Ion - Molecule Reactions between O^- and O_2 at Thermal Energies and Above", Phys. Rev. A 3 , 487, 1971.

130. J. Mauer and G. Schultz, "Associative Detachment of O^- with CO, H_2 and O_2," Phys. Rev. A 7 , 593, 1973.

131. L. McKnight, "Drift Velocities and Interactions of Negative Ions in Oxygen," Phys. Rev. A 2 , 762, 1970.

132. R. Olsen, J. Peterson and J. Moseley, "Ion-Ion Recombination Total Cross Sections - Atomic Species," J. Chem. Phys. 53 , 3391, 1970.

133. F. Fehsenfeld, E. Ferguson and A. Schmeltekopf, "Thermal Energy Associative - Detachment Reactions of Negative Ions," J. Chem. Phys. 45 , 1844, 1966.

134. E. Ferguson, R. Fehsenfeld and A. Schmeltekopf, "Ion - Molecule Reaction Rates Measured in a Discharge

Afterglow," Adv. Chem. 80 , 83, 1967.

135. F. Fehsenfeld, D. Albritton, J. Burt and H. Schiff, "Associative Attachment Reactions of O^- and O_2^- by $O_2(^1\Delta)$," Can. FJ. Chem. 47 , 1793, 1969.

136. R. Stebbings, A. Smith and H. Gilbody, "Charge Transfer Between Some Atmospheric Ions and Atomic Oxygen," J. Chem. PHys. 38 , 2280, 1963.

137. F. Niles, "Airlike Discharges with CO_2, NO, NO_2 and N_2O as Impurities", J. Chem. Phys. 52, 408, 1970.